TI Designs
Automotive 12 V 200 W (20 A) BLDC Motor Drive Reference Design

TEXAS INSTRUMENTS

TI Designs

This TI Design is a 3-Phase Brushless DC Motor Drive designed to operate in 12-V automotive applications. The board is designed to drive motors in the 200-W range and can handle currents up to 20-A. The design includes analog circuits working in conjunction with a C2000 LaunchPad™ to spin a 3-Phase BLDC motor without the need for position feedback from Hall Effect sensors or quadrature encoder. The board provides filtering and protection against reverse-polarity conditions on the input power. On-board temperature sense, voltage sense, and current sense provide a full range of diagnostic and fault-protection features.

Design Resources

TIDA-00901	Design Folder
ccstudio	Tool Folder
MOTORWARE	Tool Folder
DRV8305-Q1	Product Folder
LM53600-Q1	Product Folder
LMT86-Q1	Product Folder
DRV5013-Q1	Product Folder

TI E2E™ Community   ASK Our E2E Experts


Design Features

- Speed Control of 3-Phase Brushless DC (BLDC) Motors
- Compatible With Existing MotorWare™ Software
- Provides 3.3-V Supply for LaunchPad Operation
- Wide Range of Voltages from the 12-V Battery System
- Protection Against Faults
- Reverse Polarity Protection on 12-V Battery Input
- 2.5-inch Diameter Circular PCB
- Components Selected for Automotive Temperature and Quality

Featured Applications

- HVAC Blower
- Water Pump
- eTurbo
- Radiator Fan
- Oil Pump
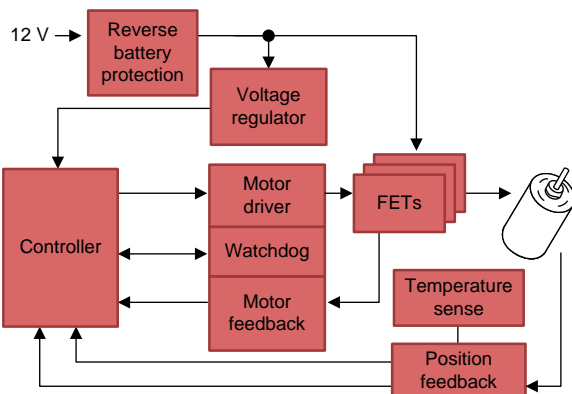
LaunchPad, Piccolo, Code Composer Studio, InstaSPIN-FOC, Insta-SPIN-MOTION are trademarks of Texas Instruments.
Webench is a registered trademark of Texas Instruments.
Diodes is a trademark of Diodes Inc.
Nichicon is a trademark of Nichicon Corporation.
Panasonic is a trademark of Panasonic Corporation.
Rohm is a trademark of Rohm Co Ltd.
ON Semi is a trademark of Semiconductor Components Industries, LLC.
Vishay is a trademark of Vishay Precision Group, Inc.

An IMPORTANT NOTICE at the end of this TI reference design addresses authorized use, intellectual property matters and other important disclaimers and information.

1 Key System Specifications

Table 1. System Specifications

PARAMETER		COMMENTS	MIN	TYP	MAX	UNIT	DETAILS
$V_{IN(VBATT)}$	Input voltage (steady-state)	12-V battery voltage range (DC)	8	12	18	V	See Section 4.3
$V_{IN(VBATT)}$	Input voltage (transient)	12-V battery voltage range	4.5		40	V	See Section 4.3
$I_{IN(VBATT)}$	Input current	8 V < $_{VBATT}$ < 18 V			20	A	See Section 4.3.1
$I_{IN(12V\ VBATT)REV}$	Input voltage reverse	Reverse battery range	− 15			V	See
f_{PWM}	PWM frequency	Motor switching frequency	15	45	50	kHz	See Section 4.6.1
V_{PHASE}	Motor phase voltage			12	40	V	See Section 4.6.1
I_{PHASE}	Motor phase current				20	A	See Section 4.6.1
$I_{3.3V}$	3.3 V – supply current	To LaunchPad through connectors J3, and J4		120	250	mA	See Section 4.4.1
Eff_{buck}	Buck efficiency	12-V input to 3.3-V output, 300-mA output current	70%				See Section 7.1.5
P_{OUT}	Output power	Power delivered to BLDC motor			200	W	See Section 7.2
	Motor current feedback gain			70		mV/A	See Section 4.7.1
	Motor current feedback bandwidth		400			kHz	See Section 4.7.1
	Motor voltage feedback bandwidth		300			Hz	See Section 4.7.2

2   System Description

Brushless DC (BLDC) motors have several advantages over brushed DC (BDC) motors; these include higher efficiency, longer lifetime and lack of brush-generated electrical noise. For these reasons, BLDC motors are increasingly being used in automotive applications, especially for equipment that operates for long periods of time.

TIDA-00901 is intended as a brushless DC motor drive design for automotive applications such as HVAC blowers, electric pumps, cooling fans, turbo compressors, and other similar equipment. The design works with typical 12V BLDC rotary motors where the rotational speed is regulated by controlling the PWM duty cycle. Commutation of the 3-phase brushless motor is demonstrated using sensorless technology, but board inputs are provided in case designers wish to use Hall sensors to determine motor commutation.

All analog components critical for the motor drive design are placed in a circular footprint (2.5-inch diameter) to replicate the typical motor drive board form factor. The board has connectors for mating to a LaunchPad™ microcontroller board, which can provide the PWM signals and communication to a graphical user interface.

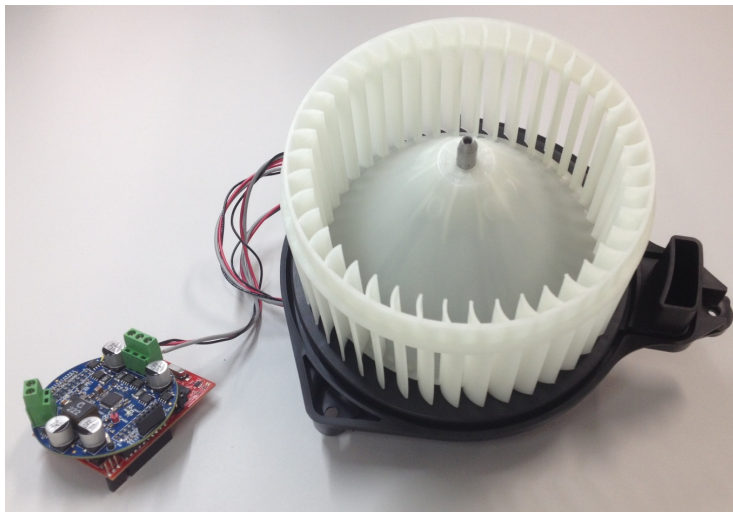Figure 1 shows the example application – automotive HVAC blower.

Figure 1. Example Application – Automotive HVAC Blower

Figure 2 shows the example application – automotive water pump.

Figure 2. Example Application – Automotive Water Pump

3   Block Diagram

Figure 2 shows the components of a typical example application. The TIDA-00901 board includes the functions highlighted in the light blue rectangle. The separate LaunchPad microcontroller board includes the C2000 real-time microcontroller and the interface to a USB connection. The brushless DC (BLDC) motor can be any appropriate three-phase model which operates on 12-V winding voltages. Hall Effect position sensors can be used to determine motor commutation, but these sensors are not needed if InstaSpin or an equivalent sensorless commutation algorithm is used.

Each of the board functions is described in the following sections, along with discussions regarding the selection of components making up each circuit.
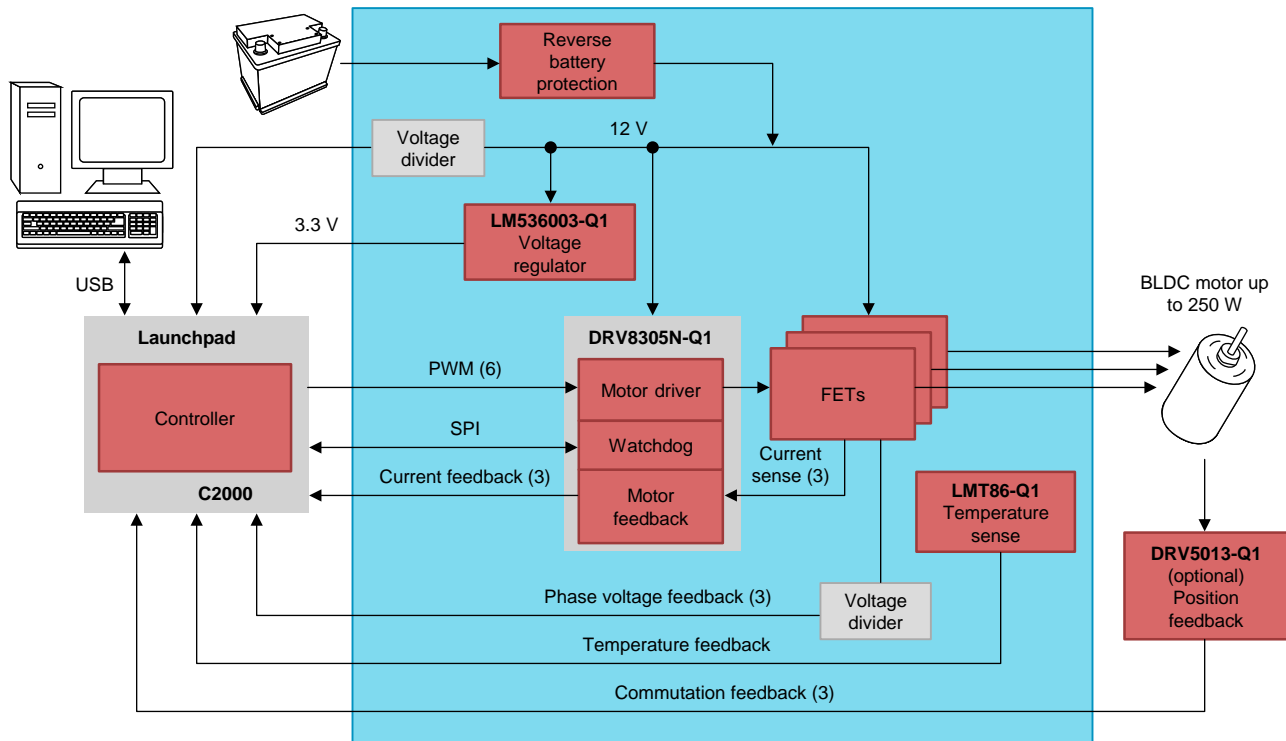
Figure 3. Detailed Block Diagram

3.1 Highlighted Products

This design uses the following TI products:

- DRV8305-Q1 is a highly-integrated gate driver with features for automotive BLDC motor drive applications.
- LM56300-Q1 is a 650mA synchronous step-down converter with up to 2.1-MHz switching rate.
- LMT86-Q1 is an analog temperature sensor with class-AB output.
- DRV5013-Q1 is a Hall Effect sensor which can be used to indicate motor position for commutation.

For more information on each device and why it was chosen for this application, see the following sections.

3.1.1 DRV8305-Q1

Figure 4 shows the internal block diagram of the DRV8305N-Q1 automotive gate driver.
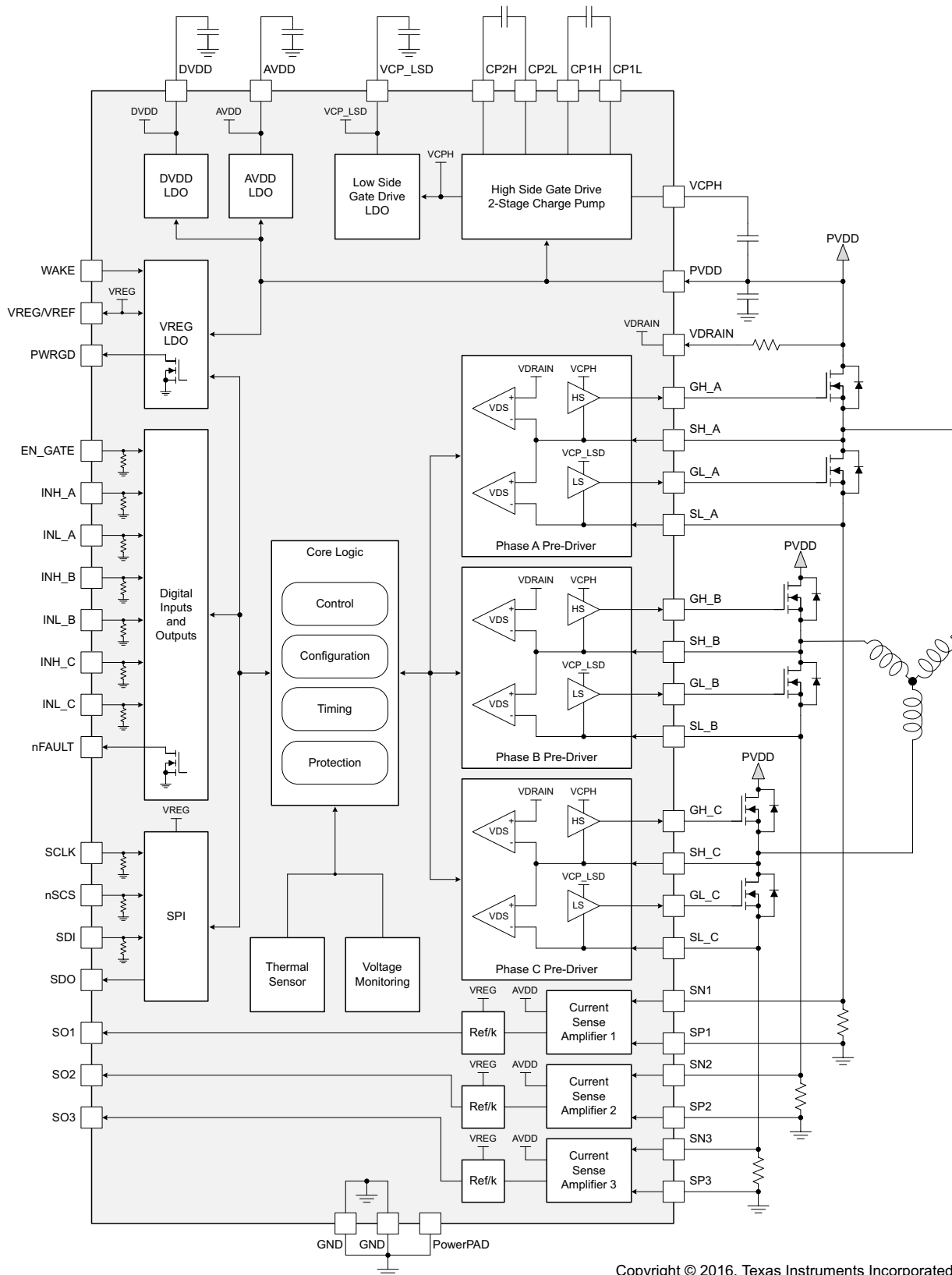
Figure 4. DRV8305N-Q1 Automotive Gate Driver

This device integrates most of the analog functions associated with controlling the drive stage for an automotive BLDC motor into a single compact package, as shown in Figure 4.

- The three half-bridge gate drivers can source and sink 1.25 A and 1 A peak gate current, respectively.
- The drive slew rate is independently programmable for the high-side and low-side FETs, with independent control of source and sink current for optimizing the motor drive performance.
- The device is rated for operation over a wide range of input voltage (4.4 V to 45 V).
- Three current shunt amplifiers are integrated with programmable gain, to provide accurate motor current feedback signals.
- Monitoring and switch control of the input power is integrated to provide protection against reverse battery faults.
- The device is available qualified to AEC-Q100 temperature grade 0 or 1, which allows for operation in automotive applications with a temperature range from –50°C to +150°C or from –40°C to +125°C, respectively.

3.1.2   LM53600N-Q1

Figure 5 shows the internal block diagram of the LM53600N-Q1 synchronous step-down (buck) converter.

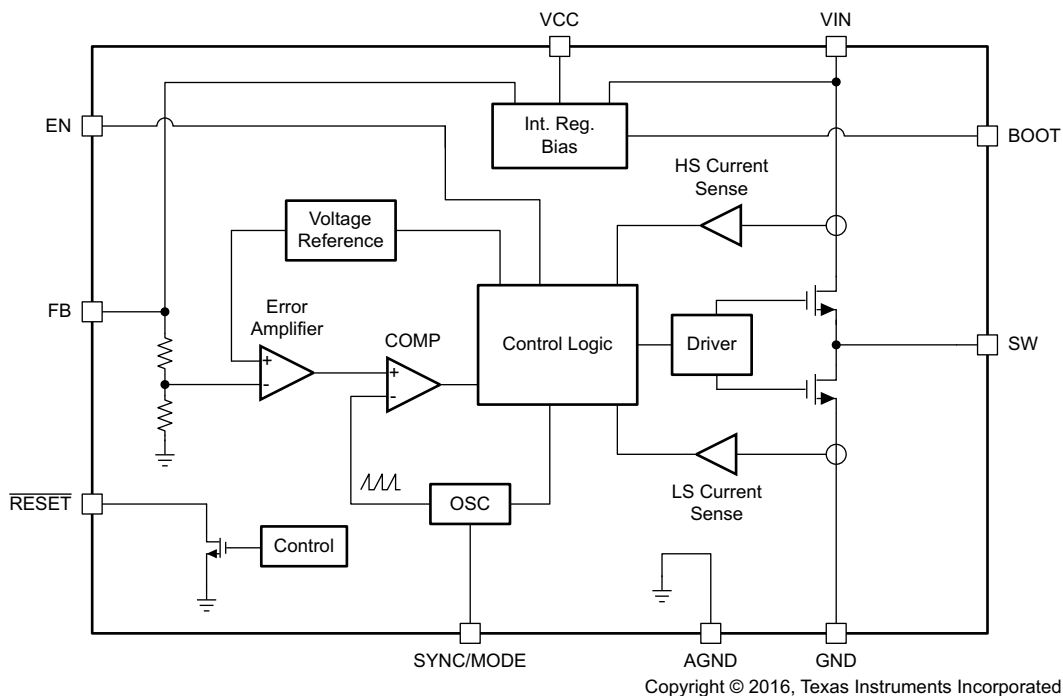Copyright © 2016, Texas Instruments Incorporated

Figure 5. LM53600N-Q1 Synchronous Step-down (Buck) Converter

- This device has a wide operating input voltage range (3.55 V to 36 V) with transient range up to 42 V.
- The device has a fixed switching frequency of 2.1 MHz, which is well above the AM radio band.
- The device is available in small 3-mm × 3-mm SON package.
- Spread-spectrum switching reduces peak switching noise for improved EMC performance.
- The device is qualified to AEC-Q100 temperature grade 1, which allows for operation in automotive applications with an ambient temperature range from –40°C to +125°C.

3.1.3 LMT86-Q1

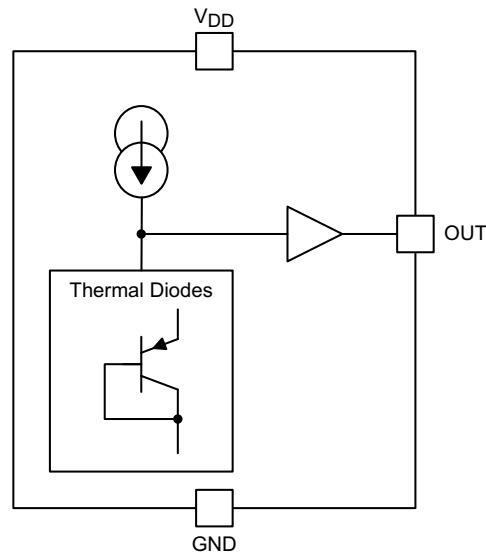Figure 6 shows the internal block diagram of the LMT86-Q1 analog temperature sensors with class-AB output.

Figure 6. LMT86-Q1 Analog Temperature Sensors With Class-AB Output

- This device has a very accurate (±0.25°C) scale factor that allows precise measurements of the board temperature.
- The devices are available in small SC70 package (2-mm × 2-mm) which facilitates placement close to the motor phase driver stages, thus reducing thermal time delay.
- A class-AB output structure gives the device strong output source and sink current capability that is well suited to an ADC sample-and-hold input.
- The device is qualified to AEC-Q100 temperature grade 0, which allows for operation in automotive applications with a temperature range from –50°C to +150°C.

3.1.4 DRV5013-Q1

Although not part of the TIDA-00901 board, the DRV5013-Q1 is an example of an appropriate Hall Effect device for use in applications where sensorless commutation is used. For these applications, the DRV5013-Q1 would typically be mounted on the motor assembly, to provide position feedback.

Figure 7 shows the internal block diagram of the DRV5013-Q1 automotive digital-latch hall effect sensor.
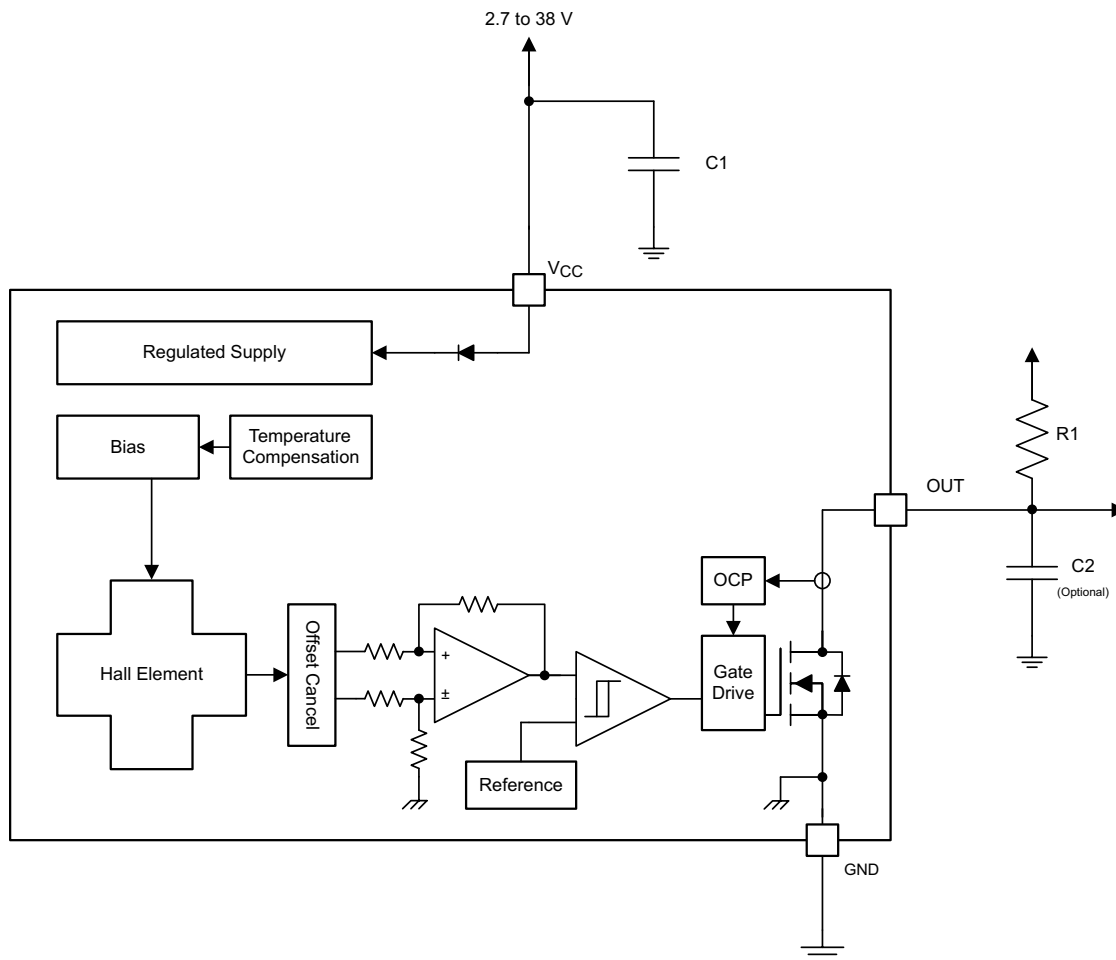
Copyright © 2016, Texas Instruments Incorporated

Figure 7. DRV5013-Q1 Automotive Digital-Latch Hall Effect Sensor

- This device supports a wide Voltage range (2.7 to 38 V) making it adaptable to a broad range of motors and interface options.
- This device has excellent temperature stability (B_{OP} ±10% over temperature) which is important for motor-mounted applications where the device will be subjected to wide temperature variations.
- The device is available in a small package for space-constrained applications.
- The device has several integrated protection features, which are important because it will be connected remotely from the bias voltage and signals may be subjected to wiring faults.
  - Protection features reverse supply protection (up to −22 V)
  - Supports up to 40-V load dump
  - Output short-circuit protection
  - Output current limitation
  - OUT short to battery protection
- The device is available qualified to AEC-Q100 temperature grade 0 or 1, which allows for operation in

automotive applications with a temperature range from –50°C to +150°C or from –40°C to +125°C, respectively.

4   System Design Theory

The following sections describe the considerations behind the design of each part of the system.

4.1   *PCB and Form Factor*

The goals for the board geometry were:

*   Compatible with LaunchPad microcontroller development platform
*   Circular board shape to demonstrate typical form factor for rotary motors
*   Easy access to significant electrical test points on LaunchPad connectors
*   Single side component mounting for ease of assembly and debug

The layout concept locates the circuitry actively driving the motor within a circular area in the center of the board. Connectors are along the outside of the circular board and were selected for ease of use, rather than suitability for a production design. The LaunchPad microcontroller board is mounted on connectors within the circle, and this arrangement allows designers to use a variety of specific microcontrollers, depending on the requirements of the application.

Figure 8 shows the TIDA-00901 board simplified board floor plan.
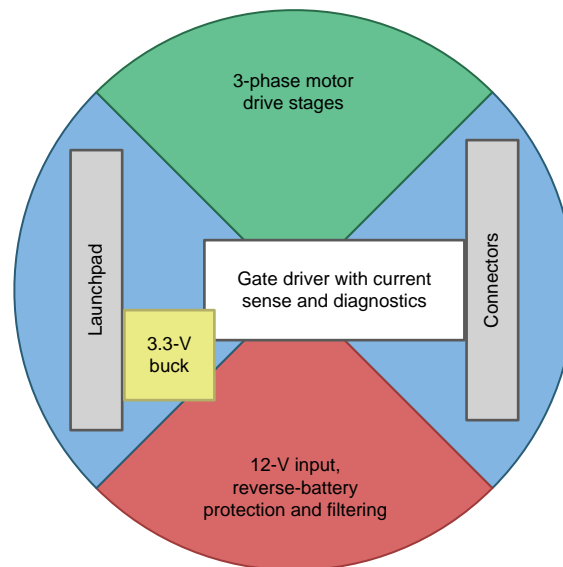
Figure 8. TIDA-00901 Board Simplified Floor Plan

4.2   *Overall Considerations for Component Selection*

In general, components were selected based on the performance requirements of the expected applications. Where practical, components with automotive ratings were selected. For active components, the components selected are AEC-Q100 qualified to either temperature grade 0 or temperature grade 1.

Capacitors are generally X7R grade (−55°C to +125°C) or higher, with size and value selected for the expected extremes of operation conditions. The voltage rating of the capacitors must be greater than the maximum voltage they could experience, and 2x the typical operating voltage to avoid DC bias effects. The amount of output capacitance used depends on output ripple and transient response requirements, and many equations and tools are available online to help estimate these values.

Consider the possible maximum voltage that could be experienced by the components. Capacitors must be derated by a minimum of 25% due to the drop in capacitance at 100% rated DC voltage of X7R and C0G/NP0 ceramic capacitors (that is, Max voltage 40 V; Capacitor voltage rating = 40V * 1.25 = 50V). The derating also helps protect components from unexpected voltage spikes in the system. During the design process the amount of BOM line items was considered. Therefore, capacitor voltage ratings may have been increased above the minimum desired rating. As an example, if there was one 1-µF, 25-V capacitor but nine 1-µF, 50-V capacitors, then the lone 25-V capacitor was modified to become a 50-V capacitor and the schematic contains a note indicating that the voltage rating was increased for BOM simplicity.

Supplies in this solution were designed for a ±2.5% (5%) total transient response. Low-ESR ceramic capacitors were used exclusively to reduce ripple. For internally compensated supplies, see device-specific data sheets, because they may have limitations on acceptable LC output filter values.

For improved accuracy, all feedback resistor dividers must use components with 1% or better tolerance. Resistance tolerance in this design was selected to reduce the total amount of BOM line items. In the design considerations, it is noted where 5% or 10% precision resistors may be used to reduce the cost of a specific individual resistor. Using less precise resistors for cost reasons should be weighed against reducing the amount of BOM line items and ordering in higher volumes to reduce total BOM cost.

Zero-Ohm (0-Ω) resistors are used at the input and output of some of the circuit sections for testing purposes only, and could be removed, if required, in a production board design.

4.3 12-V Input Protection

Reverse Battery Protection

The 12-V supply may experience several excursions from the nominal 12-V value. This design includes protection against such typical hazards as reverse battery conditions, and high-frequency electrical noise.

Reverse battery protection is required in nearly every electronic subsystem of a vehicle, both by OEM standards, as well as ISO 16750-2, an international standard pertaining to supply quality. The DRV8305 is designed to support an external reverse supply protection scheme. The VCPH high-side charge pump is able to supply an external load up to 10 mA. This feature allows implementation of an external reverse battery protection scheme using a MOSFET and a BJT, as shown in Figure 9.

The MOSFET gate and BJT may be driven by VCPH with a current limiting resistor. The current limiting resistor must be sized not to exceed the maximum external load on VCPH; R1 has a value of 10 kΩ, limiting the load on VCPH to less than 1 mA.

For this design, the Reverse Polarity MOSFET (see Section 8) must be rated at least as high as the expected input voltage; the SQJ422EP is rated for 40 V. Compared to the FETs used to drive the motor phases, there is no emphasis on switching speed for the reverse-polarity FET, therefore, this device was selected primarily based on a low on-state resistance, rather than low gate capacitance (see Table 3).

The VDRAIN sense pin is protected against reverse supply conditions by use of a current limiting resistor, R20. The current limit resistor must be sized not to exceed the maximum current load on the VDRAIN pin. As recommended, (see *DRV8305-Q1 Three-Phase Automotive Smart Gate Driver With Three Integrated Current Shunt Amplifiers and Voltage Regulator* datasheet (SLVSD12) R20 has a value of 100 Ω between VDRAIN and the drain of the external high-side MOSFET.

The BJT (Q1) and diode (D1) serve to pull the gate of the FET low when reverse battery conditions exist. This prevents any inadvertent turn-on of the reverse polarity FET due to *sneak paths*.
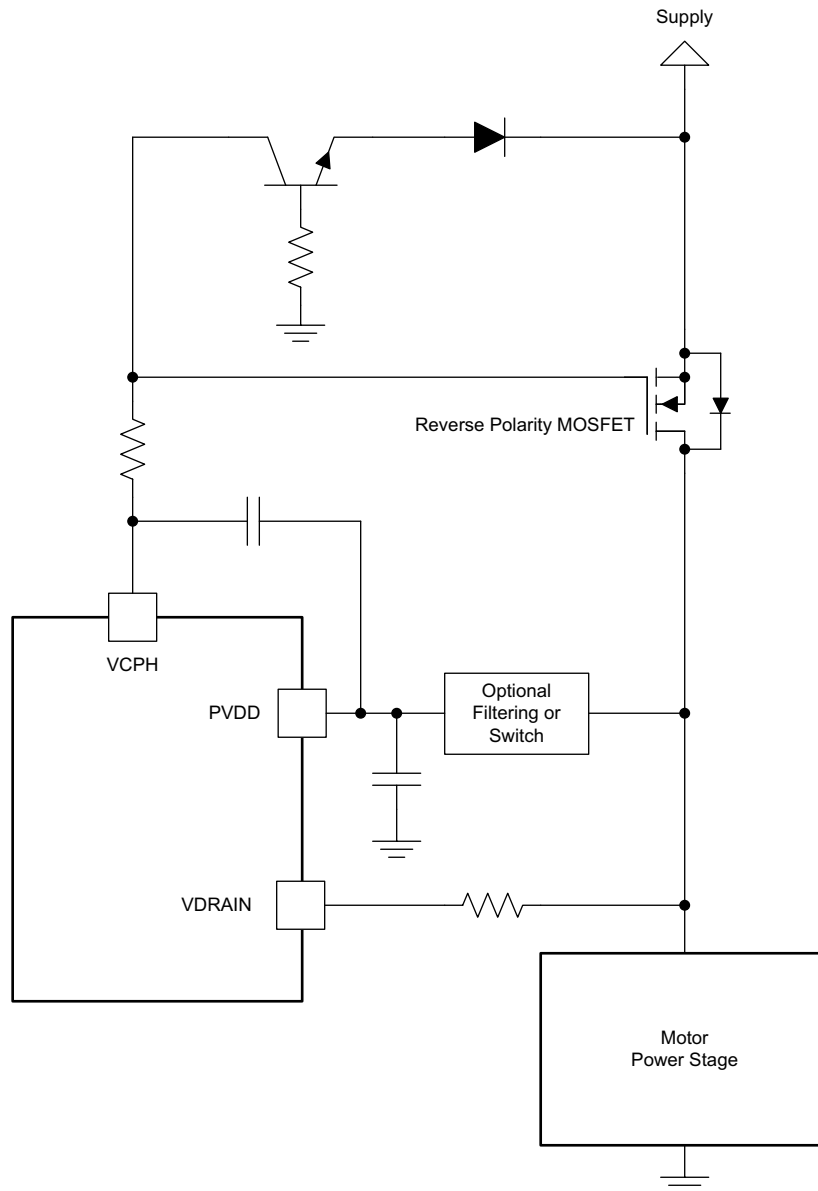
Copyright © 2016, Texas Instruments Incorporated

Figure 9. Reverse Battery Input Protection

4.3.1   12-V Input Filtering

Another consideration for the front-end protection is the input filtering. This design uses a set of capacitors and inductor to form a *pi* filter to remove unwanted AC components on the 12-V supply line. Due to the bidirectional format of the *pi* filter, incoming transients are blocked from entering the board, and any switching noise or clock noise generated on the board is blocked from propagating into the rest of the vehicle.

In general, the optimal amount of capacitance on the output side of the 12-V filtering may depend on the specifics of the application, including the current and electromagnetic compatibility (EMC) considerations. The *pi* filter implemented in this design has relatively symmetric components, providing an LC filter in both directions. The corner frequency is selected such that the fundamental of the expected PWM switching frequency, typically 20 kHz or higher, are significantly attenuated.

Figure 10 shows the input power filter with 2.2 µH inductor and 600 µF input capacitance.
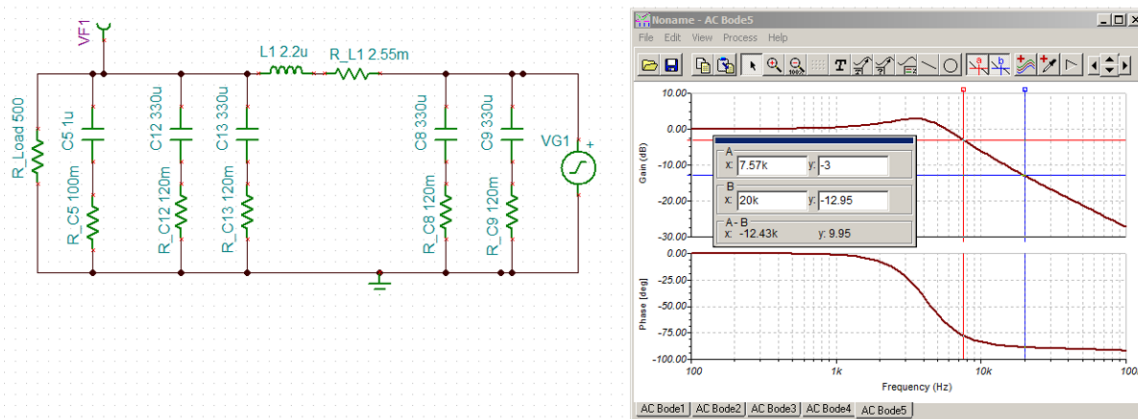
Figure 10. Input Power Filter With 2.2 µH Inductor and 660 µF Input Capacitance

Selection criteria for the input power inductor (L1) include inductance value, rated current, series resistance, power rating (internal temperature rise), and size. Table 2 shows some candidate inductors, with the parameters compared as part of the selection tradeoff. The XAL1010-222 was selected for this design based on the need for compact size and the 20-A current expectation for the applications.

With a typical DC resistance of 2.55 mΩ, the inductor dissipates approximately 1 W of power when the input current is at the design maximum of 20 A.

$$P_{L1} = \left(I^2\right) \times R_{L1} = \left(20^2\right) \times 0.00255 = 1.02 \text{ W}$$

(1)

If a lower-profile inductor were needed, the SRP1265A provides a similar set of parameters, but a larger board area is required.

lists the shielded power inductor component trade-off.

Table 2. Shielded Power Inductor Component Trade-Off

	SRP1250-1R0M	SRP1245A-1R0M	SRP1265A-2R2M	XAL6030-102ME	XAL1010-102ME	XAL1010-222	DRA127 -1R0-R
Manufacturer	Bourns **(nrnd)**	Bourns	Bourns	Coilcraft	Coilcraft	Coilcraft	Cooper Bussman
Inductance µH	1	1	2.2	1	1	2.2	1
Irms	29	29	22	**13**	32	32	**19.2**
Isat	50	50	37	**23**	55	34	40
DCR mΩ (typ)	2.5	2.5	3.8	6.2	1.1	2.55	1.7
Max Temp	150	150	150		165	165	165
Temp rise at 20A (°C)	10	15	26	20	< 20	< 20	40
Area mm2	188	179	179	44	124	124	58
Height mm	5.9	5	6	3	10	10	3.6

4.4   *Power Supplies*

The motor drive stage switches power from the filtered 12-V supply. A 3.3-V supply provides power to the LaunchPad microcontroller circuits, as well as the on-board temperature sensor and the optional Hall Effect sensors. Figure 11 shows the power supply scheme.
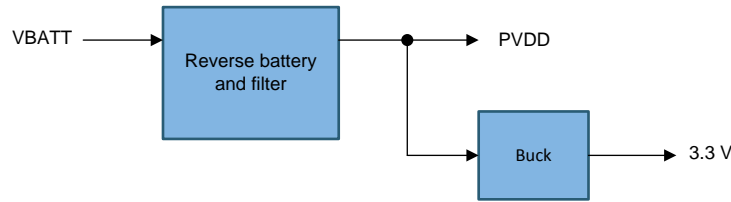
Figure 11. Power Supply Scheme

4.4.1   3.3-V Step-Down (Buck) Regulator

The design is intended to operate from a standard 12-V automotive battery. The battery voltage may vary over a range of input voltages from 4.5 V to 40 V. However, input voltages below 8 V (due to engine crank) or above 18 V (due to load dump) are expected to be short transient conditions.

The 3.3-V power supplies the C2000 real-time microcontroller LaunchPad board, the temperature sensor and reference voltage on the BoosterPack board, and the optional off-board Hall Effect sensors. Total current from the 3.3-V supply is not expected to exceed 250 mA.

To reduce component size and eliminate switching noise in the AM radio band, a synchronous buck regulator with high switching frequency is desirable. The LM536003-Q1 has a switching frequency of 2.1 MHz and provides synchronous regulation for currents up to 650 mA. The small (3 mm × 3 mm) package and few external components meet the desire for a compact design.

The *N* version of the LM53600 implements spread spectrum eliminates peak emissions at specific frequencies by spreading emissions across a wider range of frequencies than a part with fixed frequency operation. Typically, low frequency conducted emissions from the first few harmonics of the switching frequency are easily filtered. A more difficult design criterion is reduction of emissions at higher harmonics which fall in the FM band. These harmonics often couple to the environment through electric fields around the switch node. The LM53600-Q1 and LM53601-Q1 devices use a ±4% spread of frequencies which spread energy smoothly across the FM band but is small enough to limit sub-harmonic emissions below its switching frequency. Peak emissions at the part's switching frequency are only reduced by slightly less than 1 dB, while peaks in the FM band are typically reduced by more than 6 dB.

The LM53600-Q1 device uses a cycle to cycle frequency hopping method based on a linear feedback shift register (LFSR). Intelligent pseudo random generator limits cycle to cycle frequency changes to limit output ripple. Pseudo random pattern repeats by approximately 7 Hz, which is below the audio band.

Due to the fixed output voltage and internal compensation of the LM53600N-Q1, few external components are required. The choice of inductor is important, and a key feature for this design are compact footprint and sufficient current rating. The saturation current of L2 is 1.5 A, which is higher than threshold for LM53600N-Q1 hiccup feature, ensuring no issues in the event of a short-circuit fault on the 3.3-V supply output. The short-circuit falt tolerance is an important benefit because the 3.3-V supply is available on connector pins to supply the LaunchPad board.

Figure 12 shows the 12-V to 3.3-V buck regulator schematic.

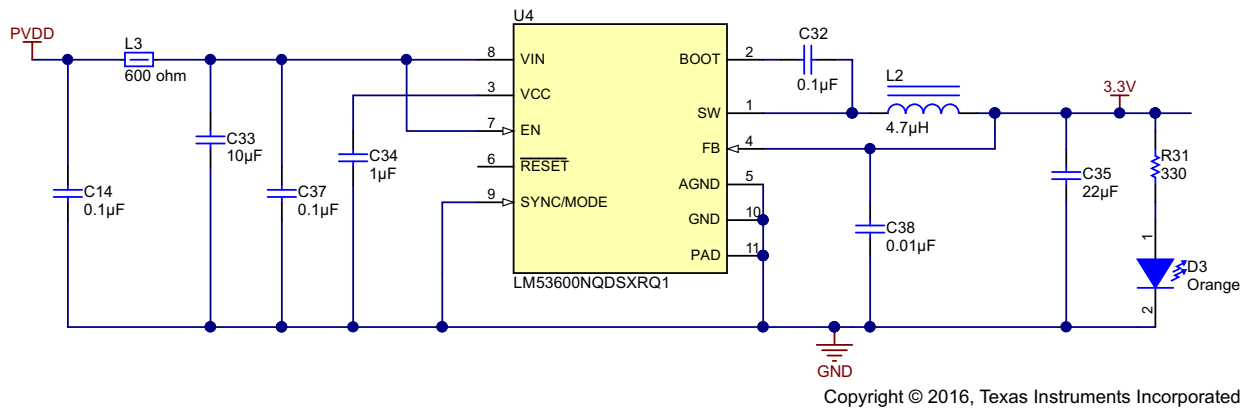Copyright © 2016, Texas Instruments Incorporated

Figure 12. 12-V to 3.3-V Buck Regulator Schematic

TI's on-line design tool, Webench® was used to select the components for the 3.3-V buck regulator. Webench also provides a means to simulate the performance of the design; some of the simulation results are shown in the following figures.

Figure 13 shows the frequency response of the 3.3-V buck regulator control loop. The zero dB crossover frequency is about 60 kHz, which is sufficient to regulate and reject any anticipated disturbances. The loop simulation shows a phase margin of approximately 50 degrees, and a gain margin of over 20 dB, indicating the loop compensation has resulted in a very stable configuration.
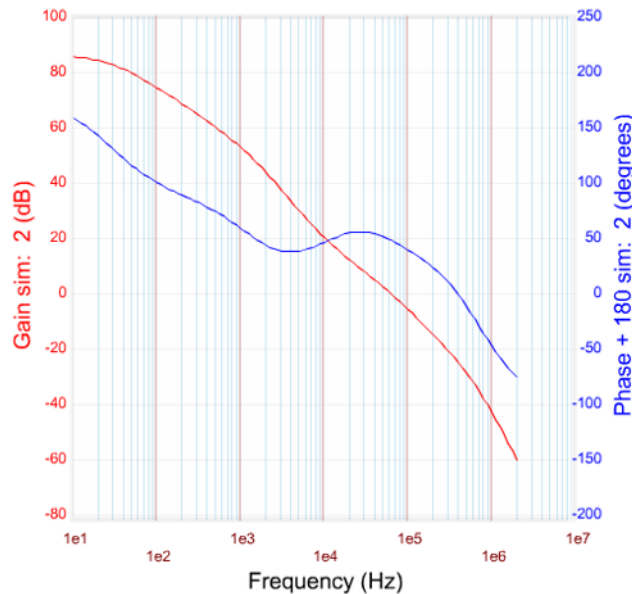
Figure 13. Bode Plot Simulation of the 3.3-V Buck Regulator Design

The response to an abrupt change in the input voltage is simulated as shown in Figure 14. Here, the input (PVDD) transitions from 5 V to 18 V and then back to 5 V. The response of the regulator is a small excursion in the output voltage, which quickly returns to the regulated value.

The abrupt changes shown in Figure 14 are intended to illustrate worst-case conditions; in real operation, even a cold-crank or stop and start event would not be expected to have this extreme of a voltage change.
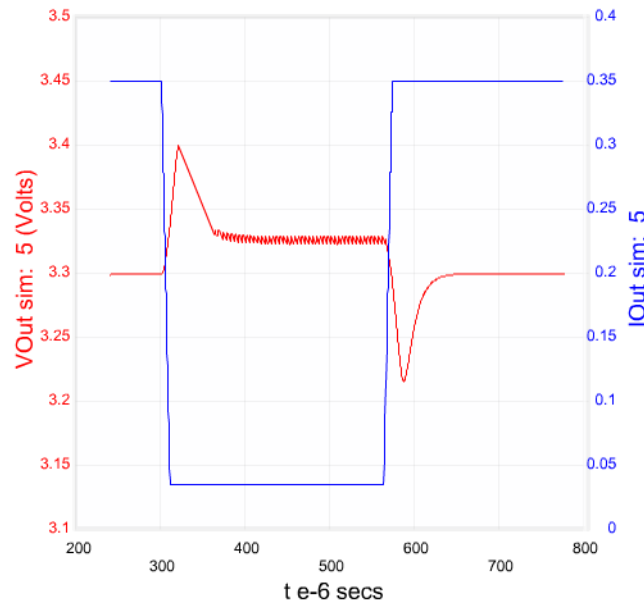
Figure 14. Simulation of Large Transient on Input to 3.3-V Buck Regulator Design

4.5 Gate Driver

The motor drive stage delivers 12-V power to the three phases of the BLDC motor as a pulse-width modulated (PWM) voltage. An overview of the gate driver circuit and motor stages is shown in Figure 15.

Each high-side and low-side pre-driver receives PWM signals from the microcontroller and generates the corresponding level-shifted (higher amplitude) signals to drive the gates of the high-side MOSFET and low-side MOSFET . The DRV8305N-Q1 gate driver is biased by the PVDD supply, with allowable supply tolerance from 4.4 V to 45 V.

The PWM switching frequency may range up to 200 kHz. This frequency is set by the parameters of the MotorWare software running on the LaunchPad microcontroller board. Unless otherwise noted, the PWM switching frequency was set to 45 kHz in the tests that follow.

Compared to other drive stage designs, there are very few external components around the drive FETs in this reference design. This reduction in external components is possible because the DRV8305-Q1 has several features that allow programming the parameters associated with the drive stage, to optimize the motor drive performance and reduce electromagnetic compatibility (EMC) concerns.

Copyright © 2016, Texas Instruments Incorporated
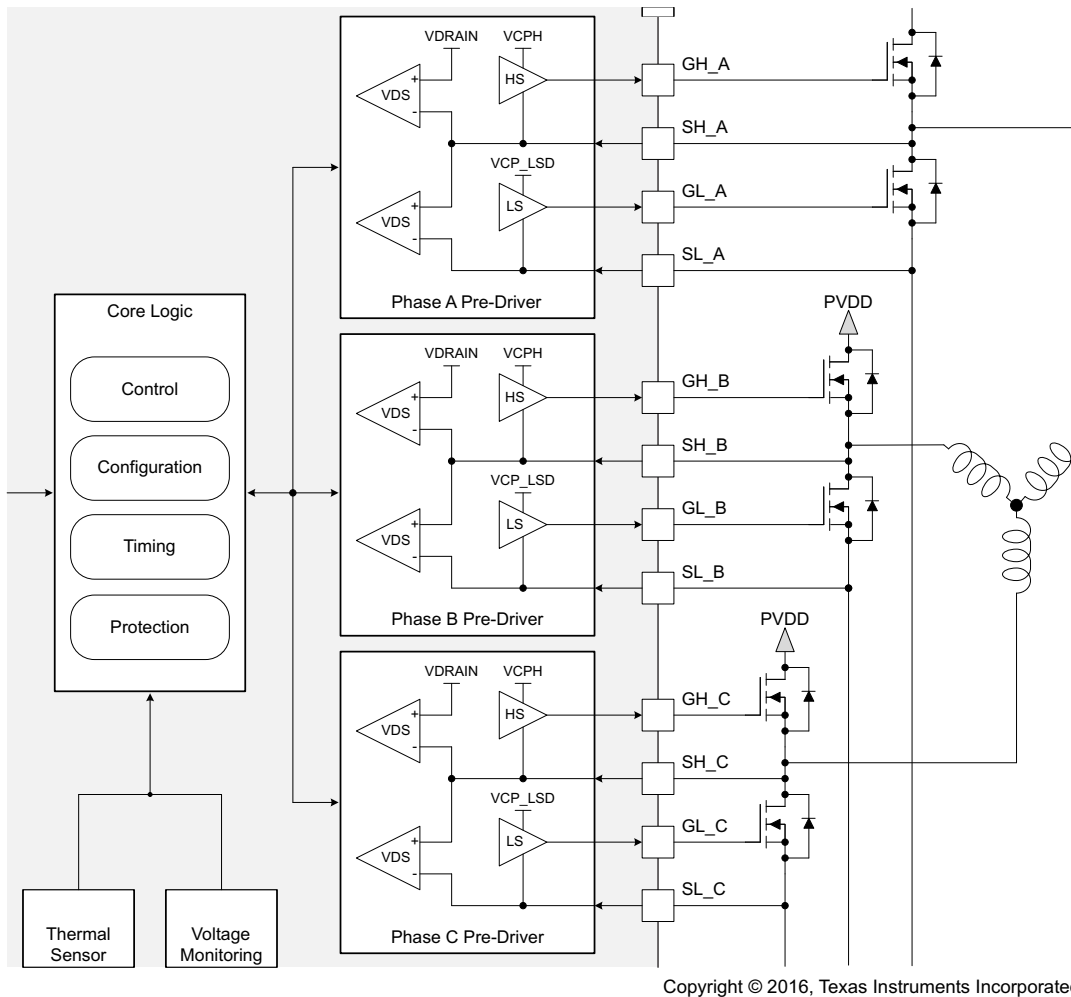
Figure 15. Motor Drive Circuit Overview

In addition to supplying gate drive current to the drive stage FETs, the DRV8305-Q1 has several other functions. These functions include three current sense amplifiers (CSA) used to amplify the signal which measures the current through each phase of the motor. The DRV8305-Q1 also controls the external circuit which disconnects the circuits on this board from the input power voltage in the case of a reverse polarity condition. These functions are discussed separately in the following sections.

4.6 Motor Drive Stages

The motor drive stage consists of the three pairs of n-channel MOSFETs (high-side and low-side), one for each of the three phases of the BLDC motor, and the large capacitors which supply the immediate bursts of current during each FET transition. Due to the integrated features of the DRV8305-Q1 gate driver, few other components are needed to optimize the performance of the drive stage.

4.6.1 FET Selection

Selection of the field-effect transistors (FETs) for the motor drive stages involves a trade-off between component size, on-state resistance, and gate capacitance or charge.

Table 3 lists some of the candidate FETs considered for the drive stages. All of the drive stages meet the requirements for high voltage specifications on the drain-to-source (at least 40 V), and a small size (32 mm^2 board area). All drive stages are rated for at least 20 A of current, and have low RDS(ON) for reducing conductive losses (<10 m

Table 3. Power FET Component Trade-Off

	CSD18540Q5B	AUIRF7648M2	AUIRFN7107	SQJ858AEP	SQJ460AEP	SQJ422EP
Manufacturer	TI	Infenion	Infineon	Vishay	Vishay	Vishay
VDS (max)	60	60	75	40	60	40
Automotive	**No**	Yes	Yes	Yes	Yes	Yes
Max Temp	**150**	175	175	175	175	175
Max Current	221	68	75	58	27 at 125 C	62 at 125 C
RDS (on) max (mΩ)	2.2 at 25 C	7	8.5	6.3 at 25 C	8.7 at 25 C	3.4 at 25 C
Total Gate Change (Max) (nC)	53	53	77	55	**106**	**100**
QGD typ (nC)	6.7	**14**	**14**	6	**12.5**	**10.3**
Package	SON 5 × 6	Direct FET 6.3 × 5	PQFN 5 × 6	SO-8L 5.13 × 6.15	SO-8L 5.13 × 6.15	SO-8L 5.13 × 6.15
Area	30	32	30	32	32	32

For this design, a PWM switching frequency of up to 50 kHz is specified; the DRV8305-Q1 allows switching rates up to 200 kHz. However, another design consideration is that the DRV8305-Q1 is rated for a maximum average gate drive current of 30 mA. This maximum gate drive current of 30 mA sets an upper limit on the product of the PWM switching frequency multiplied by the total gate charge of the drive FETs.

As discussed in the section *Gate Drive Average Current* of the *DRV8305-Q1 Three-Phase Automotive Smart Gate Driver With Three Integrated Current Shunt Amplifiers and Voltage Regulator* datasheet (SLVSD12A), the maximum switching frequency is a function of the gate charge of the FETs selected for the drive stages.

$$f_{sw(MAX)} = \frac{I_{GD(MAX)}}{N_{FETs} \times Q_G} = \frac{30 \text{ mA}}{6 \times Q_G}$$

(2)

Figure 16 shows the maximum allowable PWM switching frequencies for each of the candidate n-channel MOSFETs. Of the three FETs with significant margin above the 50 kHz design specification, the SQJ858 is selected as having both full automotive ratings and low gate-to-drain charge (QGD), in addition to the specifications mentioned earlier.

NOTE: For similar industrial applications, which do not require a full automotive component qualification, the CSD18540Q5B has excellent electrical parameters. The CSD18540Q5B also has a pin-compatible package as the SQJ858, allowing direct replacement with no board re-layout.
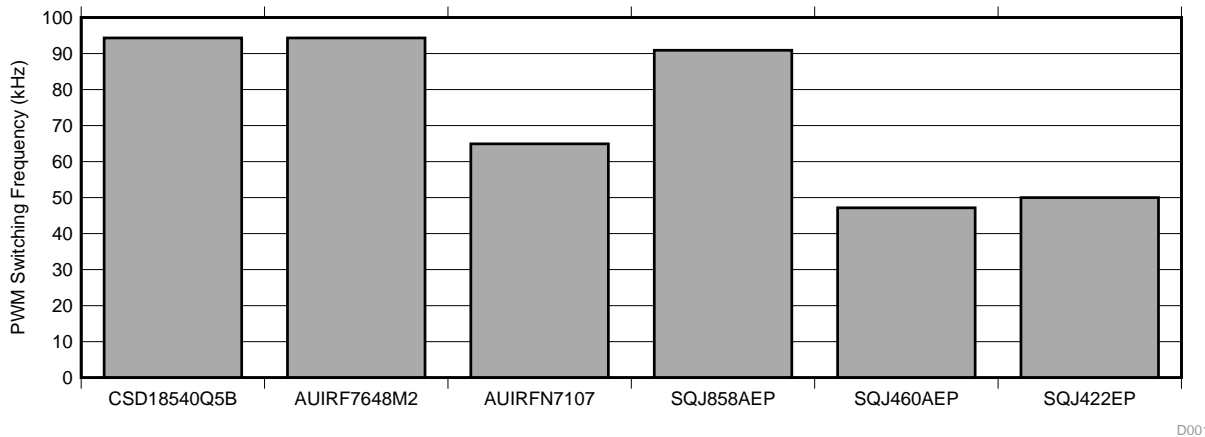
Figure 16. Maximum PWM Switching Rate for Candidate FETs

Another significant design consideration of the drive stage is the selection of the electrolytic capacitors. Selection of the electrolytic capacitors depends on meeting the requirements for high capacitance in a small size, wide temperature range, long lifetime rating, and a high value of rated ripple current. Table 4 shows the key parameters for several candidate electrolytic capacitors.

The EEE-FT1H331 capacitor was selected as having the best combination of capacitance value, size, temperature rating, ripple current, and equivalent series resistance (ESR).

NOTE: For most applications in the automotive body, the 105 °C temperature rating is sufficient, however, for application in the automotive powertrain, a higher temperature rating may be desired.

Table 4. Electrolytic Capacitor Component Trade-Off

	160 RLA	**UBC1H470**	**UBC1H101**	**EEE-FT1H101**	**EEE-FT1H331AP**	**ECA-1HM471**
Manufacturer	Vishay™	Nichicon™	Nichicon	Panasonic™	Panasonic	Panasonic
Value (µF)	100	47	100	100	330	470
Temperature	150	150	150	105	105	85
Voltage	50	50	50	50	50	50
Diameter	10	10	12.5	6.3	10	10
Height	**16**	10	13.5	7.7	10.2	**22**
Iripple (mA)	270	**100**	420	350	900	650
ESR (mΩ) at 100 kHz	260			340	120	
Endurance at Trated (Hours)	1,000	1,000	1,000	2,000	2,000	2,000

Ripple current is the AC current flowing in the capacitor due to motor switching currents. The ripple current heats the capacitor, and the maximum permitted ripple current is set by how much is permitted while still meeting the capacitor's load life specification. Too much temperature rise causes the capacitor to exceed its maximum permitted core temperature and fail quickly, however, operation close to the maximum permitted core temperature dramatically shortens expected life. The load life specifications for aluminum electrolytic capacitors operating at maximum permitted core temperature are typically 1,000 to 10,000 hours.

To keep the ripple current low, the PWM frequency should be such that the PWM period (T) is significantly shorter than the electrical time constant of the motor winding (τ = L/R).

Figure 17 shows how the motor current varies during PWM switching.
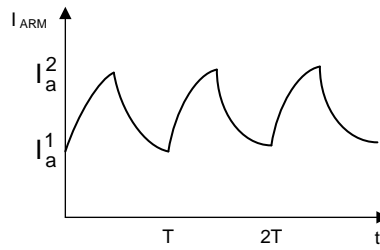
Figure 17. Motor Current Varies During PWM Switching

In a motor, the current is found for both when the controllable switch (MOSFET) is open and closed. If the switch closed current is called I_{ac} then,

$$I_{ac}\left(t\right) = I_a^1 e^{-t/\tau} + \frac{V_{IN} - E_a}{R_a}\left(1 - e^{-t/\tau}\right) \text{ in which } \tau = \frac{L_a}{R_a}$$

(3)

If the motor current when the switch, S1, is open is called Iao, then

$$I_{ao}\left(t\right) = I_a^2 e^{-(t-DT)/\tau} - \frac{E_a}{R_a}\left(1 - e^{-(t-DT)/\tau}\right) \text{ in which } \tau = \frac{L_a}{R_a}$$

(4)

The quantities of Ia2 and Ia1 may be found by recognizing that

$$I_{ac}\left(DT\right) = I_a^2 \text{ and } I_{ao}\left(T\right) = I_a^1$$

(5)

Solve the above two equations simultaneously to obtain

$$I_a^1 = -\frac{E_a}{R_a} + \frac{V_{IN}}{R_a} \times \frac{e^{-\frac{(1-D)T}{\tau}} - e^{\frac{T}{\tau}}}{1 - e^{-\frac{T}{\tau}}}$$

(6)

and

$$I_a^2 = -\frac{E_a}{R_a} + \frac{V_{IN}}{R_a} \times \frac{1 - e^{-\frac{DT}{\tau}}}{1 - e^{-\frac{T}{\tau}}}$$

(7)

The amount of ripple current is given by

$$\Delta I_a = I_a^2 - I_a^1$$

(8)

The ripple current is maximized when the duty-cycle D = 0.5 (and is zero when D = 0 or D = 1). For this 50% duty cycle condition, the worst case is when the motor is stationary (start-up or stall condition) and thus the back EMF is zero. Then the maximum ripple current is

$$\Delta I_a = \frac{V_{IN}}{R_a}\left(\frac{1}{1 - e^{-\frac{T}{\tau}}}\right)\left(1 - e^{-\frac{T}{2\tau}}\right)^2$$

(9)

For relatively short PWM periods (less than the electrical time constant of the motor), this relationship is fairly linear, as shown in Figure 18. The motor electrical time constant is typically on the order of 1 millisecond, so a typical PWM frequency of 40 kHz gives a T to τ ratio of 1 ÷ 40, or 0.025. The ripple current then is on the order of 0.6% of the motor stall current. The capacitors selected for this design have a rated ripple current of 900 mA; to keep the actual ripple current well below this value, a motor with stall current on the order of 80 A is driven with a PWM frequency of 40 kHz or more. This combination of frequency and motor stall current limits the maximum ripple current to about 500 mA.
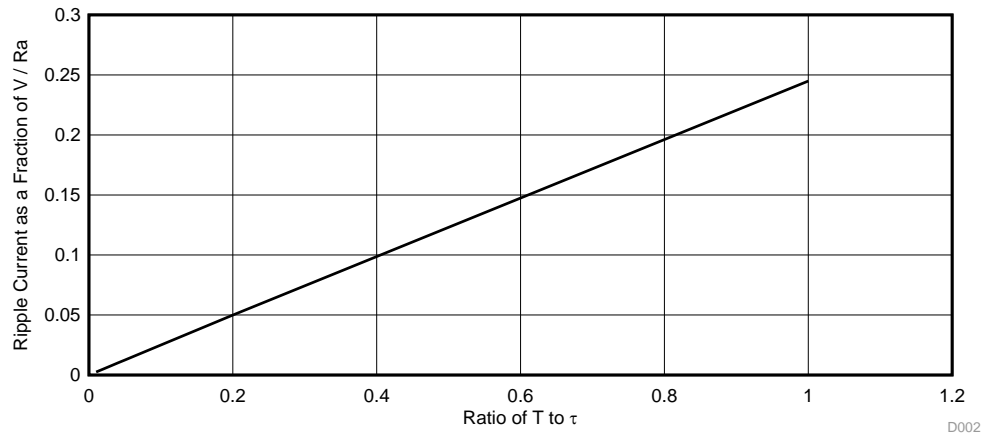
Figure 18. Normalized Plot of Ripple Current vs PWM Period

4.7   Motor Control Feedback

The algorithm for controlling the motor makes use of sampled measurements of the motor conditions, including 12-V supply voltage, the voltage on each motor phase, the current of each motor phase, and in the case of sensored communication, the position feedback from motor-mounted sensors such as Hall Effect sensors. For reliability, the temperature of the motor drive stage is also monitored.

4.7.1   Motor Current Feedback

During each PWM cycle, the current through the motor is sampled by the microcontroller as part of the motor control algorithm. The circuit shown in Figure 19 shows how the motor current is represented as a voltage signal, with filtering, amplification, and offset to the center of the ADC input range. This circuit is used for each of the three motor phases.

The low-side current through phase A flows through R3, giving a scale factor of 7 mV per amp. Differential low-pass filtering is provided by C36, with an RC time constant of 7 ps (7 mΩ × 1 nF), so this only affects very high frequencies.

The differential gain amplifier circuit (inside the dashed rectangle representing the DRV8305-Q1) has a differential gain and offset which can be selected from several settings through the SPI port. For this design, the differential setting of 10 is used, with an offset of half of the 3.3V-supply (1.65 V) provided by the DRV8305 internal voltage. After the gain provided by the op amp circuit, the motor current scale factor at the input to the ADC is 70 mV/A, with a voltage of 1.65 V representing zero motor current. Thus, with a range of 0 V to 3.3 V at the input of the ADC, motor currents of ± 23 A may be measured.

Low-pass filtering may be accomplished by selecting C28 to reduce the amplifier gain at high frequencies. However, if the filter time constant is longer than the shortest PWM pulse, the current measurement is affected.
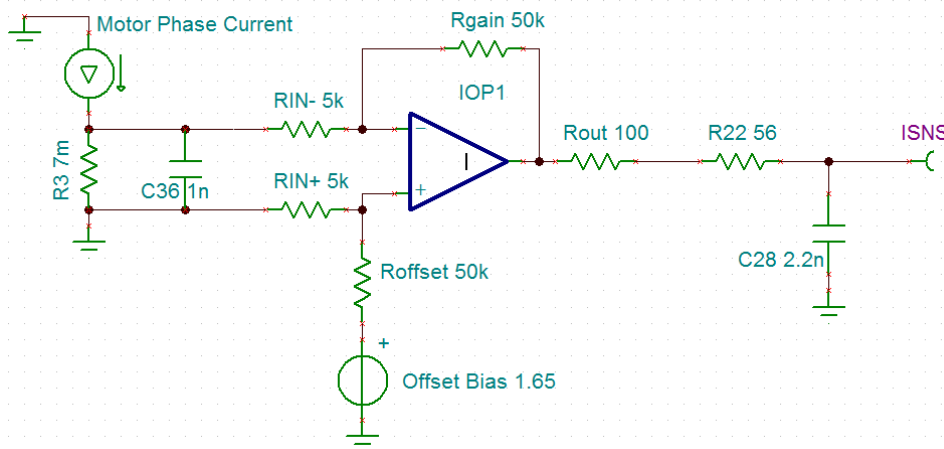
Figure 19. Motor Current Feedback Circuit

Figure 20 shows the frequency response of the motor current sense amplifier circuit as simulated in the Tina-TI circuit simulation tool. As expected, the low frequency gain is -23 dB, and the corner frequency is about 450 kHz for these values of R22 and C28.
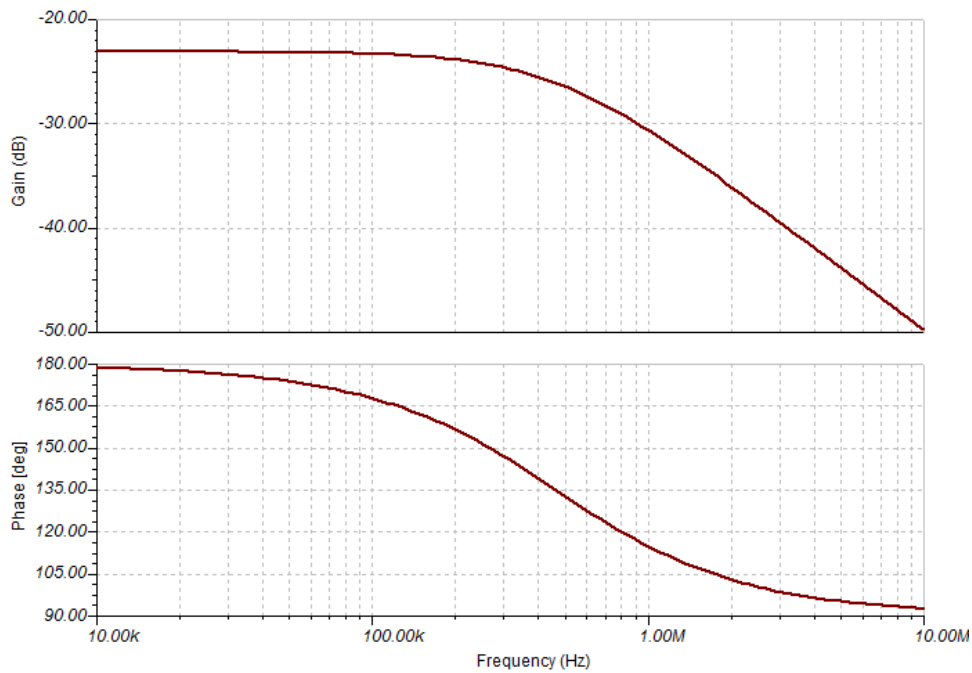
Figure 20. Simulated Frequency Response of the Current Sense Amplifier Circuit

4.7.2 Motor Voltage Feedback

The voltage of each of the three motor phases is sampled by the microcontroller as part of the motor control algorithm. The circuit shown in Figure 21 shows how the motor voltage is filtered and scaled for the ADC input range. A fourth identical circuit is used to measure the 12-V supply applied to all three of the motor phase drive circuits.
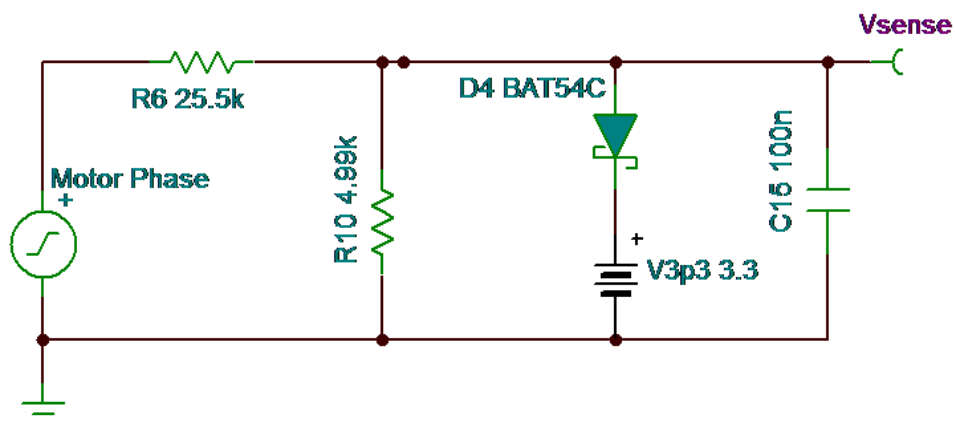
Figure 21. Motor Voltage Feedback Circuit

The resistor divider formed by R6 and R10 attenuates the motor phase voltage by a factor of 6.1:1, allowing voltages up to 20 V to be within the range of the LaunchPad ADC (0 V to 3.3 V). In case of motor voltages higher than 20 V (for example, caused by back EMF from the motor), D4 clamps the signal to slightly above the 3.3-V supply. Figure 22 shows the simulated DC transfer function of the voltage sense circuit.
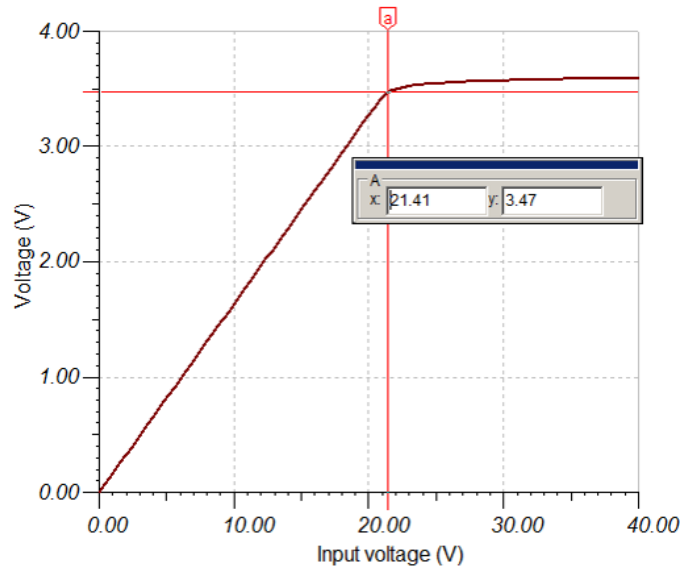
Figure 22. Simulated DC Transfer Function of The Voltage Sense Circuit

The RC time constant formed by C15 and R10 give a low-pass filter with corner frequency 318 Hz. This frequency allows all expected motor drive voltage waveforms to pass (318 Hz is 19 kRPM) while averaging the PWM switching pulses and filtering out higher frequency noise.

Software tools are available for circuit performance simulation using the TI TINA or other SPICE-based circuit analysis tools. See http://www.ti.com/tool/tina-ti for more information.Figure 23 shows a frequency transfer function analysis of the motor voltage feedback circuit. As expected, the low-frequency gain is –15.7 dB (corresponding to an attenuation of 6.1:1), and the first low-frequency corner frequency is approximately 320 Hz.
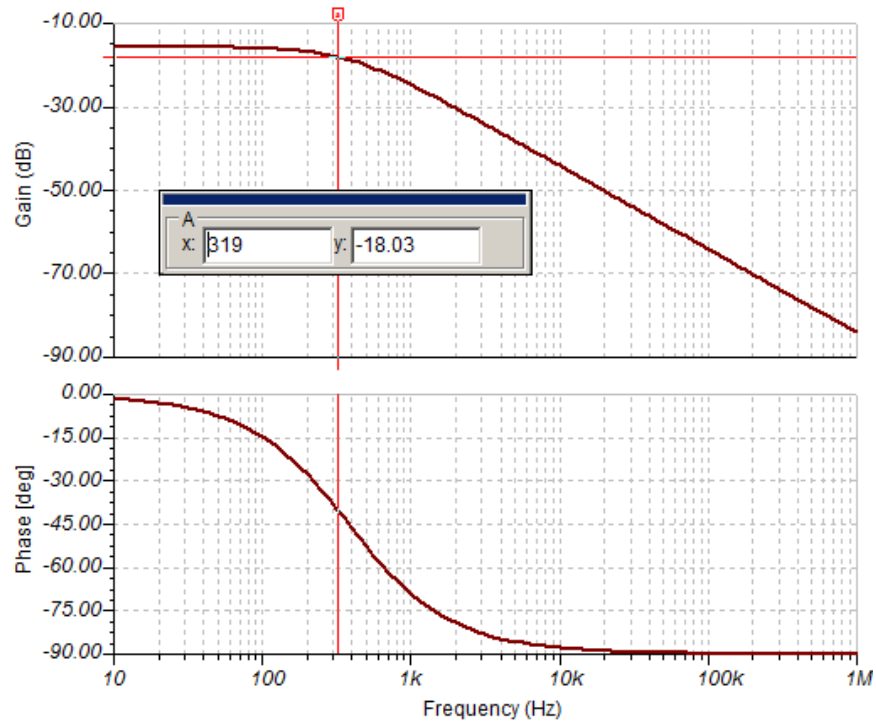
Figure 23. Simulated Frequency Transfer Results for Voltage Feedback Circuit

Selection of the clamping diodes is based on size, forward voltage drop, breakdown voltage and pad pitch. The BAT54CDW was selected as having the best combination of low forward voltage, high reverse breakdown voltage, and pad pitch easily assembled by most board shops.

Table 5 shows the clamping diode selection criteria.

Table 5. Clamping Diode Selection Criteria

	RB521ZS8A30TE61	QSG0115UDJ-7	BAT54CDW	NUP4201	1N4448
Manufacturer	Rohm™	Diodes™	Diodes	ON Semi™	Diodes
Type	Schottky	Schottky	Schottky	TVS	Fast Switching
Diodes	4	4	4	9	1
Vf at 10 mA (maximum)	370 mV	400 mV	400 mV	Not Specified	0.855
Capacitance (pF)	7 maximum	3 typical, 8 maximum	10 maximum	3 typical maximum	4 maximum
Size	1.60 × 0.80	1.05 × 1.05	2.1 × 2.0	3.00 × 2.75	1.55 × 3.7
Pad Pitch (min) mm	0.4	0.35	0.65	1.27	2.25
Breakdown Voltage	> 30 V	> 15 V	> 30 V	> 6 V	75
Maximum Temperature	150 C	150 C	125 C	125 C	150

If the maximum expected voltage on the motor signals is 40V, the current through the clamping diodes will be less than 2 mA:

$$i_{diode} = \frac{40\ V - (3.3\ V + 0.4\ V)}{25.5\ k\Omega} = 1.4\ mA$$

(10)

Therefore, power dissipation in the clamping diodes is not a concern for this level of signal.

Submit Documentation Feedback

4.7.3 Motor Drive Temperature Feedback

The temperature of the motor drive MOSFETs is sampled by the microcontroller as part of the motor diagnostic scheme. Figure 24 shows the motor drive temperature scale.
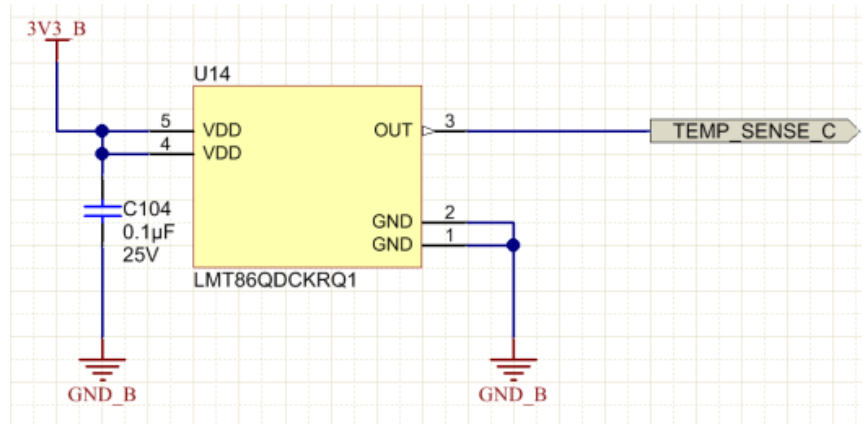
Figure 24. Motor Drive Temperature Scale

The scale factor from the LMT86 is –10.9 mV/°C with a range of –50°C to +150°C, covering an output range of 0.4 V to 2.6 V, which is within the input voltage range of the ADC. Due to the integrated features of the LMT86-Q1, very few external components are required.

4.7.4 Motor Position Feedback (Hall Effect Sensors)

Some applications may make use of Hall Effect sensors such as the DRV5013-Q1 or similar sensors to provide motor position feedback to the motor controller, facilitating simplified commutation of the 3-phase brushless motor. This design includes components to bias and buffer those signals, as shown in Figure 25.
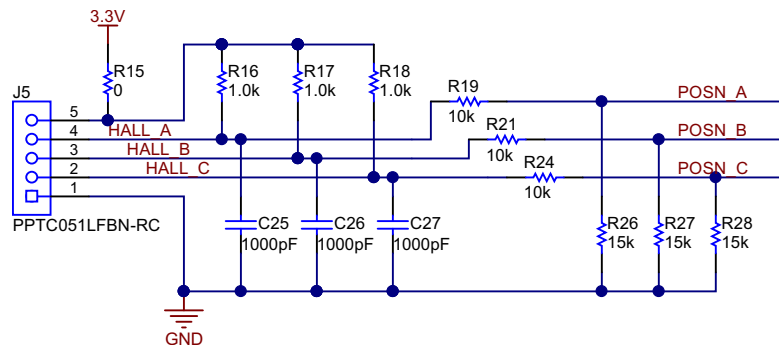
Copyright © 2016, Texas Instruments Incorporated

Figure 25. Connections to Optional External Hall Effect Sensors

The 1-kΩ resistors (R16-R18) provide pull-up to allow connection to sensors with open-collector outputs. With R15 installed, the pull-up voltage is the 3.3-V supply generated on the board. If a different pull-up voltage is needed, R15 may be removed, and the alternate voltage supplied on pin J5-5.

In all cases, the resistor values R19, R21, R24 and R26-R28 can be changed to provide any signal attenuation needed to adjust incoming Hall Effect signals with higher voltage levels to match the 3.3-V signal levels expected at the interface to the LaunchPad microcontroller board.

4.8   LaunchPad

LaunchPads are microcontroller development kits from TI. They come in a variety of types to address various needs. All LaunchPad kits include everything needed to begin developing applications in minutes.

The C2000 Piccolo™ LaunchPad evaluation kit, based on the F28027F microcontroller (MCU), is a modular, quick-launch evaluation kit that contains everything needed – device, emulation and software – to explore the latest digital control techniques in areas such as power, lighting, and motor control.

The 40 pins on the LaunchPad headers allow for easy access to all the peripherals on the F28027x device. These pins (see Figure 26) enable modularity by supporting 20-pin and 40-pin BoosterPack™ modules such as motor drive inverters, LED lighting, and much more. The TIDA-00901 board is designed with two corresponding 20-pin headers (J5 and J6) to interface with the LaunchPad pins.
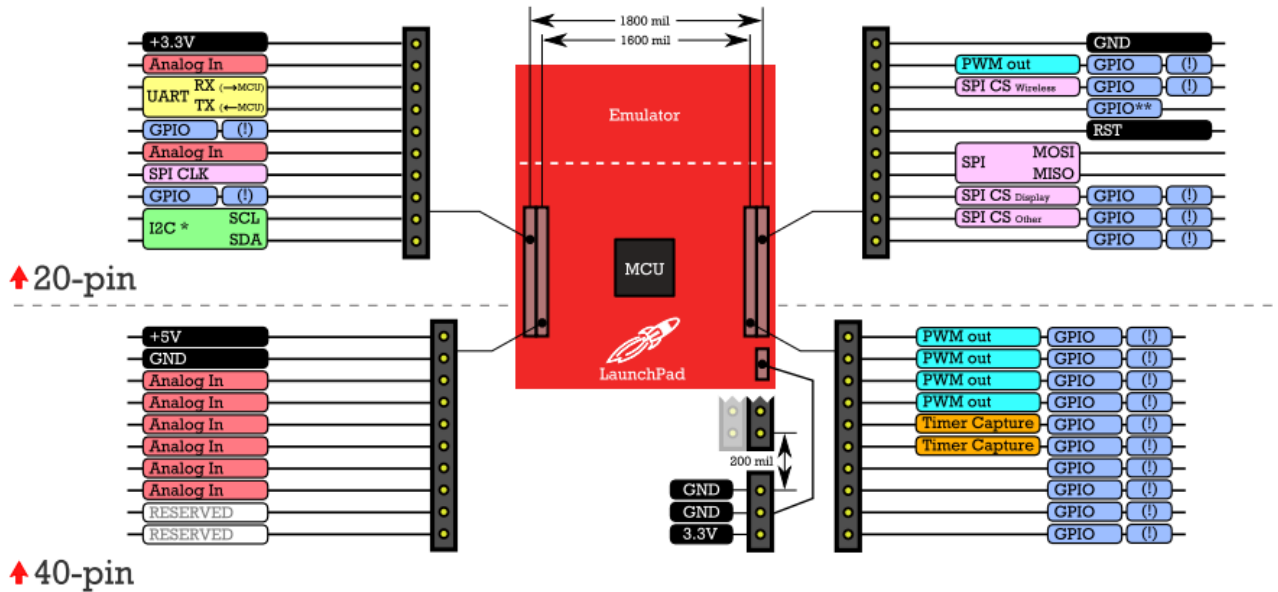
Figure 26. Connections on LaunchPad

The TIDA-00901 supplies 3.3-V power (and ground) to the LaunchPad through the standard header pins. The programing emulator and USB connection on the LaunchPad is isolated from the 3.3-V power supplied by the TIDA-00901 board (with LaunchPad jumpers JP1, JP2, and JP3 removed). For more information on the LaunchPad microcontroller development kits, see http://www.ti.com/launchpad.

Figure 27 shows the connections on the J3 and J4, both 20-pin connectors. The pin assignments are in accordance with the BoosterPack standard, allowing connection to various LaunchPad boards. All signals are referenced to the 3.3-V supply derived from the LM53600-Q1 buck regulator (U4).
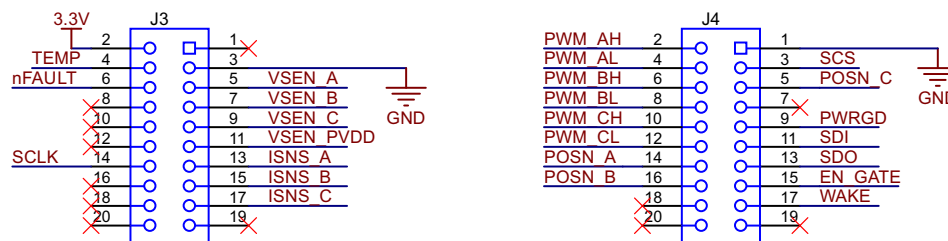
Copyright © 2016, Texas Instruments Incorporated

Figure 27. TIDA-00901 Board Connections to LaunchPad

The PWM signals are generated by the microcontroller, and connect with the DRV8305-Q1 gate driver chip. The HALL signals come from the optional motor position sensors, and connect to the microcontroller for sensored commutation. The feedback signals (voltage, current, and temperature) are scaled and filtered by RC components, to reduce high-frequency noise. These filter components can be modified if designers find specific noise frequencies which must be attenuated.

5   Getting Started Hardware

In order to fully demonstrate the TIDA-00901 design, several hardware components are required. These include:

- The TIDA-00901 motor drive board
- A LaunchPad with InstaSPIN-FOC-enabled microcontroller, such as the LAUNCHXL-F28027F
- A brushless DC motor, with or without commutation sensors (e.g. Hall Effect sensors)
- A 12-V power supply, capable of providing adequate current to power the selected motor
- A computer with the software installed to control the system

5.1   Install LaunchPad

The TIDA-00901 board is designed to accommodate connection with an F28027F LaunchPad board. The board-to-board connections are made through two 20-pin headers, in accordance with the LaunchPad/BoosterPack development environment.

Before mounting the TIDA-00901 board on the LaunchPad, verify that the switches and jumpers on the LaunchPad are set correctly.

During operation with the TIDA-00901 board, the LaunchPad is powered from the 3.3V-supply generated by the TIDA-00901 buck regulator. **Therefore, the shunts on jumpers JP1, JP2, and JP3 on the LaunchPad board must be removed.**

There are additional switches on the Launchpad which must be set correctly; S1 (boot mode selection) and S4 (serial connectivity select).

The LaunchPad's microcontroller includes a boot ROM that performs some basic start-up checks and allows for the device to boot in many different ways. S1 is provided to allow users to easily configure the pins that the bootROM checks to make this decision whether to perform an emulation boot or a boot to flash. In general, all 3 switches on S1 must be in the ON position. More information about boot mode selection can be found in the *TMS320x2802x Piccolo Boot ROM Reference Guide* (SPRUFN6).

When S4 is in the up (ON) position, the Piccolo device's SCI is connected to the XDS100 and users are able to receive and send serial information from or to the board via the USB connection. When S4 is in the down position, the Piccolo device's SCI is disconnected from the XDS100 and BoosterPacks.

> **NOTE:** Use caution when mounting the LaunchPad to the TIDA-00901 board, as misalignment of the header pins during installation may cause damage.

The TIDA-00901 board is designed to allow mounting on top of the LaunchPad board. The correct orientation of the TIDA-00901 board on the F28027F LaunchPad board is shown in Figure 28. Observe that the 3-position motor connector on the TIDA-00901 board is near the micro-USB connector on the LaunchPad board.
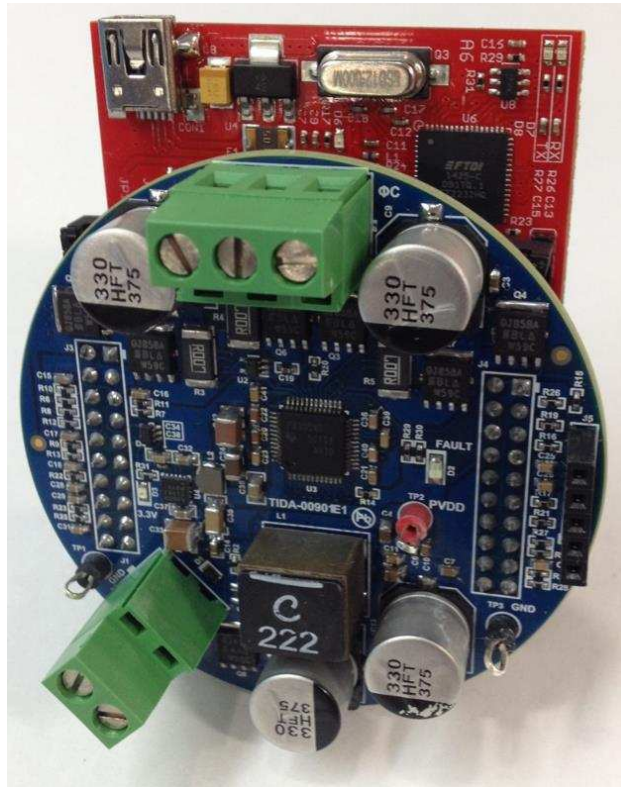
Figure 28. TIDA-00901 Board Installed on the F28027F LaunchPad

5.2 Power Connection

For operation, this design requires connection to a 12-V supply with current capability as dictated by the motor to be driven, typically in the range of several Amps. Connect leads to the 2-contact screw terminal block on the side of the TIDA-00901 board. The ground screw terminal is labeled to indicate the proper polarity of the supply connection.

5.3 Motor Connection

The motor connections consist of the drive signals to the three-phase brushless DC motor, phase A, phase B, and phase C, as well as the optional Hall Effect sensor signals, and also the bias voltage for those sensors.

5.3.1 Motor Phase Connection

The board is designed for a 3-phase brushless DC motor. The motor connections are suitable for a motor configured in either a Y or Δ configuration. The A and C phase voltages are marked next to the corresponding terminals; terminal B is in the middle.

> **NOTE:** The order of the phases is not critical, but that reversing any two phases will cause a reversal in the motor direction.

Figure 29 shows the connections to the TIDA-00901 board and LaunchPad.
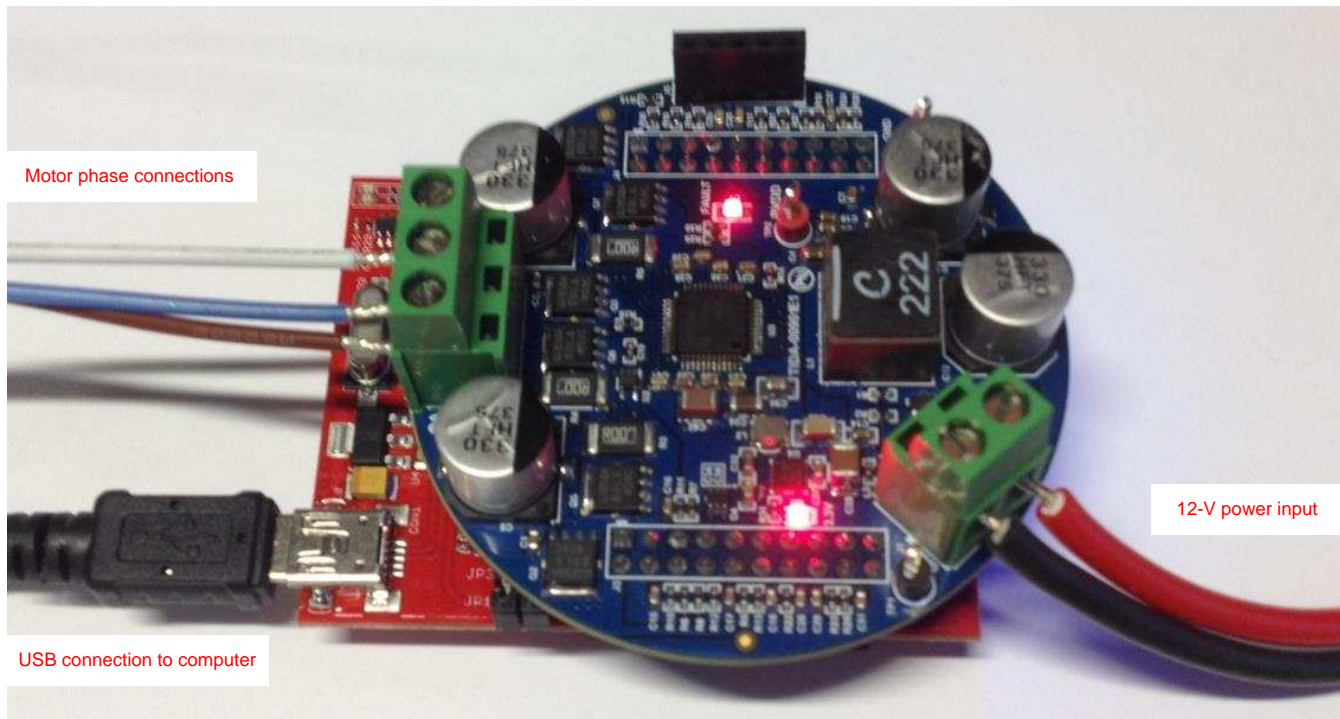
Figure 29. Board Connections

5.3.2   Motor Communication Feedback Connection

The board is designed to accept commutation feedback signals, such as Hall Effect sensors, from the motor. If these sensors are used, connect to the 5-position terminal block J5. A connection to the 3.3-V supply is included on J5, which can be used to bias the Hall effect sensors, if needed. In the case that a sensor supply other than 3.3V is used, this can be applied to pin J5-5 from an external source, provided resistor R15 is removed from the TIDA-00901 board.

6 Getting Started Software

6.1 Download and Install Code Composer Studio™

Code Composer Studio™ (CCStudio) is an integrated development environment (IDE) for Texas Instruments (TI) embedded processor families. CCStudio comprises a suite of tools used to develop and debug embedded applications. It includes compilers for each of TI's device families, source code editor, project build environment, debugger, profiler, simulators, real-time operating system and many other features. The intuitive IDE provides a single user interface taking you through each step of the application development flow. Familiar tools and interfaces allow users to get started faster than ever before and add functionality to their application thanks to sophisticated productivity tools. See the Code Composer Studio web page at http://www.ti.com/tool/ccstudio for information on downloading the integrated development environment for the C2000 code.

6.2 Download and Install MotorWare

The TIDA-00901 board may be operated using a LaunchPad microcontroller development board. In the following discussion, set-up using the C2000 LaunchPad LAUNCHXL-F28027F will be described. A link may be found in Section 9.

The TIDA-00901 board and connected LaunchPad board was tested using Texas Instruments' MotorWare software, with some additional files necessary to adapt to the specific hardware configuration of the TIDA-00901 board.

MotorWare is the software infrastructure and distribution mechanism for the InstaSPIN-FOC and InstaSPIN-MOTION motor control solutions. The software includes source code object oriented APIs for peripheral drivers and modules (including a freshly updated set of motor control functions). These APIs are used to build multiple InstaSPIN-FOC projects that demonstrate the different modes and capability, documented through the Projects and Lab User's Guide.

The MotorWare software may be downloaded from http://www.ti.com/tool/MOTORWARE . Follow the installation instructions to install on your local computer.

6.3 Run the Example Software

There are several lab projects in the MotorWare directory which can be used to exercise the TIDA-00901 board. Lab project 2b uses the InstaSPIN motor identification algorithm to determine the key motor characteristics, and then uses sensorless commutation to drive the BLDC motor.

6.3.1 Import an Existing MotorWare Lab Project

Import the existing project, for example proj_lab02b, from the MotorWare directory. In this instance, there are two projects in the directory. Depending on how MotorWare is set up, there may be several projects in the MotorWare directory to choose from.

Figure 30 shows the import existing CCS eclipse project screen.
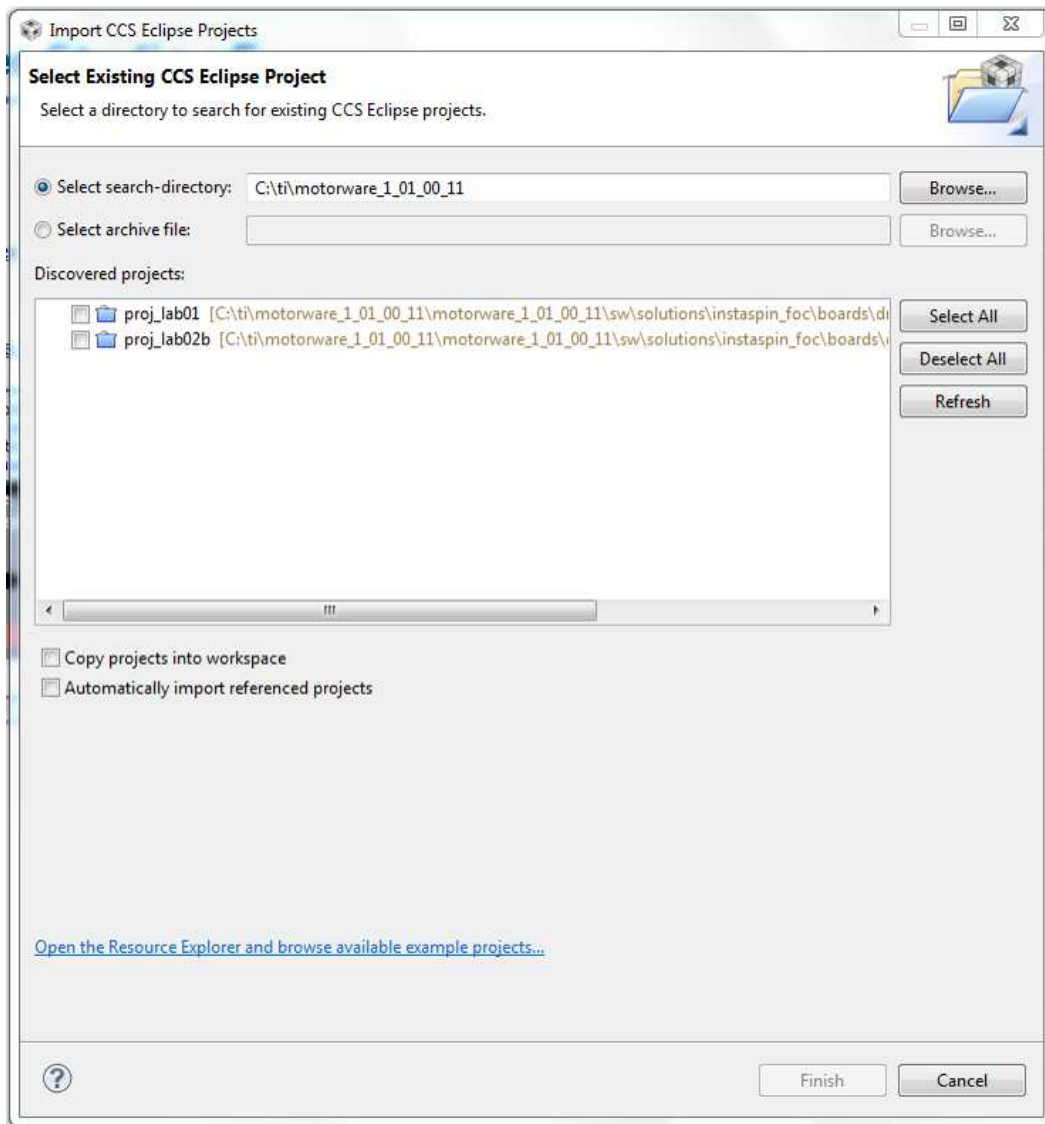
Figure 30. Import Existing CCS Eclipse Project Screen

> **NOTE:** This design works with other projects in the MotorWare libraries, but lab02b has all the features needed to exercise the design as documented in this report.

Figure 31 shows the imported project file and sub-files.
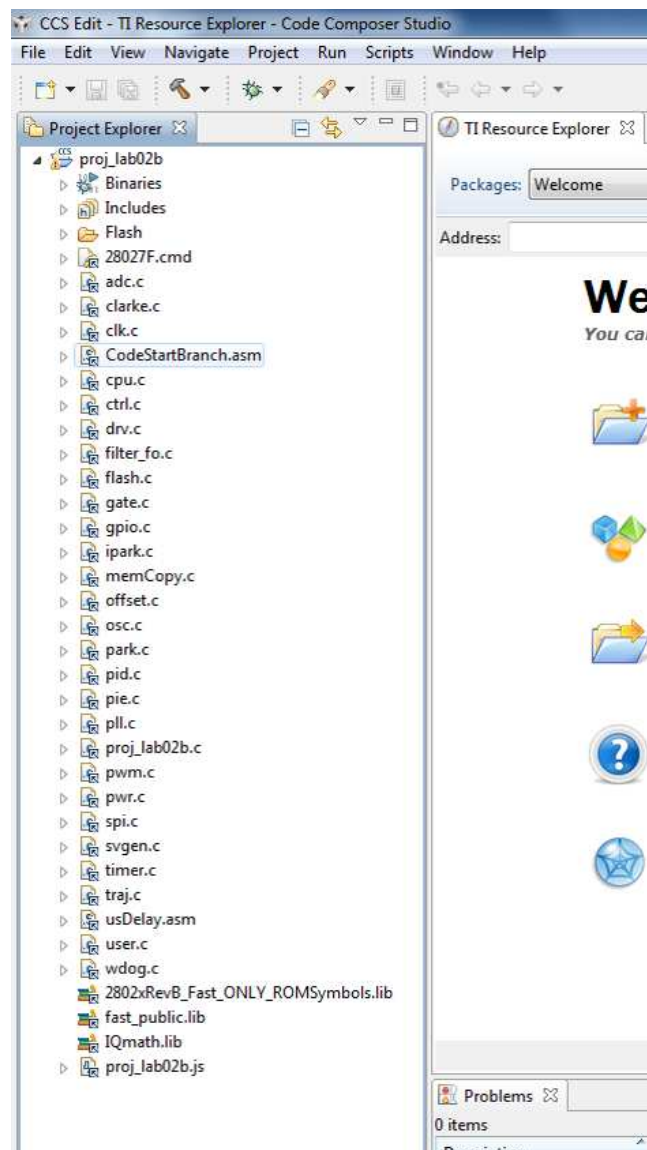
Figure 31. Imported Project File and Sub-Files

6.3.2   Set the Target Configuration

The connection will depend on the JTAG emulator in use. For the LAUNCHXL-F28027F LaunchPad:

1. Select the XDS 100 v2 emulator should be selected from the *Connection* pull-down menu.
2. The target device on this board is the TMS320F28027 piccolo microcontroller.
3. Save the configuration set-up after selecting the connection and target device.
4. Click the *Save* button.

Figure 32 shows the new target configuration screen.
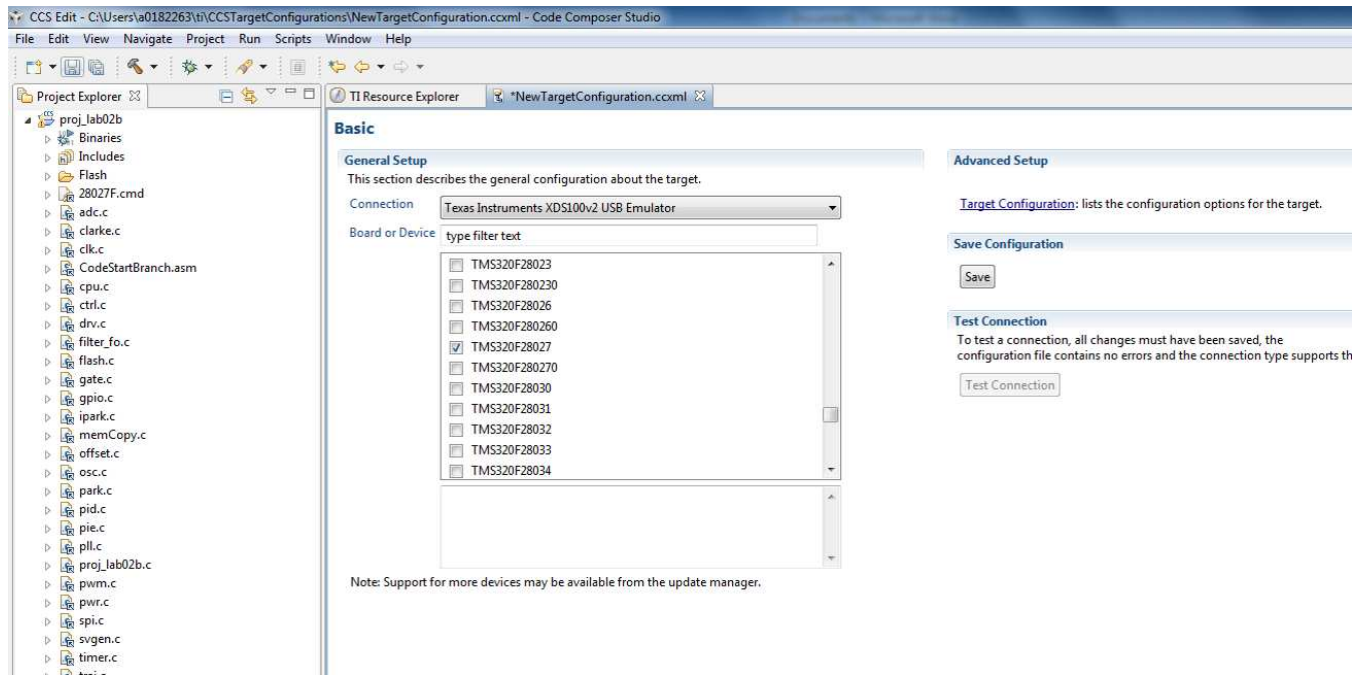
Figure 32. New Target Configuration Screen

At this point, test the connection to the target. The connection to the target board may be verified.

Figure 33 shows the test connection window after completion of a successful test.
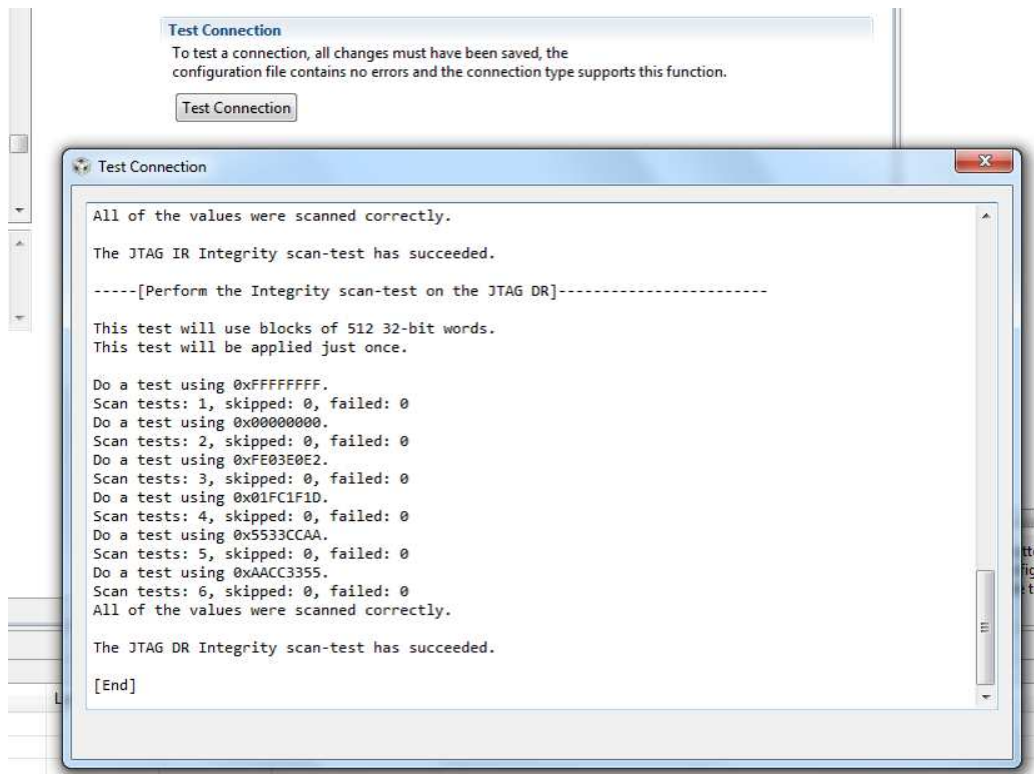
Figure 33. Test Connection Window After Completion of a Successful Test

6.3.3   Adjust the Scale Factors in the user.h File

The BOOSTXL-DRV8305EVM voltage sense circuits have a different attenuation factor than the TIDA-00901 board. Therefore, the maximum voltage setting should be modified in the user.h file (part of the MotorWare project) when using the TIDA-00901 board. Otherwise the PVDD supply voltage measurement and motor phase voltage measurements are not correct.

1. In the file user.h, starting at line 90, change the USER_ADC_FULL_SCALE_VOLTAGE_V value:

```
//! \brief Defines the maximum voltage at the input to the AD converter

//! \brief The value that will be represented by the maximum ADC input (3.3V)
                     and conversion (0FFFh)

//! \brief Hardware dependent, this should be based on the voltage sensing and
                     scaling to the ADC input #define USER_ADC_FULL_SCALE_VOLTAGE_V (20.13) //
BOOSTXL-DRV8305EVM =
                     44.30 V

 // TIDA-00901 Board = 20.13V full-scale
```

2. The default setting of 47.14 Amps full-scale which corresponds to the BOOSTXL-DRV8305EVM hardware also works with the TIDA-00901 board. This value is set in the user.h file, and further depends on the amplification setting for the current sense amplifiers (CSAs) in the DRV8305-Q1. If a different gain setting (or modified current sense circuitry) is of interest to best match a specfic application, this full-scale value can be modified as shown in the following code fragment. In the file user.h, starting at line 105,

```
//! \brief Defines the maximum current at the AD converter

//! \brief The value that will be represented by the maximum ADC input (3.3V)
                     and conversion (0FFFh)

//! \brief Hardware dependent, this should be based on the current sensing and
                     scaling to the ADC input

#define USER_ADC_FULL_SCALE_CURRENT_A (23.57) // BOOSTXL-DRV8305EVM = 47.14 A
```

6.3.4 Build the Project

To build the project:

1. Click on the project name (for example, proj_lab02b) in the *Project Explorer* window to make sure that the project is active.
2. Click the hammer icon on the CCS Edit toolbar to build the project.
3. If the project builds correctly, the message *Build Finished* is shown at the end of the text in the console window.

NOTE: In case of errors during build or execution, there may be states where the project build encounters problems due to previous build or execution. Performing a *Clean* build (select *Clean* under the *Project Menu*) rebuilds the project from a completely reset state.

Figure 34 shows the *CCS Console* window after successful build of the project.
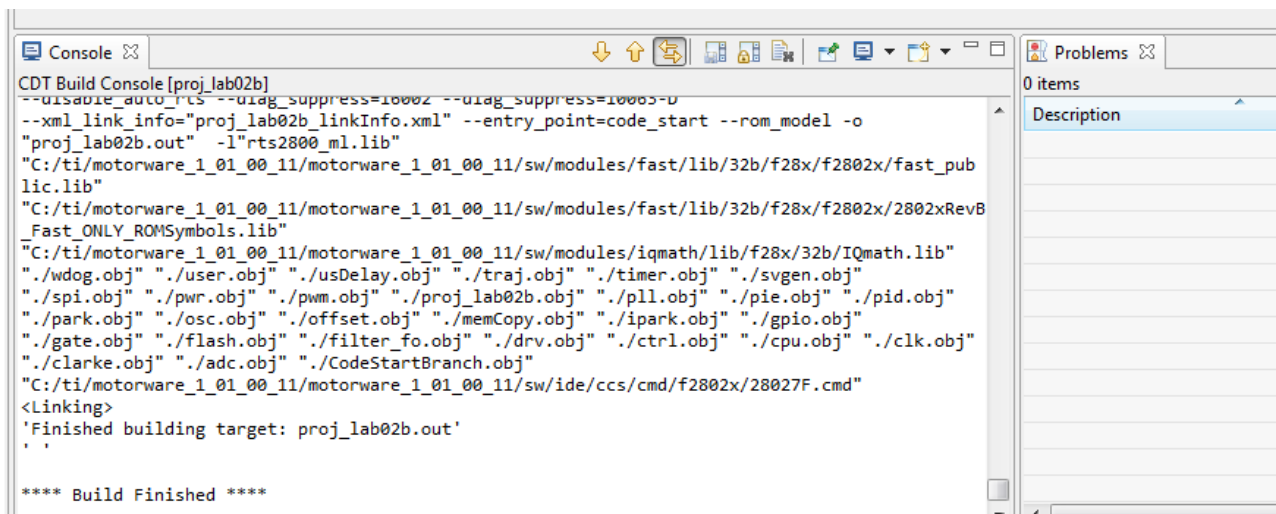
Figure 34. CCS Console Window After Successful Build of the Project
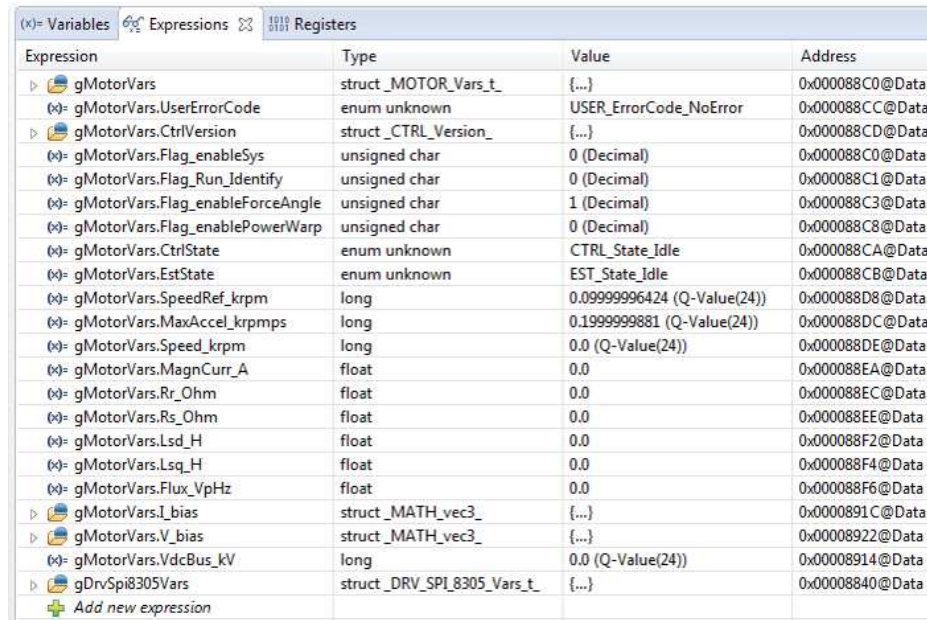
6.3.5 Start a Debug Session With the Project

Start a debug session by clicking the bug icon on the CCS Edit toolbar. The built project will be downloaded to the LaunchPad microcontroller through the USB port and JTAG emulator.

6.3.6 Run the Project

To run the project:

1. Click the green *Run/Resume* icon in the CCS debug toolbar to run the project.
2. Click the clock icon in the CCS debug toolbar to enable *Silicion Real-Time Mode*.
3. Open the Expressions tab which is populated with the motor variable expression, as shown in Figure 35.

Expression	Type	Value	Address
▷ 🖳 gMotorVars	struct _MOTOR_Vars_t_	{...}	0x000088C0@Data
(x)= gMotorVars.UserErrorCode	enum unknown	USER_ErrorCode_NoError	0x000088CC@Data
▷ 🖳 gMotorVars.CtrlVersion	struct _CTRL_Version_	{...}	0x000088CD@Data
(x)= gMotorVars.Flag_enableSys	unsigned char	0 (Decimal)	0x000088C0@Data
(x)= gMotorVars.Flag_Run_Identify	unsigned char	0 (Decimal)	0x000088C1@Data
(x)= gMotorVars.Flag_enableForceAngle	unsigned char	1 (Decimal)	0x000088C3@Data
(x)= gMotorVars.Flag_enablePowerWarp	unsigned char	0 (Decimal)	0x000088C8@Data
(x)= gMotorVars.CtrlState	enum unknown	CTRL_State_Idle	0x000088CA@Data
(x)= gMotorVars.EstState	enum unknown	EST_State_Idle	0x000088CB@Data
(x)= gMotorVars.SpeedRef_krpm	long	0.09999996424 (Q-Value(24))	0x000088D8@Data
(x)= gMotorVars.MaxAccel_krpmps	long	0.1999999881 (Q-Value(24))	0x000088DC@Data
(x)= gMotorVars.Speed_krpm	long	0.0 (Q-Value(24))	0x000088DE@Data
(x)= gMotorVars.MagnCurr_A	float	0.0	0x000088EA@Data
(x)= gMotorVars.Rr_Ohm	float	0.0	0x000088EC@Data
(x)= gMotorVars.Rs_Ohm	float	0.0	0x000088EE@Data
(x)= gMotorVars.Lsd_H	float	0.0	0x000088F2@Data
(x)= gMotorVars.Lsq_H	float	0.0	0x000088F4@Data
(x)= gMotorVars.Flux_VpHz	float	0.0	0x000088F6@Data
▷ 🖳 gMotorVars.I_bias	struct _MATH_vec3_	{...}	0x0000891C@Data
▷ 🖳 gMotorVars.V_bias	struct _MATH_vec3_	{...}	0x00008922@Data
(x)= gMotorVars.VdcBus_kV	long	0.0 (Q-Value(24))	0x00008914@Data
▷ 🖳 gDrvSpi8305Vars	struct _DRV_SPI_8305_Vars_t_	{...}	0x00008840@Data
➕ Add new expression			

Figure 35. Expressions Window in the Debug View of CCS, Program Running, Drive Not Enabled

6.3.7 Enable the System

To enable the system:

1. Click the value field and enter a 1 to set the *Flag_enableSys* to 1.
2. At this point the operation of the system may be verified. Observe that the 12-V supply voltage is correctly monitored.
3. If required, right-click inside the value field.
4. Select the Q values and 24 to change the expression VdcBus_kV to Q-Value(24).
5. Verify that the value for VdcBus_kV corresponds to the DC supply voltage.

Figure 36 shows that the supply voltage is 12.17 V.

If the VdcBus_kV value does not correspond to the input voltage on VBATT, check that the voltage gain in User.h is correctly set, as discussed in Section 6.3.3.

Figure 36. Expressions Window in the Debug View of CCS, Program Running, and Drive Enabled

6.3.8   Identify the Motor Parameters

Click inside the value field and enter 1 to set the *Flag_Run_Identify* to 1. The motor is driven with small and large motions, drawing up to several Amps. During the identification procedure, the motor stator winding resistance *Rs_Ohm* variable is estimated, as well as the winding inductance *Lsd_H* and *Lsq_H*, and the flux *Flux_VpHz*. The estimated values for each are updated in the Expressions window, highlighted in yellow after each update.

shows the motor winding resistance is 84-mΩ, and the winding inductance is 0.64 mH.

Figure 37. Expressions Window in the Debug View of CCS, During Motor Identification

6.3.9 Operate in Speed Control Mode
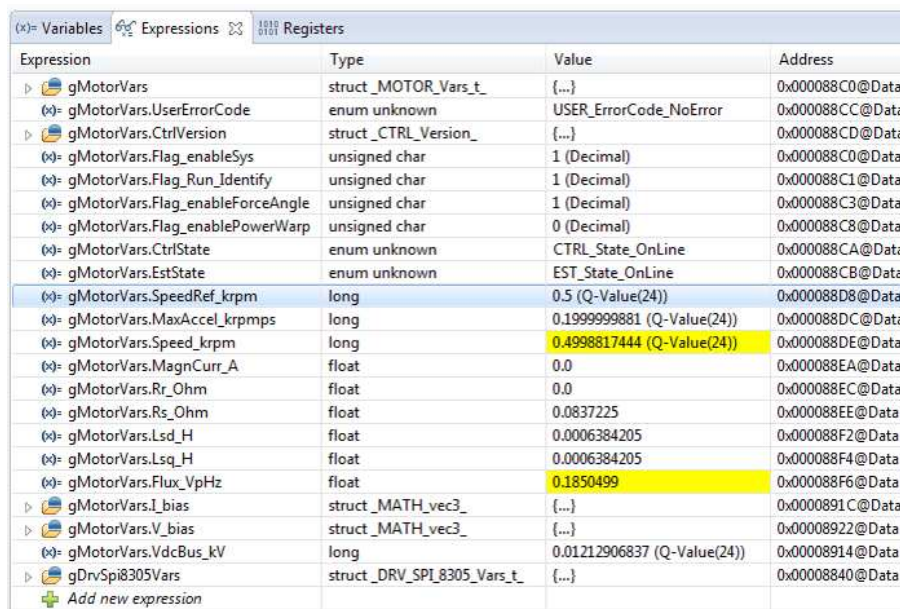
When the motor has been successfully identified, the *Flag_Run_Identify* is reset to 0.

At that point:

1. Again, click inside the value field and enter 1 to set the *Flag_Run_Identify* to 1.

   This allows the system to operate with the motor parameters already determined. After a moment, the motor begins to spin at the speed set by the *SpeedRef_krpm* parameter value.

2. Click inside the value field of *SpeedRef_krpf* and enter a new value (in kRPM) to change the command speed.

3. Click inside the value field of *MaxAccel_krpmps* and enter a new value (in kRPM per second) to change the acceleration.

NOTE: The speed reference may be either positive or negative, affecting whether the motor rotating is clockwise or counterclockwise.

Figure 38 shows the expressions window, motor speed 500 RPM (left) and –400 RPM (right).

Figure 38. Expressions Window, Motor Speed 500 RPM (left) and –400 RPM (right)

6.3.10 Operate With InstaSPIN Universal GUI to Adjust DRV8305-Q1 Parameters

To have easy access to the DRV8305-Q1 motor drive parameters, the board may also be operated using the InstaSPIN_F28027F_UNIVERSAL graphical user interface (GUI). For information about this GUI, see http://www.ti.com/tool/INSTASPINUNIVERSALGUI.

The InstaSPIN Universal GUI allows you to instrument bound variables for each compiled MotorWare project (.out) on the Piccolo MCU. Use CCStudio to compile a MotorWare project into a .out that may be loaded onto the Piccolo MCU. Select the MotorWare project that meets your application requirements. See the InstaSPIN-FOC™ and Insta-SPIN-MOTION™ User's Guide (SPRUHJ1) for a list of available projects. The user.h file specifies the settings for your motor. Make sure that the appropriate settings are selected in the user.h, and that the file is saved before building the project as mentioned in Section 6.3.3.

To install:

1. Rename the compiled MotorWare project (the binary, for example proj_lab2b.out, as shown in Figure 39) to *appProgram.out*.

---

2. Copy the file to the appropriate webapp folder, in this case InstaSPIN_F2802xF_UNIVERSAL, typically under C:\ti\guicomposer\webapps (depending on how MotorWare was installed).

Name	Date modified	Type	Size	Folder
proj_lab02b.out	3/10/2016 4:13 PM	OUT File	394 KB	Flash (C:\TI\motorware\motorware_1_01_00_16\sw\solutions\instaspin_foc\boards\boostxldrv8305_revA\f28x\f2802xF\projects\ccs5\proj_lab02b)

Search again in:
Libraries Computer Custom... Internet File Contents
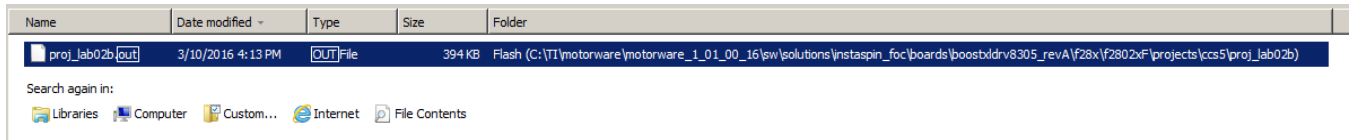
Figure 39. Directory Path for .out File for Lab_2b

3. Run the executable from the webapp folder: InstaSPIN_UNIVERSAL.exe or by starting the MotorWare application

4. Select *Run Universal GUI* under the Piccolo F28027F >> GUI directory, as shown in Figure 40.
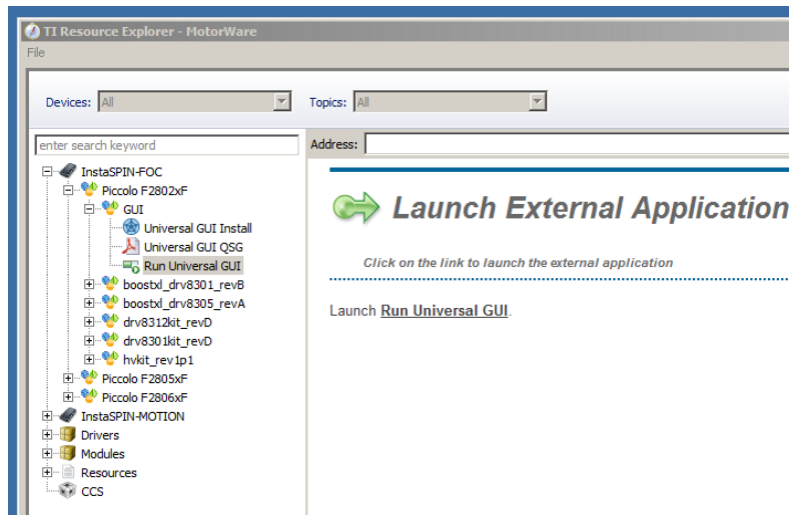
Figure 40. Universal GUI Application Entry Point

During the GUI launch, the USB link to the LaunchPad emulator is initialized and connected, the associated firmware is flashed into the LaunchPad, and the C2000 program is executed. Figure 41 shows the configuration tab of a successful GUI launch.
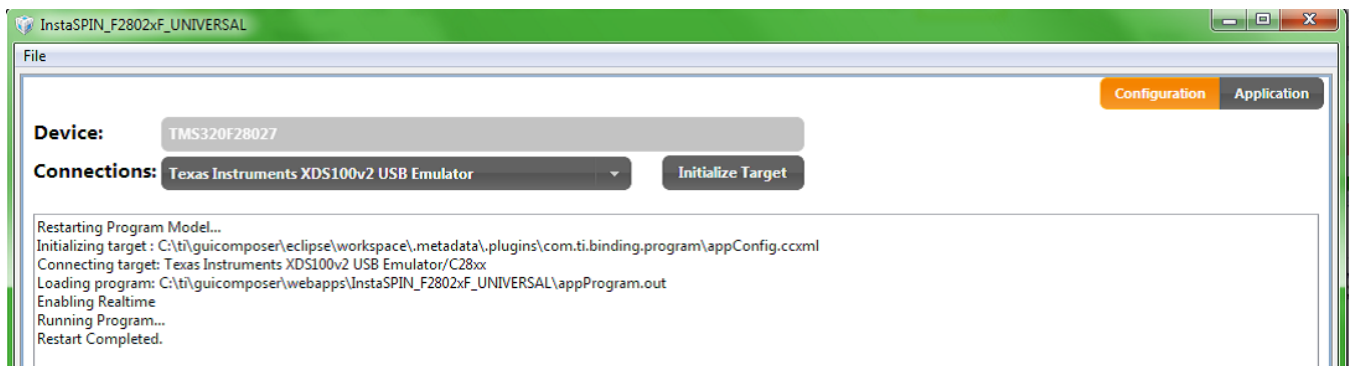
Figure 41. Configuration Tab of a Successful GUI Launch

When the GUI is running, a screen with several tabs is available for controlling both the motor operation and the control parameters resident in the DRV8305-Q1 registers. Figure 42 shows the Field-Oriented Control tab which has options for setting the state of the motor drive, and for entering speed control targets.

5. Click the *Enable System* button to command operation of the motor.

6. Click the *Run* button.

The system uses InstaSPIN to identify the motor parameters.

Copyright © 2016, Texas Instruments Incorporated

7. Turn off the *Run* button when the motor is identified.

8. Click the *Run* button again to operate the motor drive.

Motor speed may be set in the Speed_Ref_RPM parameter window.

Figure 42 shows the field-oriented control (FOC) tab of the graphical user interface (GUI).
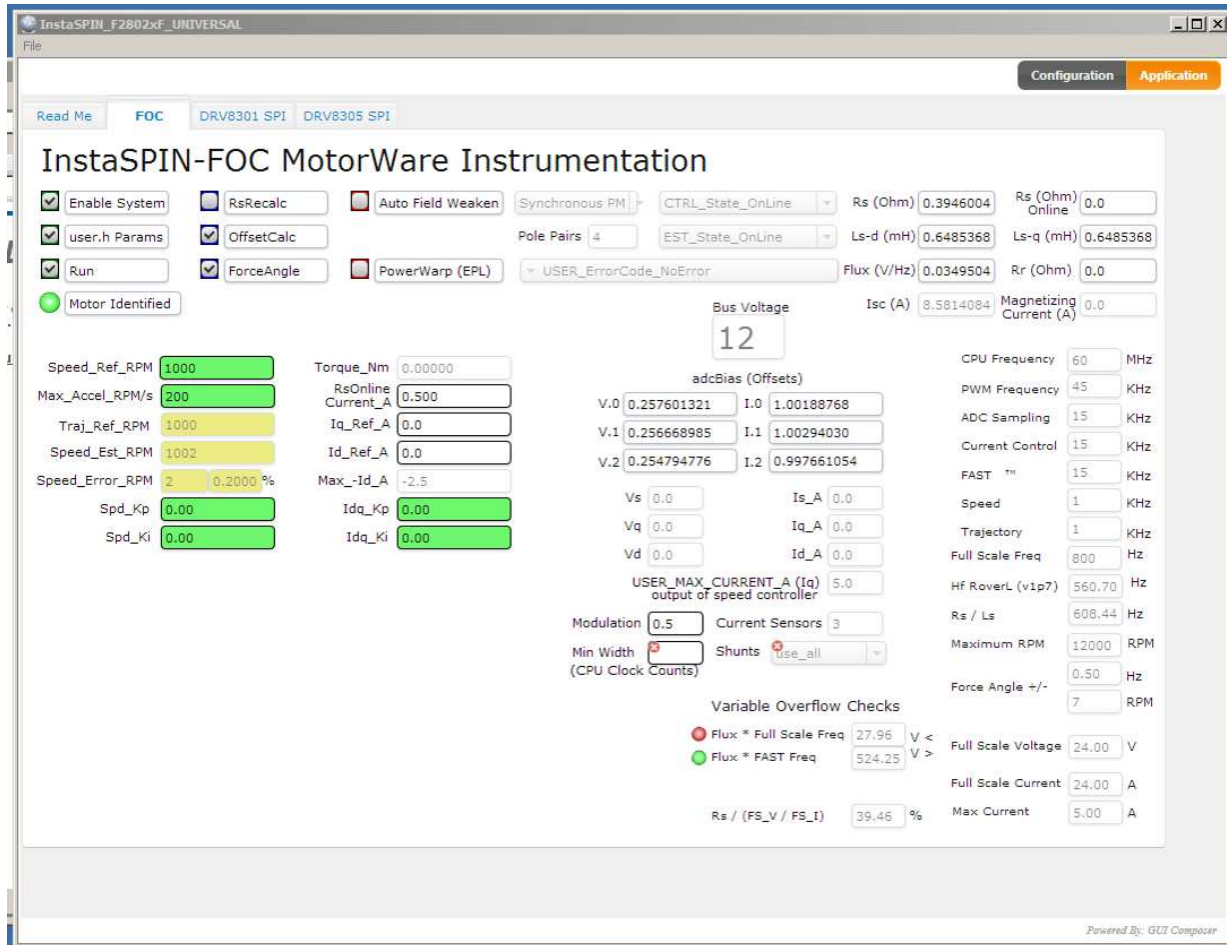
Figure 42. Field-Oriented Control of the Graphical User Interface (GUI)

Figure 43 shows the DRV8305 SPI tab in the GUI application. In this tab, the various parameters of the DRV8305-Q1 may be adjusted to investigate their affect on motor performance. Only those parameters that have been referenced in the lab project which was copied to the GUI directory is available for adjustment.

NOTE: Not all of the parameters are enabled by each of the MotorWare lab projects.

Only those parameters that have been referenced in the lab project which was copied to the GUI directory are available for adjustment.

See http://www.ti.com/tool/motorware for the MotorWare lab projects, the InstaSPIN Graphical User Interface, and the DRV8305-Q1 for more information on the details of operation of these tools.
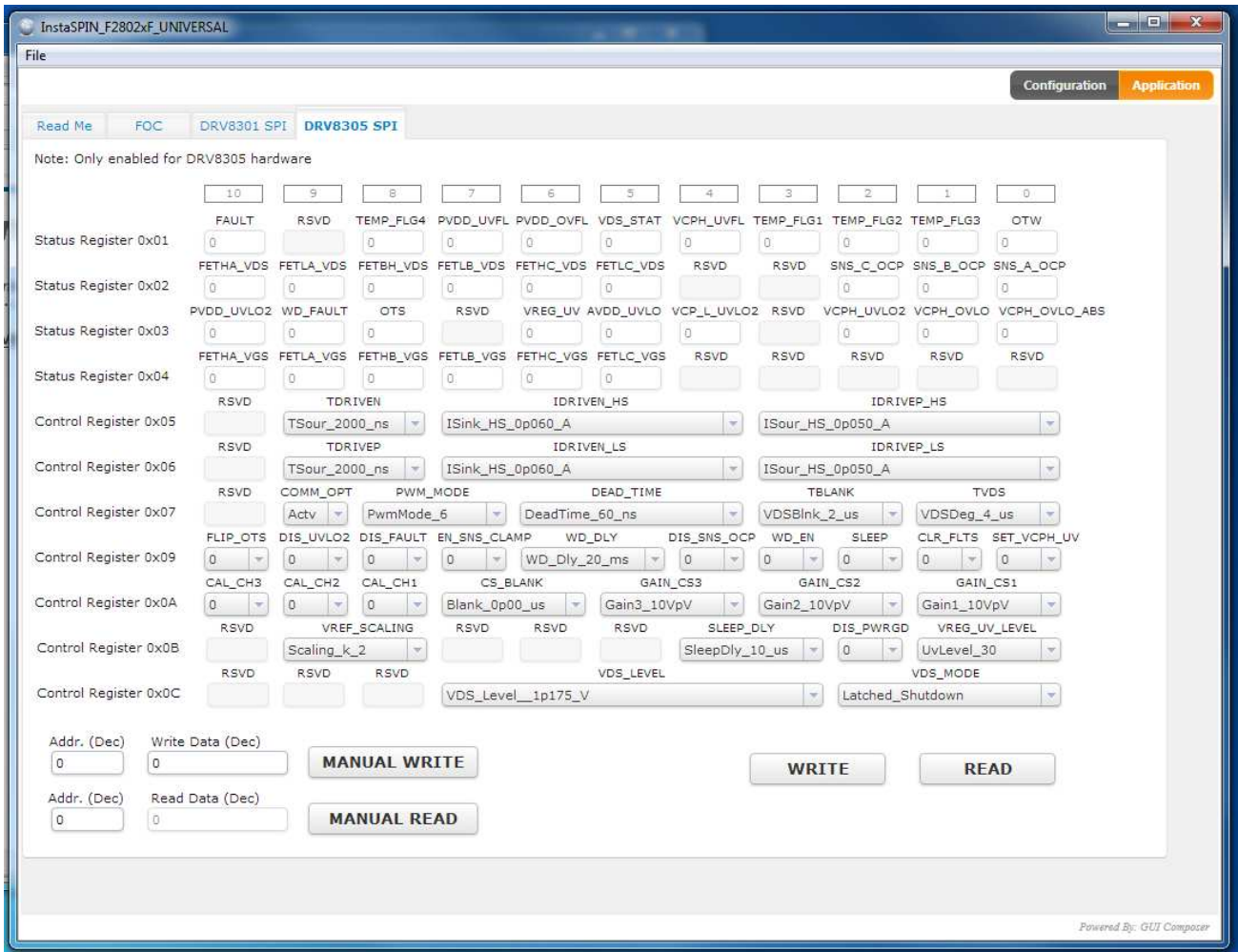
Figure 43. DRV8305 SPI Tab in the GUI

7   Testing

The following sections show the test data which characterize the design. These results indicate typical performance with equipment similar to that expected in the intended applications.

7.1   *Power Supplies*

7.1.1   12-V Supply Current

Table 6 lists the supply current under various conditions with a 12-V (nominal supply). A motor was not connected to the board for these measurements.

Table 6. Supply Current Under Various Operating Conditions

CONDITION	CURRENT (mA)
No load (no LaunchPad)	8
With LaunchPad Installed (C2000 idle)	33
With LaunchPad Installed (C2000 running, DRV8305 disabled)	66
With LaunchPad installed (C2000 running, DRV8305 enabled)	68

7.1.2   12-V Supply Range of Operation

The design is intended for operation with a range of voltage on the 12-V automotive battery supply. Figure 44 shows the measured output of the 3.3-V supply for a positive range of input voltage on J1 with no LaunchPad installed. The curve indicates operation beginning at about 5 V, where the 3.3-V regulator circuit begins to operate.
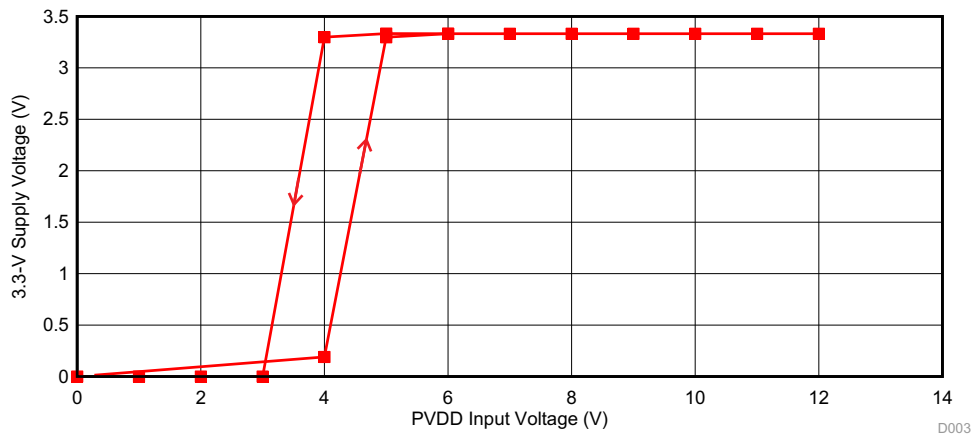
Figure 44. 3.3-V Regulator Output Voltage vs Positive Input Voltage on PVDD

The reverse-battery performance is shown in Figure 45. Observe that the reverse current is primarily due to the path through R2 through the base-emitter junction of Q1 and D1 (refer to Figure 9). The collector of Q1 pulls the gate of Q8 below the threshold point, keeping Q8 in the off state.
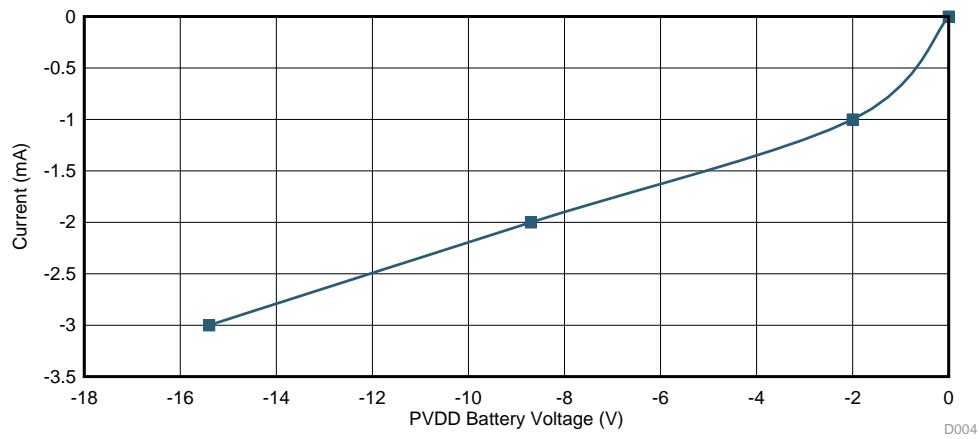
Figure 45. Input Current vs Negative Input Voltage on PVDD

7.1.3   3.3-V Buck Turn-On Transitions

Although not a key parameter for most applications, the turn-on time after application of battery power is of interest. The plots in Figure 46 and Figure 47 show that the 3.3-V buck supply is regulating at 3.3 V within 4 ms of the battery voltage being applied.
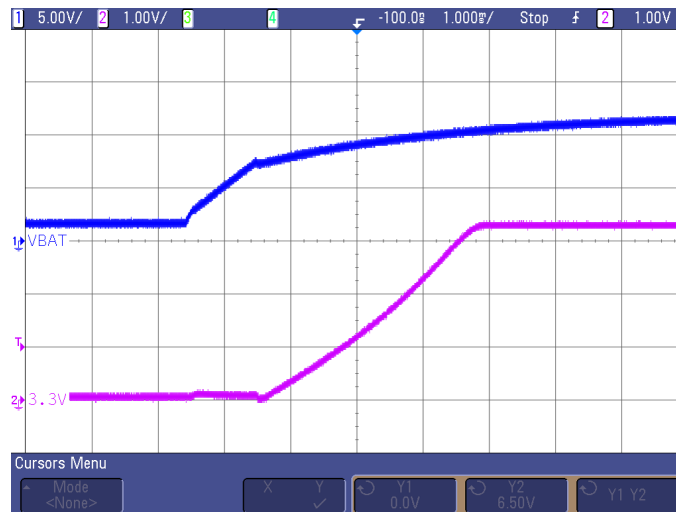
Figure 46. 3.3-V Buck Supply Turn-On During VBAT Supply Transition to 12 V
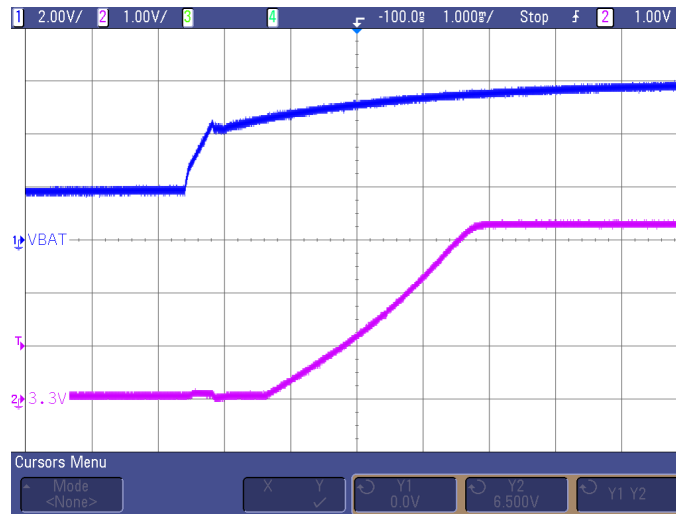
Figure 47. 3.3-V Buck Supply Turn-On during VBAT Supply Transition to 6 V

7.1.4   3.3-V Buck Load Regulation

The 3.3-V regulator is designed to supply current to the on-board temperature sensor, Hall Effect interface, and LED indicators, as well as the off-board microcontroller. The regulator is designed to supply up to 350 mA of current to the off-board controller; this is more than sufficient for a typical device such as the C2000 real-time microcontroller, as implemented on the C28027F LaunchPad.

Figure 48 shows the regulation of the 3.3-V supply with various external loading conditions. With no external load, the supply is about 30 mV above 3.3 V, or about 1% above the design set-point. With a load of 400 mA, the supply is about 75 mV below 3.3 V, or about 2.4% below the design set-point.
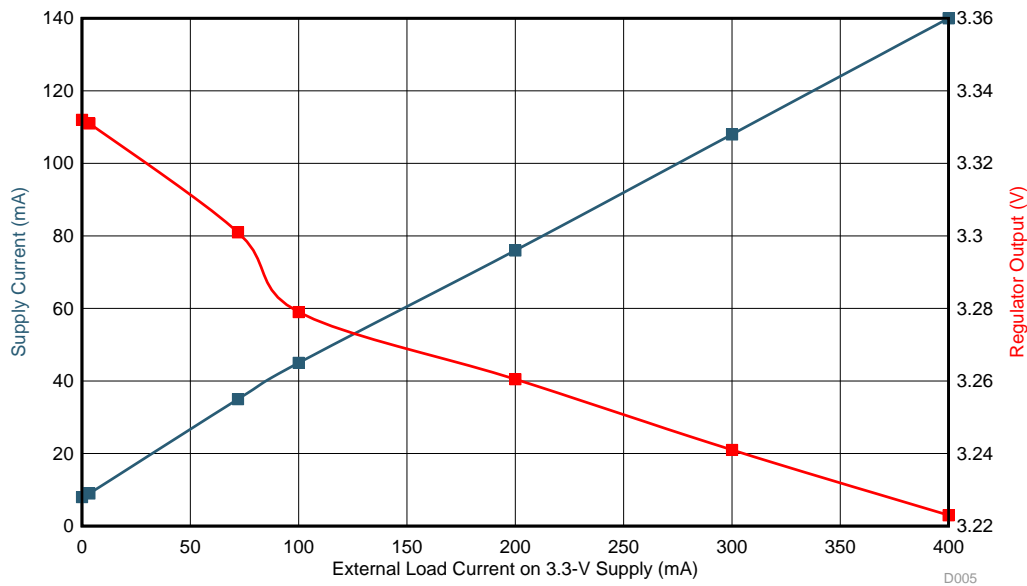
Figure 48. 3.3-V Supply Load Regulation

7.1.5   3.3-V Buck Efficiency

The efficiency of the 3.3-V regulator is determined by measuring the power delivered to an external load on the 3.3-V supply and the 12-V power supplied to the board. Based on the incremental power supplied to the external load, and the incremental power supplied by the 12-V supply, the overall 3.3-V regulator efficiency is measured as approximately 81%.

Table 7 lists the efficiency measurements for the 3.3-V regulator.

Table 7. Efficiency Measurements for the 3.3-V Regulator

EXTERNAL LOAD (mA)	12-V SUPPLY (mA)	REGULATOR OUTPUT	INPUT POWER	OUTPUT POWER	3.3-V POWER EFFICIENCY
0	8	3.332	96	0	
3.4	9	3.331	108	11.3254	94%
72	35	3.301	420	237.672	73%
100	45	3.279	540	327.9	75%
200	76	3.2605	912	652.1	87%
300	108	3.241	1,296	972.3	83%
400	140	3.223	1,680	1,289.2	83%
OVERALL:					81%

7.1.6   Input Power Filtering

The plots shown in Figure 49 and Figure 50 were taken with the ElectroCraft motor rotating at 100 RPM, with another motor connected as a braking generator load and 3 parallel 33-Ω resistors on each phase, loading the generator. The left plot is measured at PVDD test point. The right plot is measured at the J1-2 power input for VBAT, showing the effect of the filtering, which has attenuated the maximum peak by 27 dB, or an attenuation factor of 23.
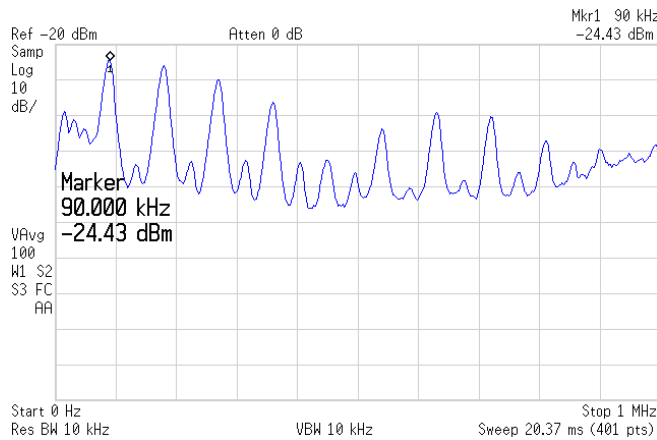
Figure 49. Without Input Power Filter, Showing Attenuation of PWM Harmonics
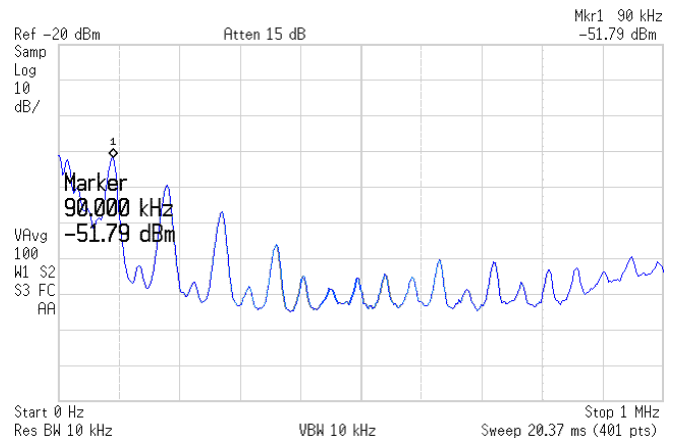
Figure 50. With Input Power Filter, Showing Attenuation of PWM Harmonics

Figure 51 and Figure 52 show the filter attenuation on the LM53600-Q1 buck regulator switching frequency. The filter on the input power reduces the conducted voltage at 2.06 MHz by 13.5 dB, or an attenuation factor of 4.7.
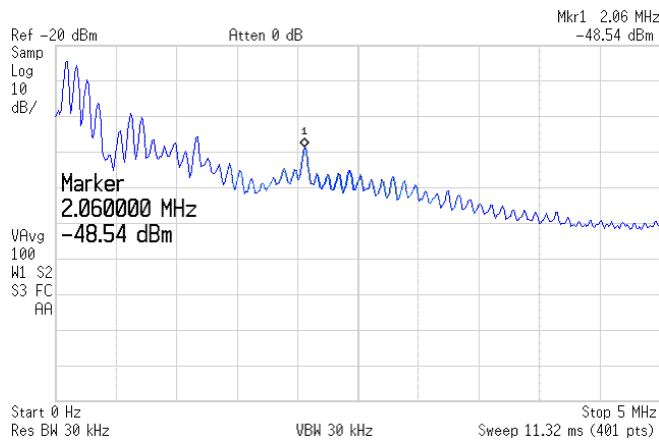
Figure 51. Without Input Power Filter, Showing Attenuation of Buck Regulator Switching Frequency
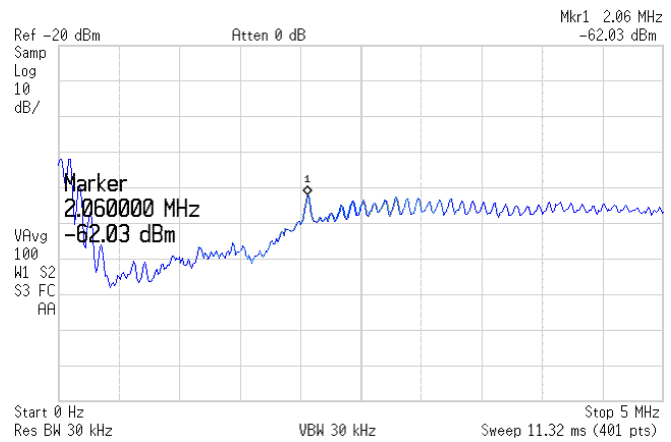
Figure 52. With Input Power Filter, Showing Attenuation of Buck Regulator Switching Frequency

7.1.7 Input Voltage Monitoring

One of the functions of the DRV8305-Q1 is to monitor the filtered input voltage (PVDD) and indicate when it is not within the intended range of operation. As the input voltage declines, three levels of indication are available. If the voltage drops below 7.7V, an undervoltage warning is activated, the nFAULT signal begins to toggle, illuminating the red FAULT LED (D2). A register bit is also set in the DRV8305-Q1, which may be read through the SPI port. This function is shown in Figure 53 where the nFAULT signal begins to toggle when the input supply voltage drops from 8 V to 7 V.
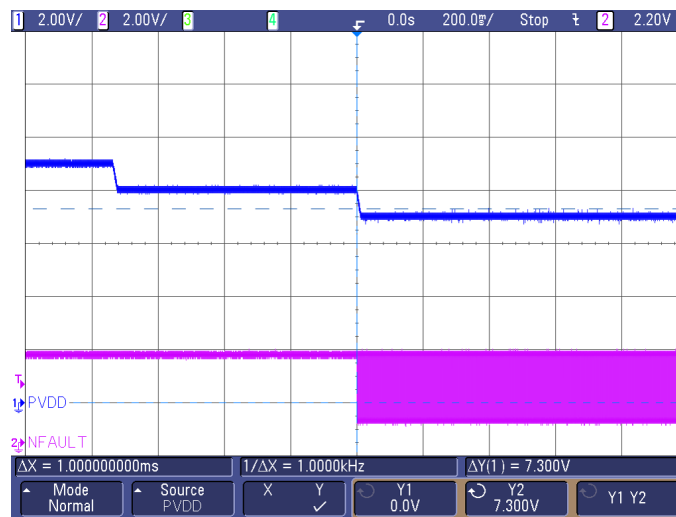
Figure 53. nFAULT Signal Begins to Toggle When VBATT Falls Below 7.7 V

7.2 Motor Operation

7.2.1 Motor Drive Signals

The overall motor drive function of the TIDA-00901 board is shown in Figure 54. Here, the six PWM commands from the C2000 LaunchPad, which are the input signals to the TIDA-00901 board, are shown in light blue at the bottom of the oscilloscope plots. Note that each of the three pairs of signals is comprised of complementary commands for the high-side and low-side gate drivers of each motor phase. (As discussed later, the dead-time between complementary transitions can be set to a minimum, as the DRV8305-Q1 has integrated programmable dead-time control.) The three motor phase voltages are shown in color; these are the main outputs from the TIDA-00901 board. Note that the high and low segments of each motor phase are roughly aligned with the corresponding PWM input commands. The time shift between command and phase voltage is due to the charge-up time and transition slew rate of the drive FETs, as well as the dead-time inserted between complementary transitions. The DRV8305-Q1 allows users to adjust the motor drive parameters in terms of both time shift and slew rate by programming the internal registers through SPI transactions.
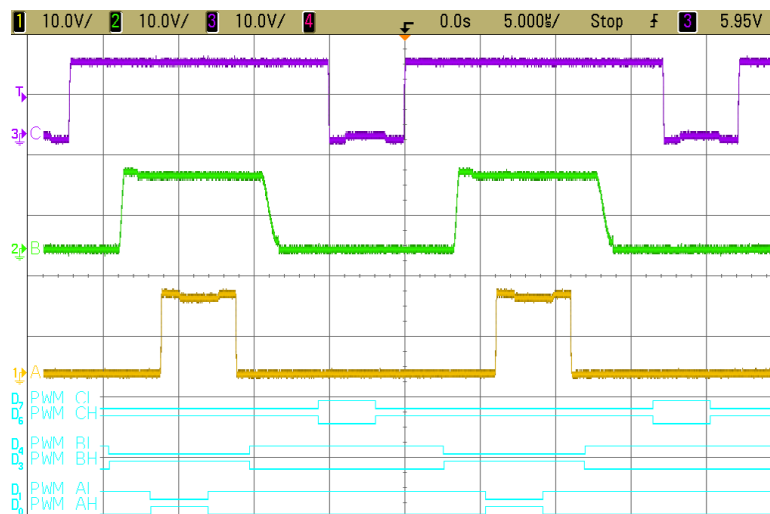
Figure 54. Inputs and Outputs During Normal Operation, 12-V Supply, 45 kHz PWM Frequency, No-Load Motor

7.2.2 Motor Operation Test Setup

This design was tested with various 3-phase BLDC motors. Brief specifications for these are listed in the appendix. To provide a known load for the motor, a dynamometer was coupled to the motor shaft. Figure 55 shows one such motor coupled to the dynamometer, with the boards being tested driving the motor.

Several items must be noted related to dynamometer testing:

• The motor may be rotating at high speeds, and may have sufficient torque to cause damage or injury. Care must be taken to keep clothing, tools, and more away from the rotating shaft during testing.

• Alignment of the motor shaft to the dynamometer shaft is important for safe operation and for accurate measurement of the motor performance. Misalignment may lead to damage of the coupling or incorrect torque readings.

• Rapid changes of the motor speed may lead to overvoltage generated by the motor. Be aware that the generated voltage may exceed the voltage set-point of the 12-V supply.
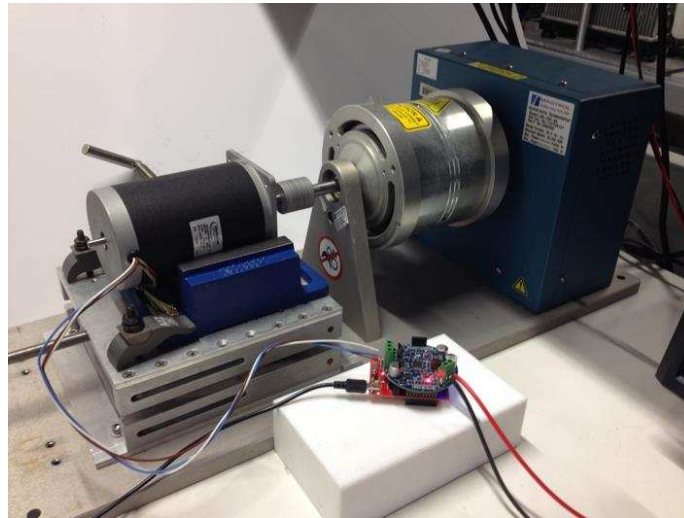
Figure 55. Test Setup With BLDC Motor and Dynamometer

The dynamometer used during this testing was the Magtrol model HD-705-6N, which is rated for 300W continuous operation, with maximum power up to 1400W for short periods. The dynamometer is capable of rotation up to 25,000 RPM, and may apply up to 55 in-lb (6.2 N-m) of torque. The dynamometer controller was a Magtrol model DSP6001, which may be controlled manually or using the M-TEST software through a serial link to an external computer.

Figure 56 shows one of several user interface screens available in the M-TEST software to set the dynamometer. Later figures will show M-TEST screens which display various dynamometer measurements, including rotational speed, applied load torque (also called dynamometer braking) and power delivered to the load (dynamometer).
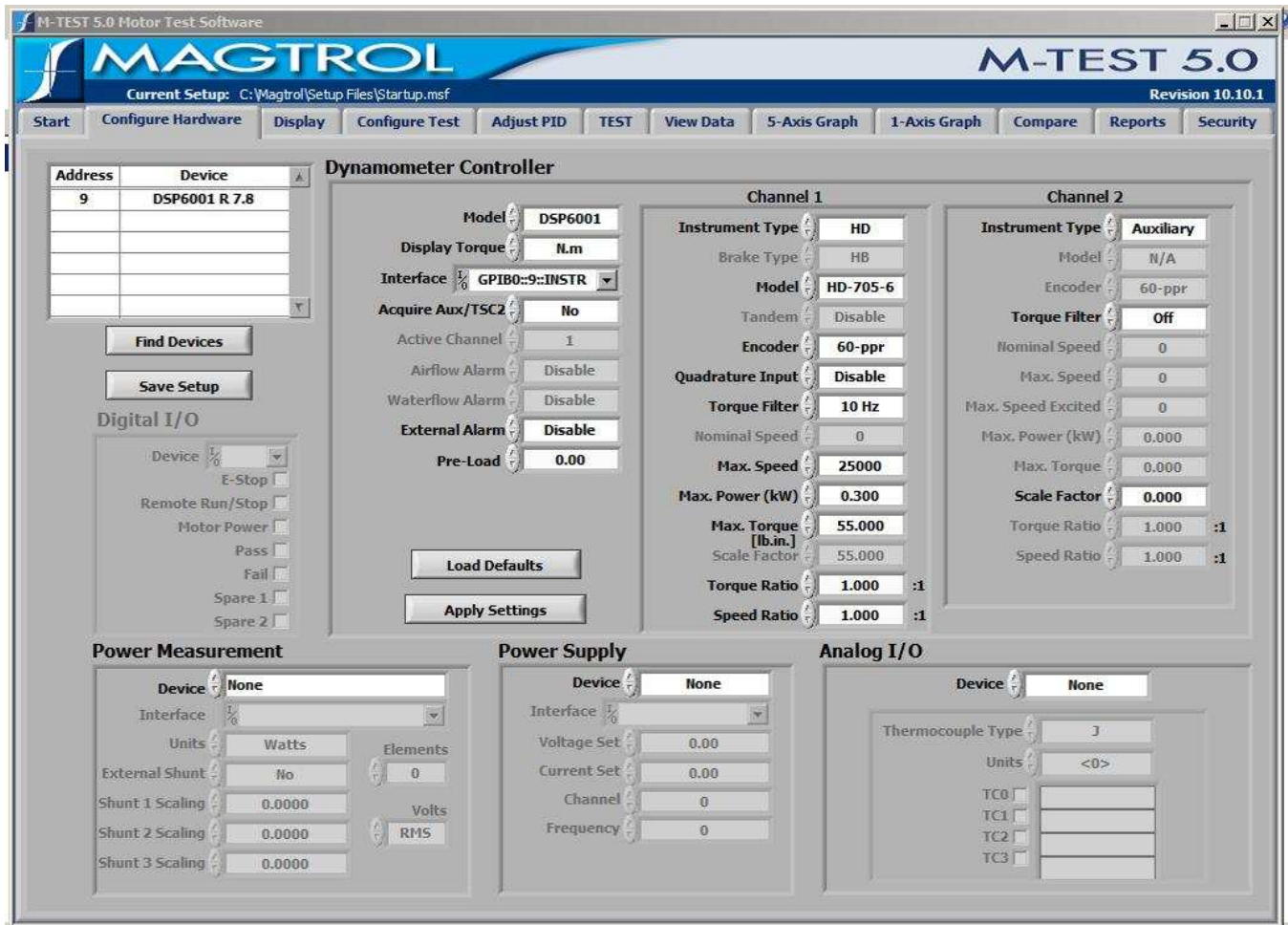
Figure 56. User Interface for Control of the Dynamometer Hardware Configuration

7.2.3 Motor No-Load Operation

The 12-V automotive battery supply is expected to vary in real-world applications. This design must maintain control of the motor over a range of at least 8 V to 18 V, but the motor drive performance is affected by the supply voltage.

- At any given supply voltage, the current required to maintain a specific speed varies more or less directly with the speed.
- Assuming a constant load, the maximum attainable speed increases as the applied supply voltage increases.
- At any given speed, the motor current varies inversely with the applied voltage, assuming a constant load.

The plots shown in Figure 57 show these relationships for the IHN06576 motor. Observe that these measurements were with no dynamometer attached. The maximum no-load speed for each supply voltage is indicated by the endpoint of the corresponding line.

Unless otherwise specified in later sections, the motor supply for all remaining measurements was set to the nominal value of 12 V.
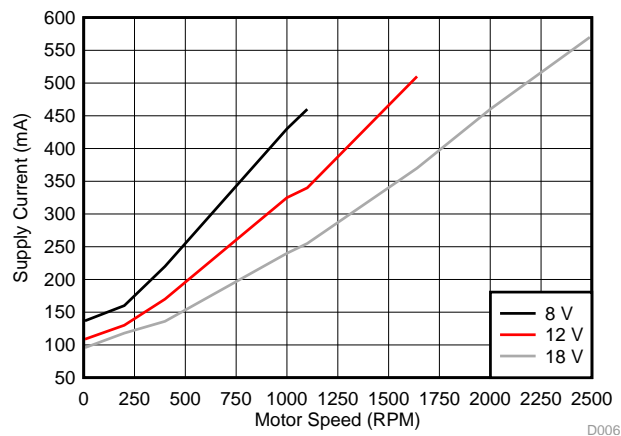
Figure 57. Motor No-Load Current vs Speed for Various Supply Voltages

7.2.4 Motor Operation With HVAC Blower Wheel

The plots in Figure 58 show these relationships for the IHN06576 motor with a six-inch (150 mm) blower wheel. The maximum speed for each supply voltage is indicated by the endpoint of the corresponding line.
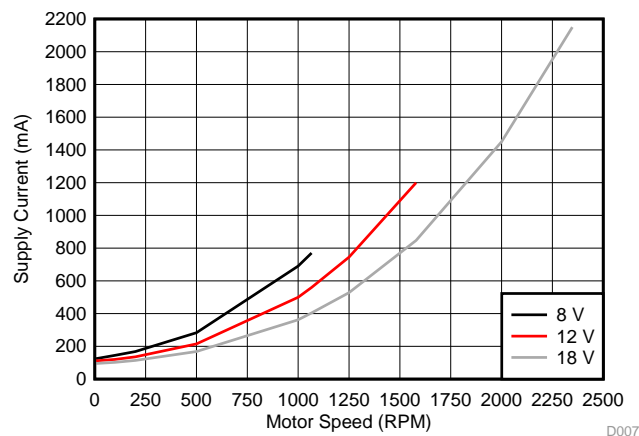
Figure 58. Motor Operation With HVAC Blower Wheel

Unless otherwise specified in later sections, the motor supply for all remaining measurements was set to the nominal value of 12 V.

7.2.5   Operation With BLDC Pump

Automotive pump applications include water pumps for engine cooling and for auxiliary cooling, fuel pumps, oil pumps, and others. These pump applications are similar to the HVAC blower in that the rotation speed is controlled rather than position, and the rotation is typically in only one direction.

Figure 59 shows the simple water pump hardware.

Figure 59. Simple Water Pump Hardware

To demonstrate operation of the TIDA-00901 design in a pump application, an automotive 50-W water pump was used, with colored water (for visibility) pumped between two tanks. In this simple example, the fluid system is unpressurized, and the dynamic head is less than 1 meter. The test system is shown in Figure 59.

For this water pump system, the relation between flow rate, electrical current from the 12-V supply, and motor speed is shown in Figure 59.

> **NOTE:** While the flow rate increases more or less linearly with motor speed, the supply current increases rapidly as the speed increases. For motor speeds below 500 RPM, there was no water flow, as the resulting pump pressure was insufficient for the system head.

shows the flow rate and supply current vs pump speed.
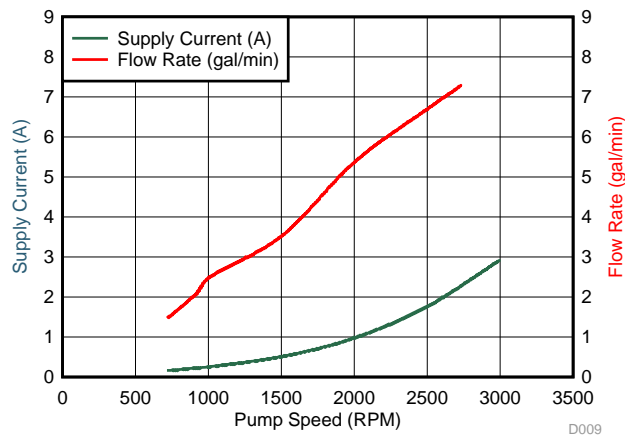
Figure 60. Flow Rate and Supply Current vs Pump Speed

shows the relation between the water flow rate and the total electrical power. This shows that as the power is increased, the incremental increase in water flow becomes progressively smaller. This is due to viscous loses in the system. For this system, the maximum flow rate is less than 10 gallons per second, with a maximum pump power of 50 Watts (about 4 Amps from the 12-V supply).
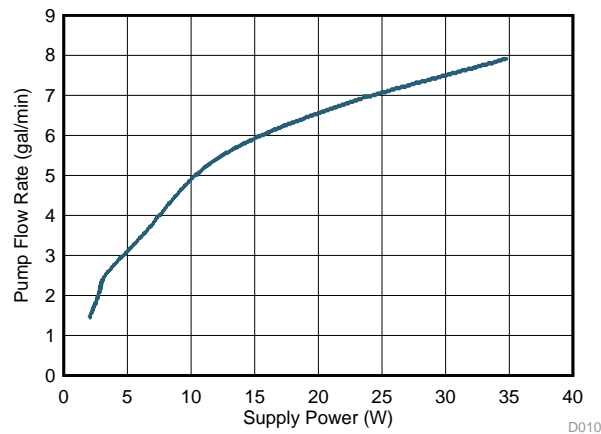
Figure 61. Flow Rate vs Electrical Power

7.2.6 System Response to Change in Speed Command

The response of the system to a change in the commanded speed is of particular interest to applications where the motor speed, rather than motor position or motor torque, is directly related to the performance of the system. For example, HVAC blowers, fans, and pumps typically have a desired target speed setting during operation.

The following plots were obtained by testing the ElectroCraft motor on a dynamometer. Unless otherwise specified, the input voltage (VBAT) was set to 12 V. The MotorWare software was used to control the LaunchPad commands to the TIDA-00901 board. The time scale factor is 1,000 samples per second (1 ms per sample) unless stated otherwise.

Figure 62 shows the response of the system to a step increase in the commanded speed, from 200 RPM to 600 RPM. Note that the speed overshoots the final speed, rising to 720 RPM before settling at the target speed. This overshoot is due to the settings of the P-I (proportional integral) speed control loop in MotorWare. If tighter control of the speed dynamics is needed for a specific application, these parameters can be optimized; several of the later MotorWare lab projects address how to set these parameters.
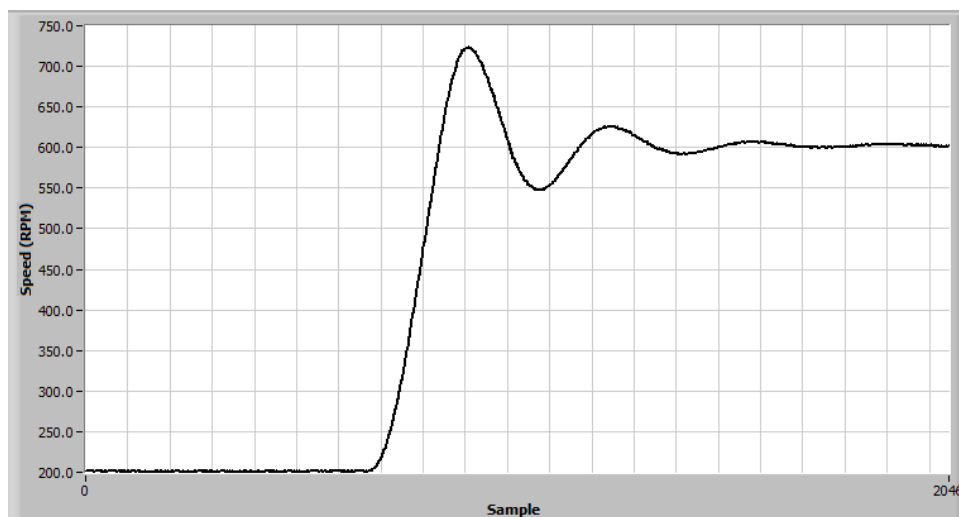
Figure 62. Dynamometer Test, Speed Step From 200 RPM to 600 RPM

Figure 63 shows the system response to a step increase in motor speed from 600 RPM to 1,000 RPM. Again the overshoot in the response is evident, with a maximum overshoot value of almost 40% of the commanded speed increase. The speed settles to within a few percent of the commanded rate in less than a second.
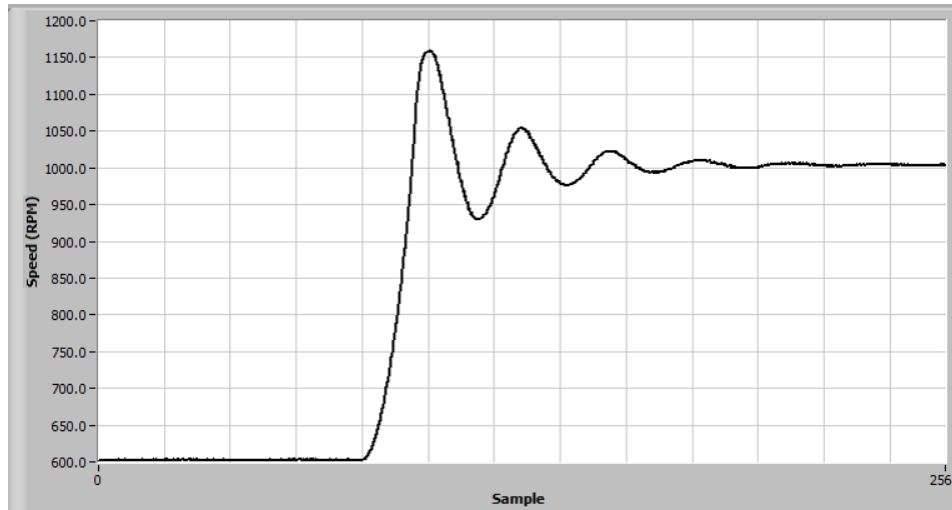
Figure 63. Dynamometer Test, Speed Step From 600 RPM to 1,000 RPM

Figure 64 shows the system dynamic response to a step decrease in commanded rate from 1000 RPM to 200 RPM. The overshoot is less pronounced, but still evident. The motor settles into the new commanded speed after a few cycles of ringing.
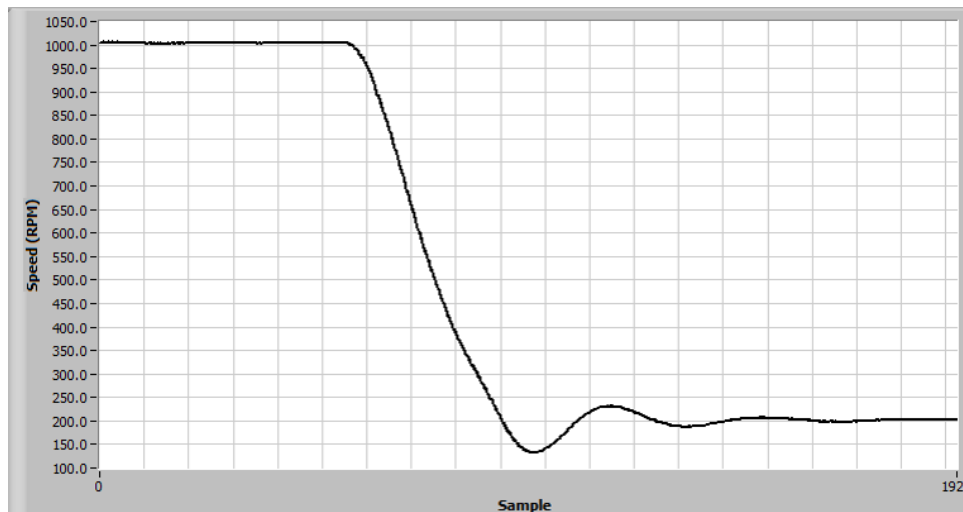
Figure 64. Dynamometer Test, Speed Step From 1,000 RPM to 200 RPM

Figure 65 shows the measured speed, torque, and power during a commanded speed decrease from 800 RPM to 0 RPM (stopped motor). As the motor approaches zero speed, the rotor begins to make small oscillations around a final position, which show up as torque oscillations. For applications such as blowers or fans, these small oscillations do not have a significant effect.
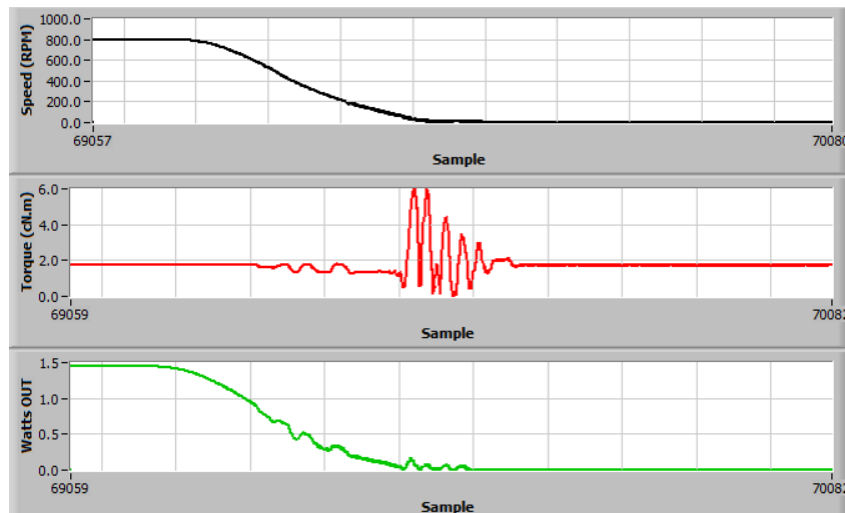
Figure 65. Speed Decrease Showing Torque and Power

7.2.7 System Response to Change in Load Torque

The following plots were obtained by testing the ElectroCraft motor coupled to a dynamometer with variable brake torque settings. Unless otherwise specified, the input voltage (VBAT) was set to 12 V. The MotorWare software was used to control the LaunchPad commands to the TIDA-00901 board. The time scale factor is 1,000 samples per second (1 ms per sample) unless stated otherwise.

Figure 66 shows the response of the system running at 200 RPM to a step increase in the braking torque applied by the dynamometer. Note that the rotational torque of the dynamometer is non-zero (about 1.3 cN-m) even when the active brake is not applied. When the braking torque is stepped up to 5 cN-m, the motor speed originally drops by about 15% before recovering and eventually settling back at the commanded 200 RPM rate. This performance is based on using the default settings of the MotorWare P-I speed control loop; these parameters can be adjusted if better torque rejection performance is necessary.
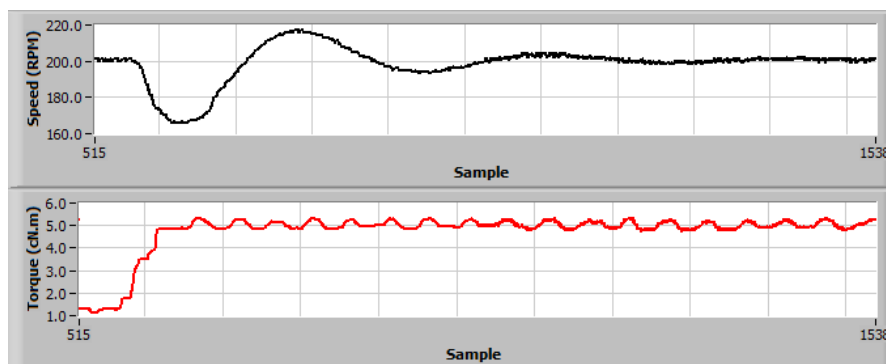
Figure 66. Dynamometer Test, Response to Small Torque Step Increase

Figure 67 shows the response of the system running at 800 RPM to a larger step increase in the braking torque applied by the dynamometer. Note that the rotational torque of the dynamometer is somewhat higher (about 2 cN-m) even when the active brake is not applied, indicating a viscous (speed-dependent) component of the dynamometer friction torque.

When the braking torque is stepped up to 12.5 cN-m, the motor speed originally drops by about 17% (to about 660 RPM) before recovering and eventually settling back at the commanded 800 RPM rate. This plot also shows the power dissipated in the dynamometer, rising from about 2 Watts before the brake is applied, to about 11 Watts when the speed regains the commanded setting after the brake torque step.
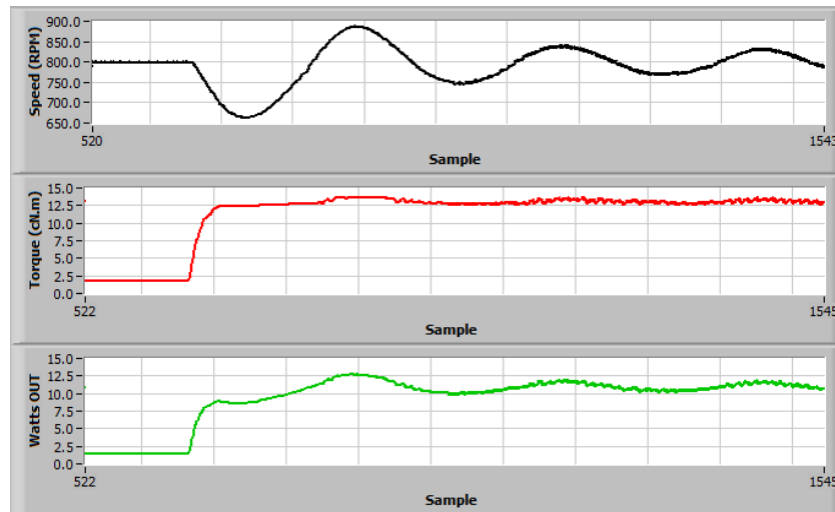
Figure 67. Dynamometer Results, Response to Step Increase in Load Torque

7.3   *Motor Current Feedback*

The current through the motor is sensed with an in-line (shunt) resistor between each low-side driver FET and ground. The resistor value is small (7 mΩ) and gain is provided by the current sense amplifiers in the DRV8305 before the signal is sampled by the microcontroller.

Figure 68, Figure 69, and Figure 70 show how the motor current increases as the torque load on the motor increases. These plots show the envelope of the phase A current sense signal ISNS_A which is connected back to the microcontroller through J3-13. In each of these plots, the motor was rotating at a constant speed.
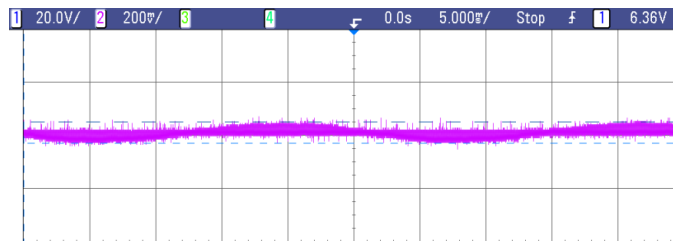
Figure 68. Phase A Current With Low Torque Load
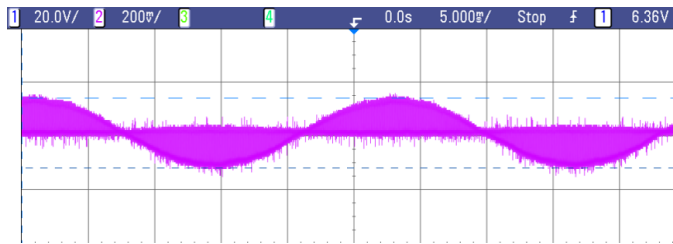
Figure 69. Phase A Current With Medium Torque Load
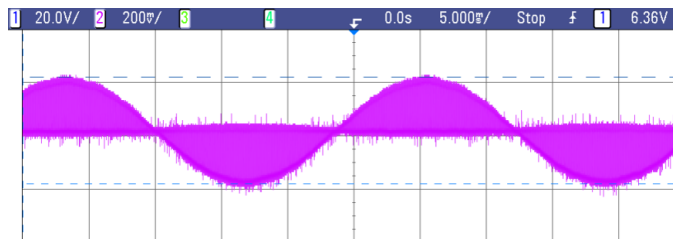
Figure 70. Phase A Current With High Torque Load

For the plots in Figure 71 and Figure 72, the ElectroCraft motor was running with a constant load, with total supply current of about 1.5 A. The PWM signals from the microcontroller to the DRV8305 are shown at the bottom of each plot. The blue trace is the phase A motor voltage, and the pink trace is the phase A current sense (ISNS_A) with a DC offset on the channel to position the trace on the oscilloscope screen.

> **NOTE:** The time and voltage scales in both plots are not changed; about two PWM periods (1/45 kHz) are shown in each plot.
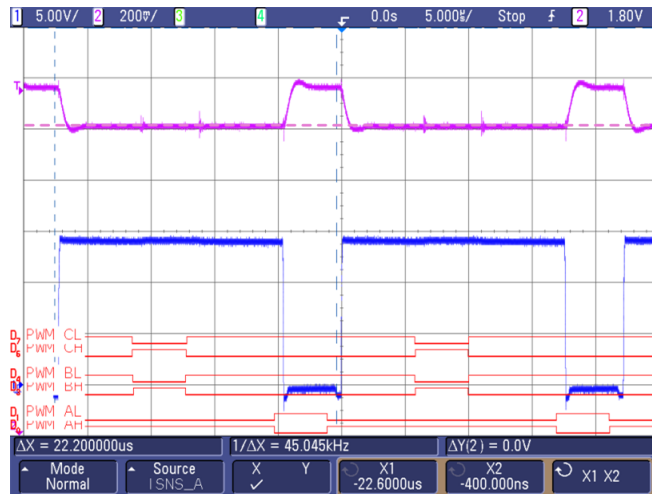
Figure 71. Phase A Voltage High
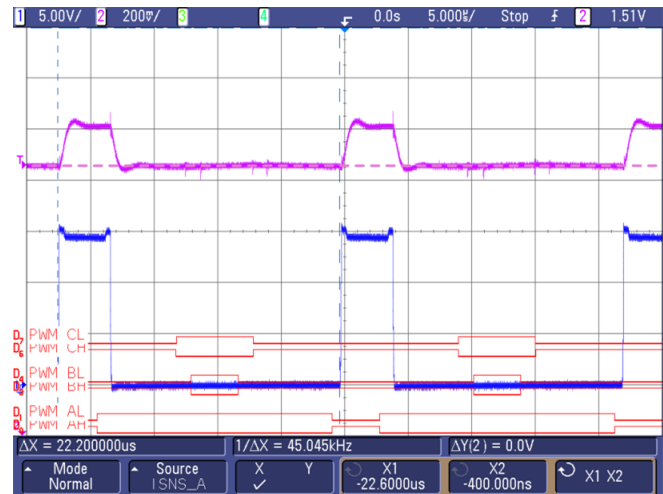
Figure 72. Phase A Voltage Low

In Figure 71, the phase A voltage (blue) is high for most of the PWM period, and the phase A current is flowing from the board terminal (J2-3) into the motor phase A winding. During the majority of the PWM period, the phase A high-side FET (Q2) is on in response to the high level on PWM_AH. While Q2 is on, the phase A low-side FET (Q5) is off, and the current sense voltage corresponds to the zero current level. For the short time that the motor phase A voltage is low, the A-phase low-side FET is on, and current is flowing from ground through the sense resistor and out to the motor phase. Thus the pink ISNS_A waveform goes above the dashed *zero current* line, indicating a current from ground to Q5 through R3, the phase A current sense resistor. (The inverting terminal of the current sense amplifier is on the motor side of R3, and the non-inverting terminal is at ground potential.)

In Figure 72, the phase A voltage (blue) is high for a small fraction of the PWM period, and phase A current is flowing from the motor winding into the phase A terminal. For the short time when the phase A voltage is high, the A phase high-side FET (Q2) is on. During this time, the A phase low-side FET (Q5) is off, and the current through the A phase current sense resistor (R3) is zero. During the longer time in the right plot, the phase A voltage is zero, indicating the A phase low-side FET (Q5) is on, and the current through R3 is from the motor towards ground, producing a current sense reading (pink) below the dashed *zero current* line.

7.4   *Motor Phase Voltages and Feedback Signals*

The voltage supplied to each phase of the motor is controlled by the C2000 Real-time microcontroller on the LaunchPad, which sends pulse-width modulated (PWM) signals to the DRV8305-Q1 gate drivers. The DRV8305-Q1 outputs alternately switch the high-side and low-side FETs for each motor phase, supplying the motor phase current needed to create torque in the brushless DC motor.

Figure 73 shows the relationships between the PWM inputs to the board in light blue, and the motor phase voltages which are the outputs from the board. Here, the overall envelope of command and drive shows the phase shifts between the three motor phases.
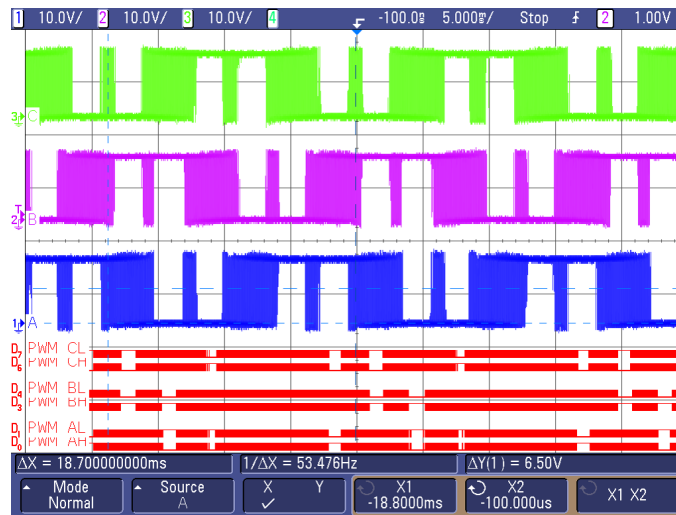
Figure 73. Phase Voltages, 800 RPM, No Load

Figure 74 shows an expansion of the horizontal time axis, such that the individual PWM edges can be discerned. Here the strict correspondence between the complementary PWM commands for each phase and the responding motor phase voltage transitions is evident.
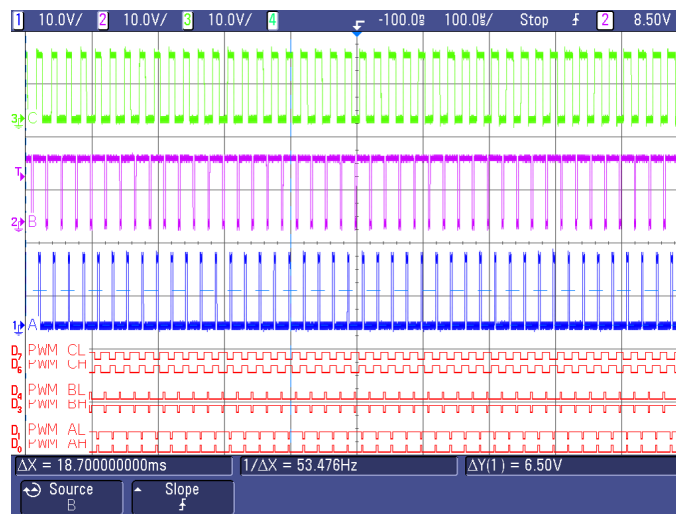
Figure 74. Phase Voltages, 600 RPM, No Load

In addition to the PWM signals and motor phase voltages, the feedback signal to the microcontroller is also of interest. The motor commutation algorithm and control loops require information on the present voltage on each of the motor phase windings. The motor phase current is filtered and scaled to fit the 3.3-V analog-to-digital converter (ADC) inputs on the C2000, providing a feedback signal for the digital control loop.

7.5 Dead-Time Settings and PWM Signals

The pulse-width modulation signals to the drive FETs must incorporate sufficient *dead-time* such that the high-side FETs and low-side FETs for any motor phase are never on at the same time. This causes a short-circuit between the 12-V supply and ground through the high-side and low-side FETs, resulting in high *shoot through* current.

The algorithms in the MotorWare code include provisions for setting a variable dead-time between the edges of the PWM signals from the LaunchPad to the TIDA-00901 board. The DRV8305-Q1 also has integrated logic to prevent current shoot through. TI recommends using the logic in the DRV8305-Q1 to control the dead-time, as this logic monitors the states of the FETs directly.

The dead-time on the rising and falling edges of the PWM signal from the C2000 on the LaunchPad can be independently set, by altering the code in the hardware abstraction layer file, hal.h, as shown in Figure 75.

NOTE: The unit of time is system clock periods, which for the TMS320F28027F LaunchPad is 16.7 nanoseconds (the reciprocal of the 60 MHz system clock frequency). Integer multiples of the clock period are valid settings for these parameters.

```
115
116 //! \brief Defines the PWM deadband falling edge delay count (system clocks)
117 //!
118 #define HAL_PWM_DBFED_CNT        1        // orignally was 4
119
120
121 //! \brief Defines the PWM deadband rising edge delay count (system clocks)
122 //!
123 #define HAL_PWM_DBRED_CNT        1        // originally was 4
124
```

Figure 75. Code Fragment in hal.h, Allowing Setting the PWM Dead-Time Parameters

Due to the integrated features of the DRV8305N-Q1 such as programmable dead time control and shoot-through protection, the dead-time setting for the microcontroller can be reduced below the default value of 4 system clock cycles (67 nanoseconds). Figure 76 and Figure 77 show the two PWM signals associated with motor phase A, and illustrate the adjustability of the dead-time parameter, in this case for the falling edge.

In both plots, the measured dead-time between transitions is as expected.
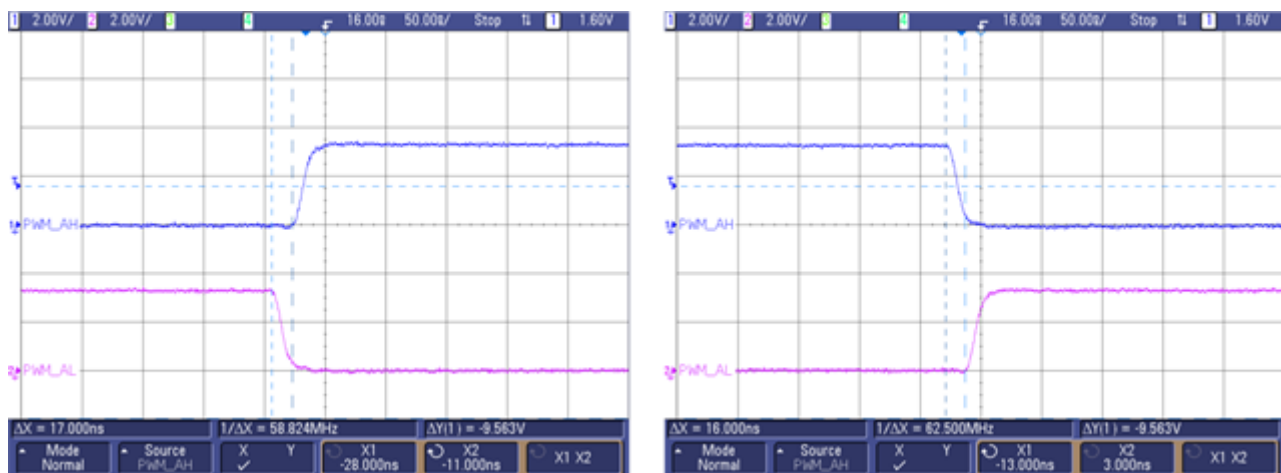
Figure 76. PWM Phase A HI (Blue) and Low (Magenta) With C2000 Dead-Time = 1

In Figure 76, the C2000 dead-time is set to 1 clock cycle, and the delay between falling edge on one PWM command signal and the rising edge of the complementary signal is approximately 17 ns. In Figure 71, the C2000 dead-time is set to 5 clock cycles, and the delay between falling and rising edges has increased to about 82 ns.
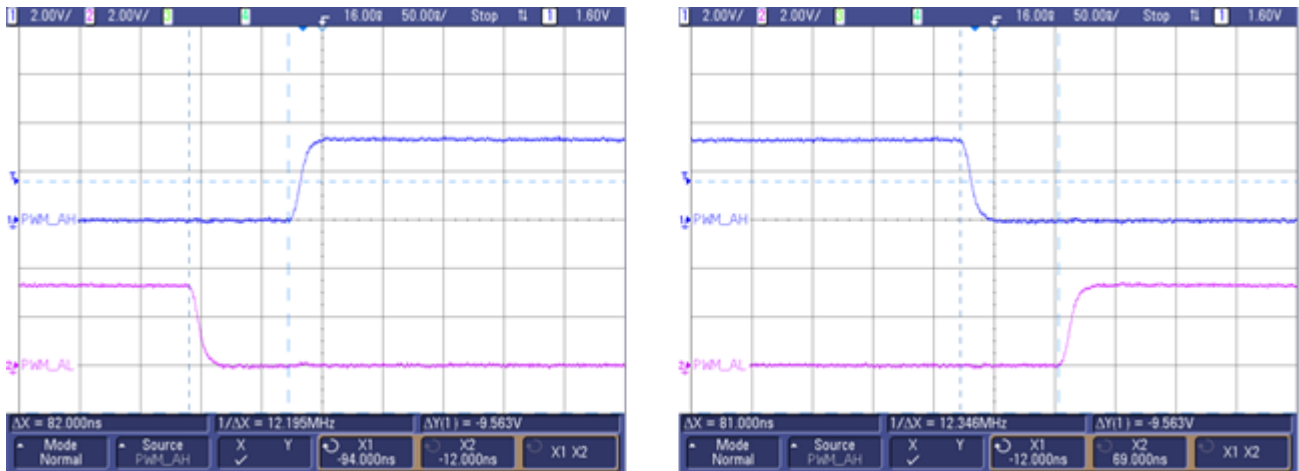
Figure 77. PWM Phase A HI (Blue) and Low (Magenta) With C2000 Dead-Time = 5

7.6 Effect of Adjusting the DRV8305 Parameters

The DRV8305N-Q1 provides programmability for several key motor drive parameters. Designers can modify these parameters through the SPI port. This can ease motor drive development by allowing optimization of the design without the need to remove and replace discrete components for each motor phase.

In several of the following plots, the specific settings for motor drive parameters are noted below the figures.

7.6.1 Adjusting Dead-Time in DRV8305 Registers

The dead-time between falling edge of one gate and the rising edge of the complementary gate can be adjusted through the register settings of the DRV8305-Q1. In Figure 78, the adjustability is shown; the left plot shows a delay of about 780 ns between the falling edge on the low-side gate drive signal and the rising edge of the high-side gate drive signal. The right plot shows that after changing the dead-time setting through the DRV8305-Q1 SPI port, the delay between falling edge and rising edge has been increased to about 1.62 µs.
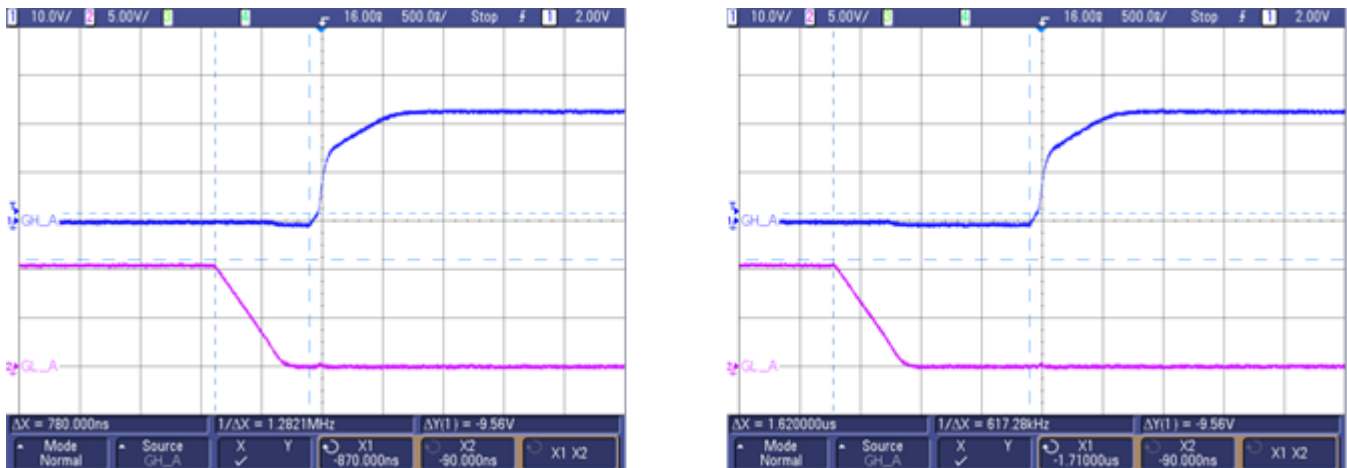
Figure 78. Gate Drive Signals for Motor Phase A Illustrating Programmable Dead-Time

Copyright © 2016, Texas Instruments Incorporated

7.6.2 Adjusting Gate Drive Current Affects Switching Delay

The gate drive current settings determine how quickly the gate capacitance is charged and discharged. This affects the delay between transition commands (from the microcontroller) and the beginning of the transition at the motor phase. It also affects the slew rate of the FET turn-on or turn-off transition. In this section the switching delay between the PWM command signal and the beginning of FET state transition is illustrated.

Figure 73 shows that with a relatively weak gate drive current, the delay between the rising edge of PWM_BH and the rising edge of the phase B motor voltage is about 670 ns.
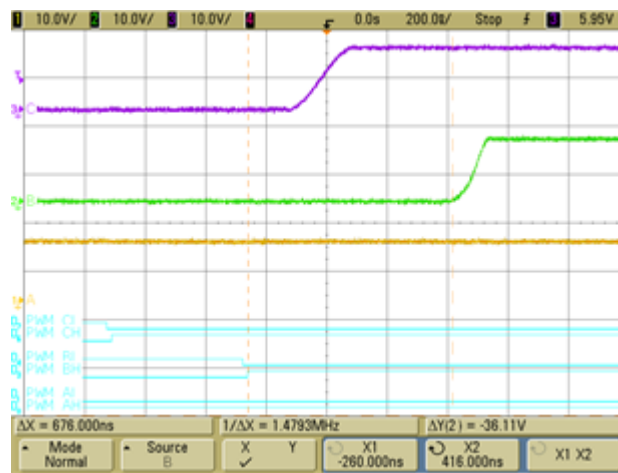
Figure 79. DRV8305-Q1 and FET Signals With Weak Gate Drive Current

Table 8. Parameter Settings Corresponding to Figure 79

TDN	TDP	IN_HS	IN_LS	IP_HS	IP_LS	T DEAD	T BLANK	TVDS
2,000	2,000	60	60	50	50	1,000	2	4

By increasing the gate source and sink current to 250 mA, as shown in Figure 80, the delay between rising edge of PWM_B and the rising edge of the motor phase B voltage has decreased from 676 ns to 320 ns.
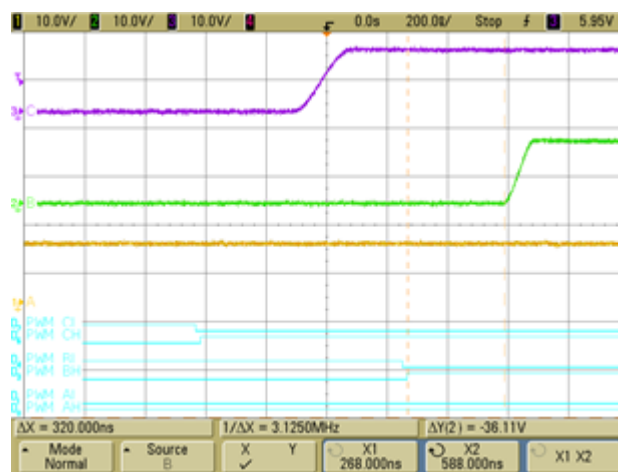
Figure 80. DRV8305-Q1 and FET Signals With Strong Gate Current Drive

Table 9. Parameter Settings Corresponding to Figure 80

TDN	TDP	IN_HS	IN_LS	IP_HS	IP_LS	T DEAD	T BLANK	TVDS
2,000	2,000	250	250	250	250	1,000	2	4

7.6.3   Adjusting Gate Drive Current Affects Transition Noise

In addition to timing, the effect of the gate drive current setting can be seen on the waveform shape of the motor phase voltage.

Figure 81 shows undesirable switching noise on the three motor phases.

> **NOTE:** There are two undesirable effects visible; the overshoot on each phase transition, and the coupling of transients from one phase to another.

These effects are due to the high gate drive settings (1.25 A sink, 1.0 A source) for the DRV8305.
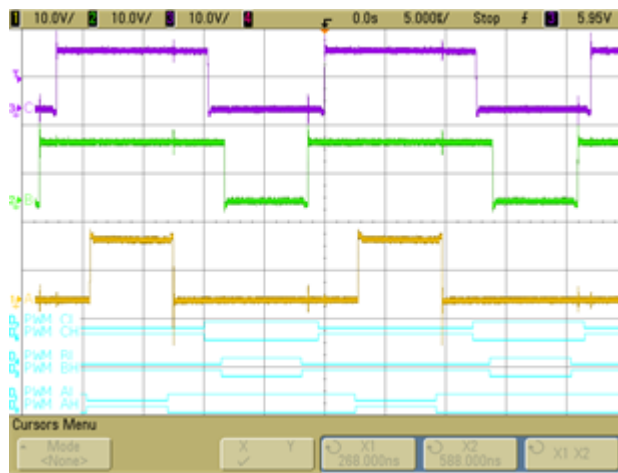
Figure 81. DRV8305-Q1 Parameter Settings

Table 10. Parameter Settings Corresponding to Figure 81

TDN	TDP	IN_HS	IN_LS	IP_HS	IP_LS	T DEAD	T BLANK	TVDS
2,000	2,000	1,250	1,250	1,000	1,000	40	2	4

Figure 82 shows that reducing the gate drive to 50 mA has reduced the undesirable effects previously seen with the strong gate drive levels. Both the overshoot on each transition and the cross-coupling has been eliminated.
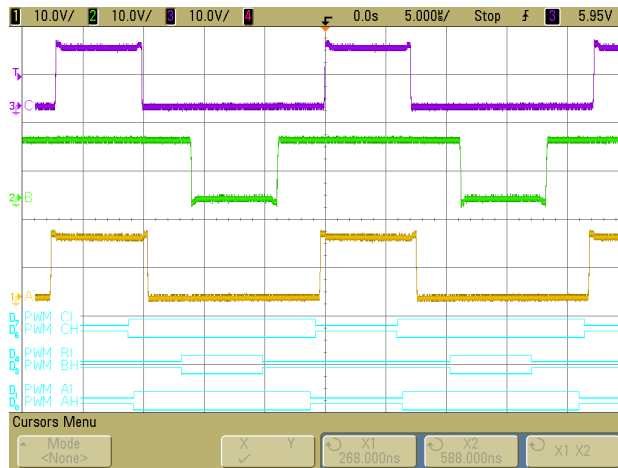
Figure 82. DRV8305-Q1 Parameter Settings

Table 11. Parameter Settings Corresponding to Figure 82

TDN	TDP	IN_HS	IN_LS	IP_HS	IP_LS	T DEAD	T BLANK	TVDS
2,000	2,000	50	50	50	50	40	2	4

7.6.4   Adjusting Gate Drive Current Affects Transition Ringing

Examining the motor phase voltage transition edge more closely, a very high gate drive current level shows both overshoot and ringing, as seen in Figure 83. This ringing, with an oscillation frequency of approximately 130 MHz, may cause undesired electromagnetic emissions. In this example, the source current for both the high side and low side FET gates is set to 1 A, and the sink current for the high-side and low-side FET gates is set to 1.25 A.
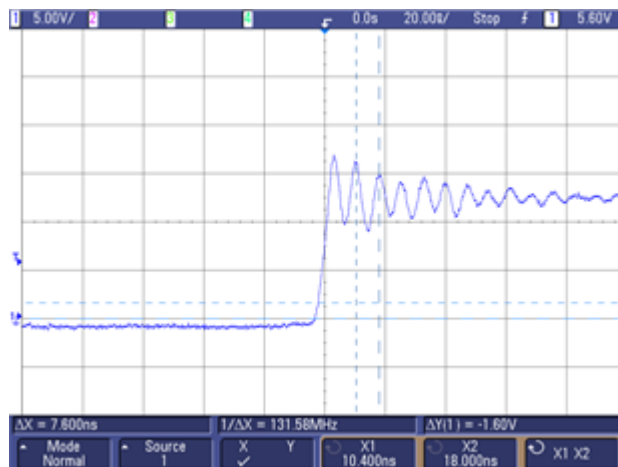
Figure 83. Strong Gate Drive Current Causes Ringing on Drive FET Edges

Table 12 lists the ElectroCraft motor, no load, 12-V supply, 300 RPM.

Table 12. Parameter Settings Corresponding to Figure 83

TDN	TDP	IN_HS	IN_LS	IP_HS	IP_LS	T DEAD	T BLANK	TVDS
2,000	2,000	1,250	1,250	1,000	1,000	60	2	4

In Figure 84, the effect of reducing the gate drive current to the minimum settings is evident. With a sink current of 20 mA and a source current of 10 mA, the ringing has been eliminated. However, observe the change of time scale and the greatly increased rise time of the motor voltage. With a high gate current, the rise time was less than 10 ns, and with a weak gate current, the rise time is about 800 ns.
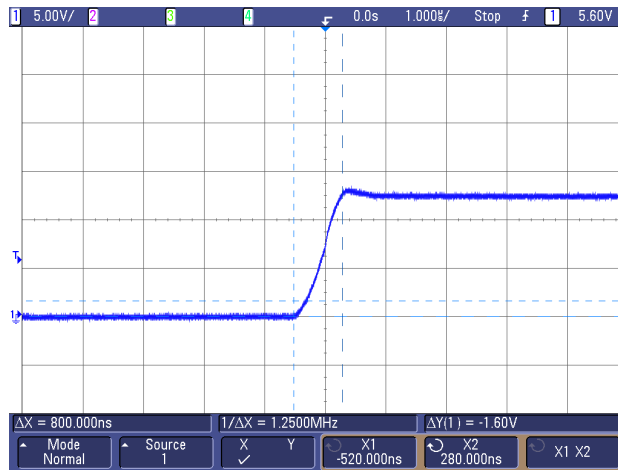
Figure 84. Weak Gate Drive Current Gives Slow FET Rise Time, With No Ringing

Table 13 lists the ElectroCraft motor, no load, 12-V supply, 300 RPM.

Table 13. Parameter Settings Corresponding to Figure 84

TDN	TDP	IN_HS	IN_LS	IP_HS	IP_LS	T DEAD	T BLANK	TVDS
2,000	2,000	1,250	1,250	1,000	1,000	60	2	4

The effect of changing the gate drive current setting may also be observed in the frequency domain. In Figure 85, the frequency spectrum of the motor drive signals is shown. The left plot shows the spectrum with strong gate drive, the right plot shows the spectrum with the gate drive current reduced. The peak amplitude and overall spectrum are both reduced with the weaker gate drive current.
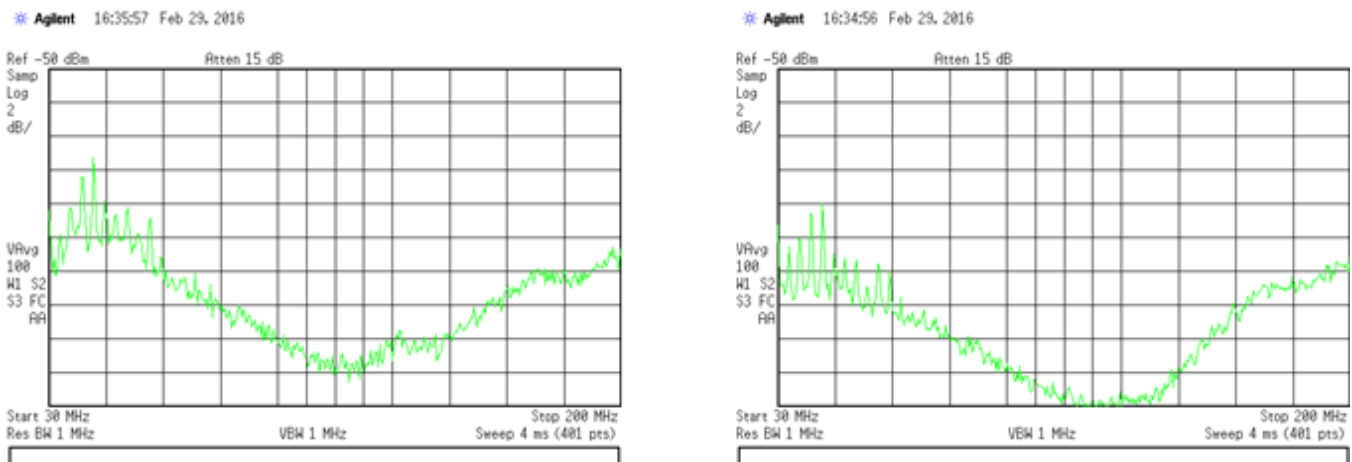
Figure 85. Frequency Domain Plots Show Effect of Gate Drive Current Setting

Another example of this effect is shown in Figure 86 and Figure 87. Here the time domain oscilloscope plots illustrate the effect of reducing the gate drive on the motor drive voltage transitions. The rising edge of the phase C motor voltage changes from a few nanoseconds with the minimum gate drive to about 250 nanoseconds with the gate current at the maximum setting.
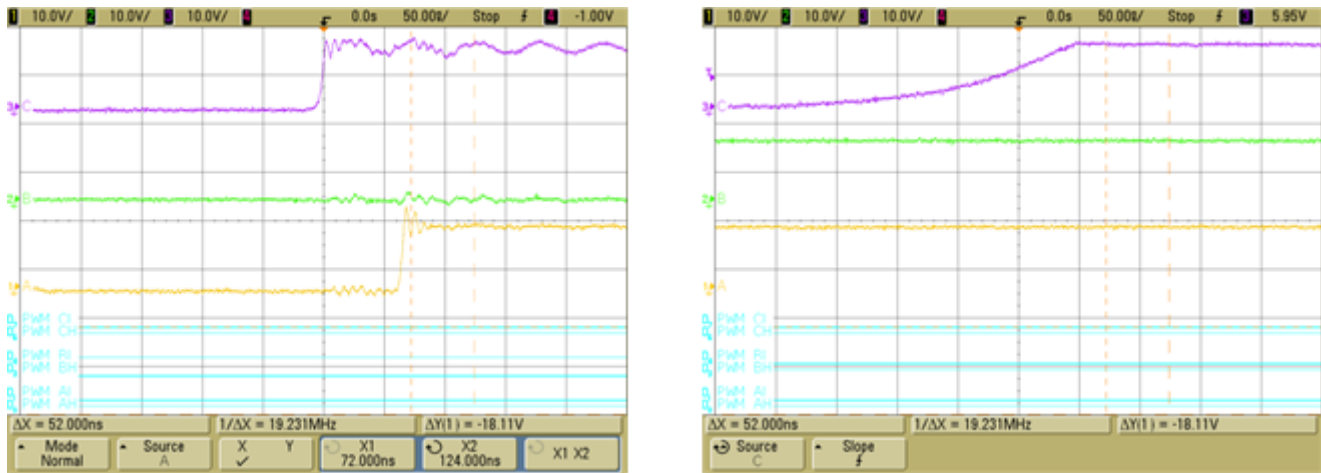
Figure 86. Time Domain Plots, Gate Current Set to maximum (Left), Gate Current Set to Minimum (Right), EC motor Unloaded at 100 RPM

Figure 87 shows the frequency spectrum corresponding to the two cases above. The left plot shows a spectrum peak at 19.25 MHz with the maximum gate current setting. The right plot shows a significant reduction in this peak when the gate current is set to the minimum value.

In general, each application may be optimized by selecting the best combination of gate current drive, dead-time, and other motor parameters. The programmability of the DRV8305-Q1 facilitates this optimization by allowing designers to change the parameters through simple SPI commands.
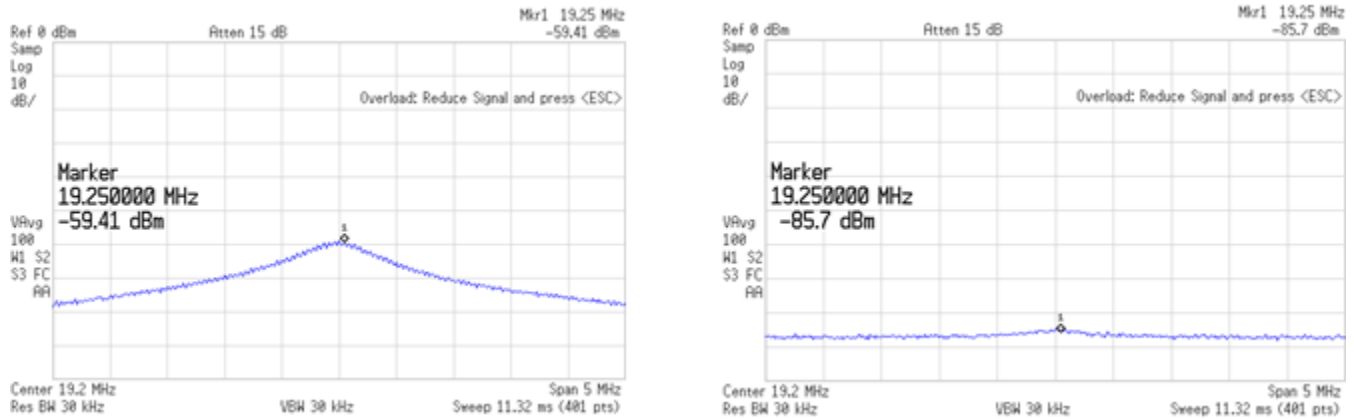
Figure 87. Frequency Domain Plots, Gate Current Set to Maximum (Left), Gate Current Set to Minimum (Right), EC Motor Unloaded at 100 RPM

Optimization of the gate drive current involves reducing the undesired high-frequency content of the transitions, without causing loss of efficiency due to excessively slow transition times.

7.7 *Hall Effect Signal for Motor Communication*

If Hall Effect sensors are available in the motor, these can be used to determine phase position for commutation of the motor without the need for sensorless commutation algorithms. Sensors such as the DRV5013-Q1 will provide signal indicating which phases of the motor should be driven high and low to maintain the desired direction of travel.

Typical Hall Effect signals during motor rotation are shown in Figure 88, showing the phase relation between the 3 sensor signal, as well as the effect of varying the motor speed.
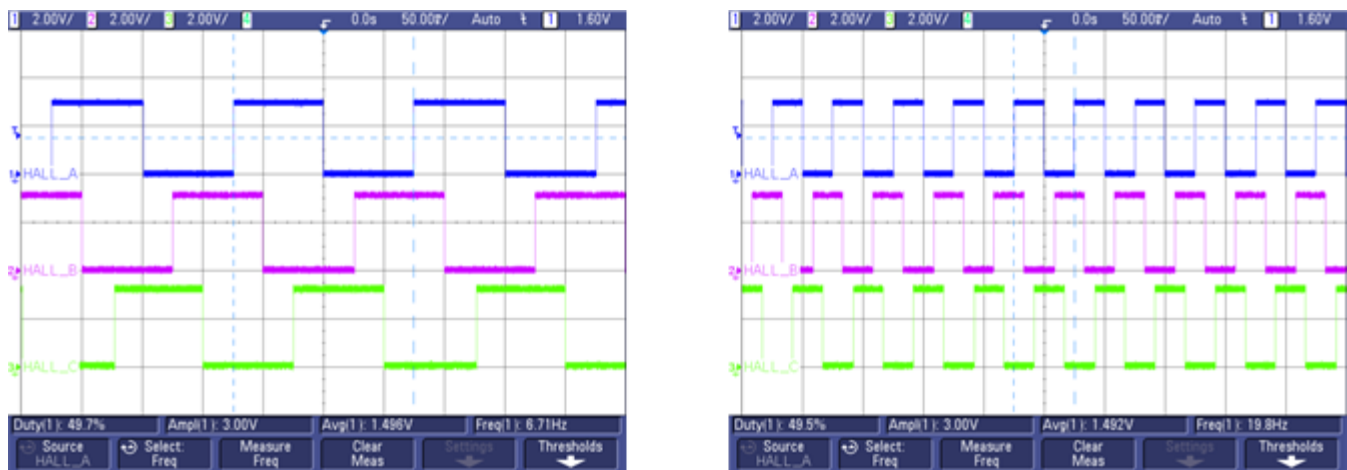
Figure 88. Hall Effect Signals, 100 RPM (Left) and 300 RPM (Right)

7.8   *Motor Identification Algorithm Testing*

One of the features of InstaSPIN-FOC is the ability to identify the parameters of the BLDC motor automatically. The InstaSPIN FOC Motor Identification algorithm measures all the required electrical motor parameters of an unloaded motor in under two minutes (typical). The motor identification is based on measures of the current and voltage for the motor phases, as shown in Figure 89.

> **NOTE:** These measurements are also the basis for sensorless commutation, as the FAST estimator calculates the motor flux, angle, speed, and torque.

Copyright © 2016, Texas Instruments Incorporated
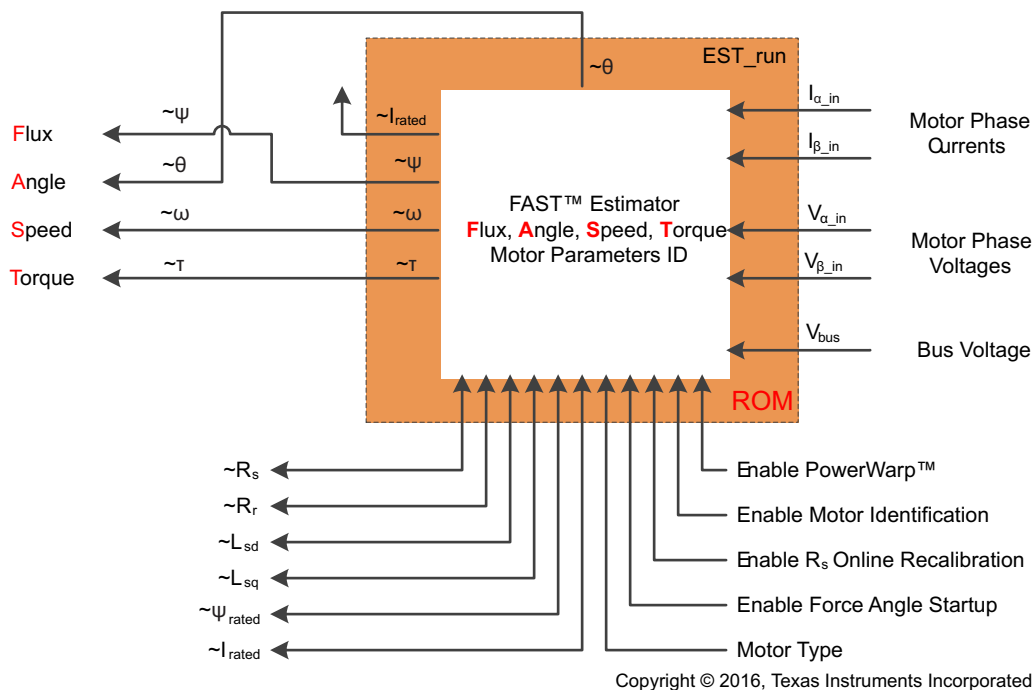
Figure 89. Automatic Motor Identification Using InstaSPIN

For the testing below, the nominal conditions of 12-V supply, and motor with no dynamometer brake load were used. Table 14 and Table 15 list the results of repeated runs of motor identification, and illustrate the repeatable nature of the identification process.

Table 14. Results of Repeated Motor Identification (EC Motor)

TRIAL	WINDING RESISTANCE (Ω)	WINDING INDUCTANCE (mH)
1	0.08298	0.6118
2	0.08226	0.6164
3	0.08317	0.6179
4	0.08225	0.6045
5	0.08259	0.6167
6	0.08311	0.6270
7	0.08362	0.6679
8	0.08266	0.6331

Table 15. Results of Repeated Motor Identification (IHN06576 Motor)

TRIAL	WINDING RESISTANCE (Ω)	WINDING INDUCTANCE (mH)	FLUX (V/Hz)
1	0.2890801	0.2800229	
2	0.2887801	0.2821203	0.1291758
3	0.2871601	0.2943898	0.1292939
4	0.2865	0.2513	
5	0.2872	0.2873	
6	0.2843	0.2859	0.12896

7.9 Temperature Sensor

Inclusion of a temperature sensor near the drive FETs allows monitoring of the anticipated highest-temperature section of the board. Table 7 shows the relation between motor drive power during operation and temperature sensor readings from the LMT86-Q1. In Section 7.11, infrared camera images of the board during these various levels of motor power show the distribution of temperature across the board.

Table 16. Temperature Readings During Board Operation

BRAKE LOAD (%)	SUPPLY POWER (W)	LOAD POWER (W)	TEMP SIGNAL (V)	TEMPERATURE
0	6.9	1.9	1.660	40
10	13.9	7.9	1.658	41
15	21	15.4	1.646	42
20	34	26.8	1.617	45
25	58	46	1.540	52
30	91	68	1.34	70

In Table 17 and Figure 90 the temperature readings from the LMT86-Q1 show how the board heats up as the motor drive is operating for a length of time.

Table 17. Temperature Readings vs Time

ELAPSED TIME (MINUTES)	TEMP SIGNAL VOLTAGE	TEMPERATURE (ºC)
1	1.73	34
3	1.71	36
5	1.69	38
8	1.67	39
10	1.66	40
15	1.64	42
21	1.62	44
22	1.61	45
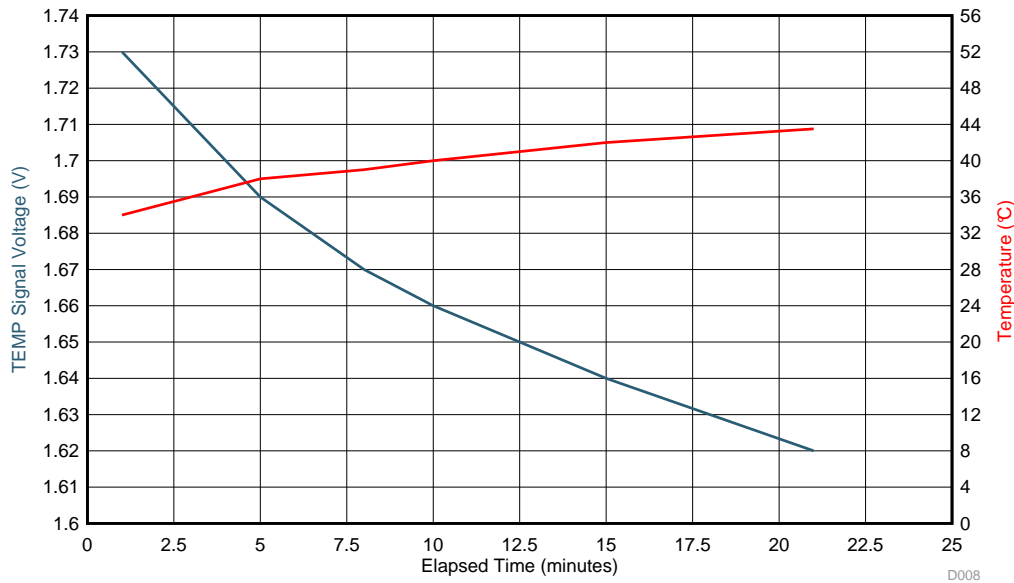
Figure 90. Temperature Readings vs Time

7.10 Thermal Shutdown

In order to illustrate the over-temperature fault feature of the DRV8305, the board was subjected to a high-temperature source causing a quick increase in temperature. Figure 91 shows the TEMP signal from the LMT86-Q1 (U2) decreasing in voltage as the board temperature rises. The nFAULT signal goes low when the temperature reaches the limit.
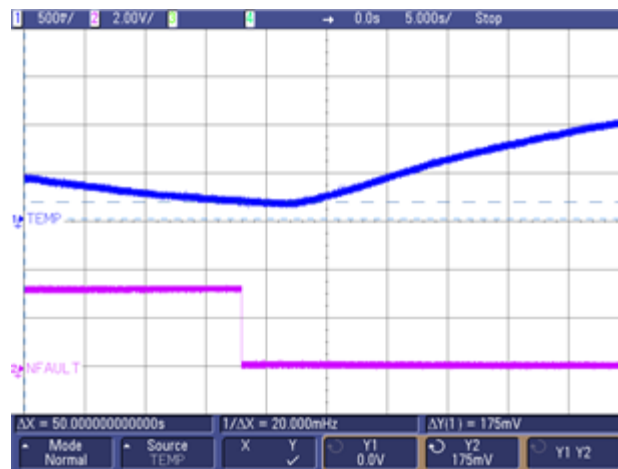
Figure 91. Over-Temperature Fault Caused by Externally-Applied Heat Source

7.11 Thermal Images

In Figure 92 and Figure 93, the surface temperature of the various components is visible. Each of the images represents a different level of total system power, set by varying the motor speed and brake load of the dynamometer attached to the motor. Note that due to the auto-ranging feature of the Fluke Ti-110 thermal imaging camera, the various colors in each image represent varying temperature levels. The background (ambient) temperature in each case was room temperature.

Figure 92 shows the temperature profile of the board with the LaunchPad processor running, about 2 Watts dissipated in the dynamometer, and about 7 Watts of total system power. Note that the hottest part of the image is the C2000 LaunchPad board; the motor drive stages are not dissipating any significant amount of power.
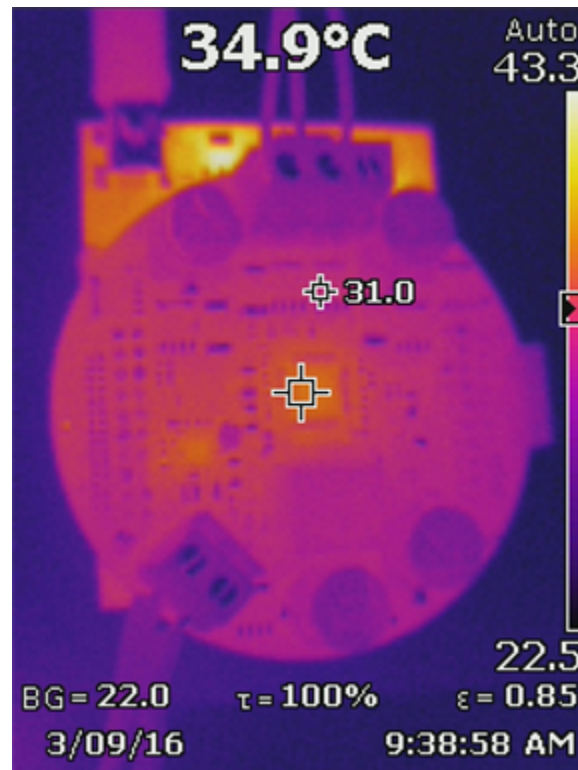
Figure 92. Thermal Image – No Dynamometer Brake

In Figure 93, the dynamometer brake load is engaged at 10%, dissipating about 8 Watts in the dynamometer; with total system power about 14 Watts. The DRV8305-Q1 has increased in temperature, while the microcontroller is about the same temperature, and is still the hottest component in the image. The maximum temperature in the image has increased slightly to 46.5 degrees Centigrade.
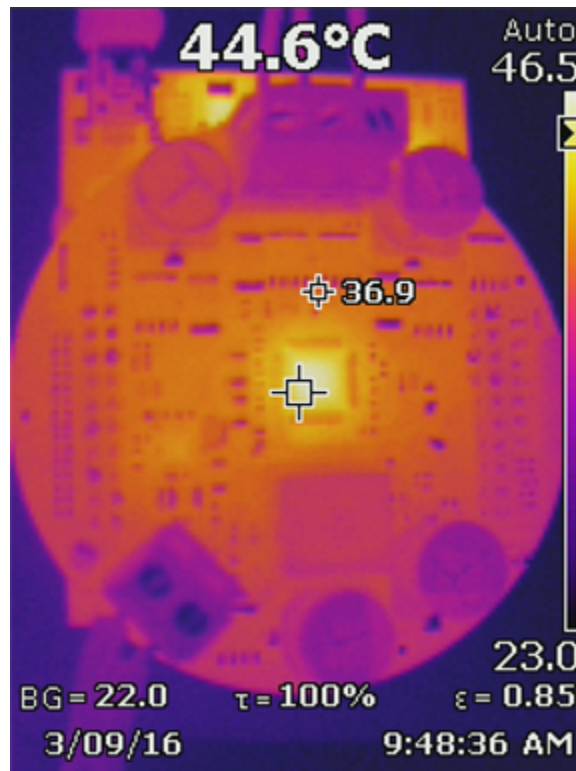
Figure 93. Thermal Image – 10% Brake

In Figure 94, the dynamometer brake load has been increased to 15%. This gives a mechanical power delivered of 15 W, and the electrical power from the 12-V supply is 21 W. Under these conditions, the drive components such as FETs and sense resistors are beginning to rise significantly in temperature.
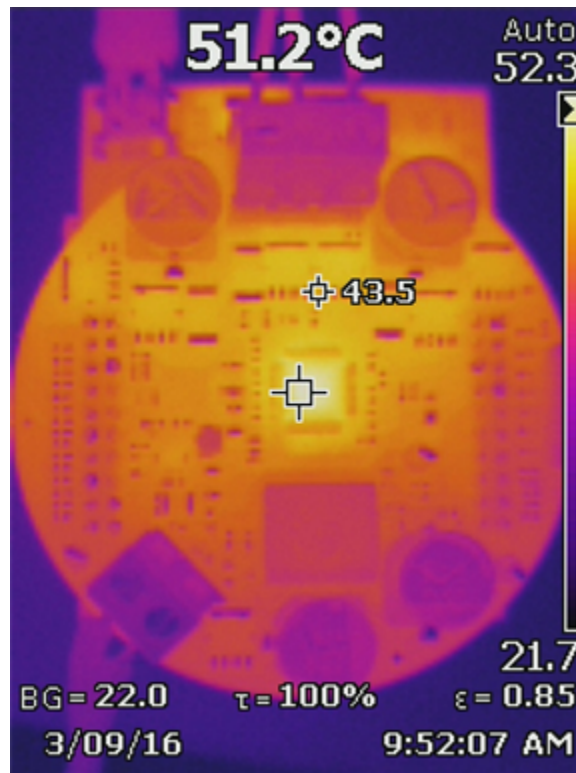
Figure 94. Thermal Image – 15% Brake

In Figure 95 the dynamometer brake load has been increased to 20%. This gives a mechanical power delivered of 27 W, and the electrical power from the 12-V supply is 34 W. Although the highest temperature has risen to 54.3 degrees, the DRV8305N-Q1 (U3) still appears to be the hottest component on the board.
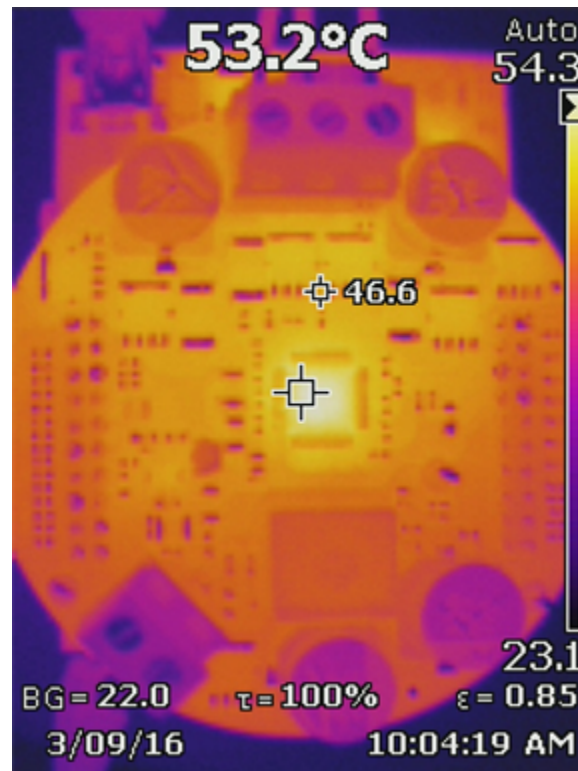
Figure 95. Thermal Image – 20% Brake

In Figure 96, the dynamometer brake load is 25%. This gives a mechanical power delivered of 46 W, and the electrical power from the 12-V supply is 58 W. In these conditions, the FETs for the motor drive are similar in temperature as the DRV8305N-Q1. The FETs for phase B appear to be the highest temperature, due to their location in the center of the board.
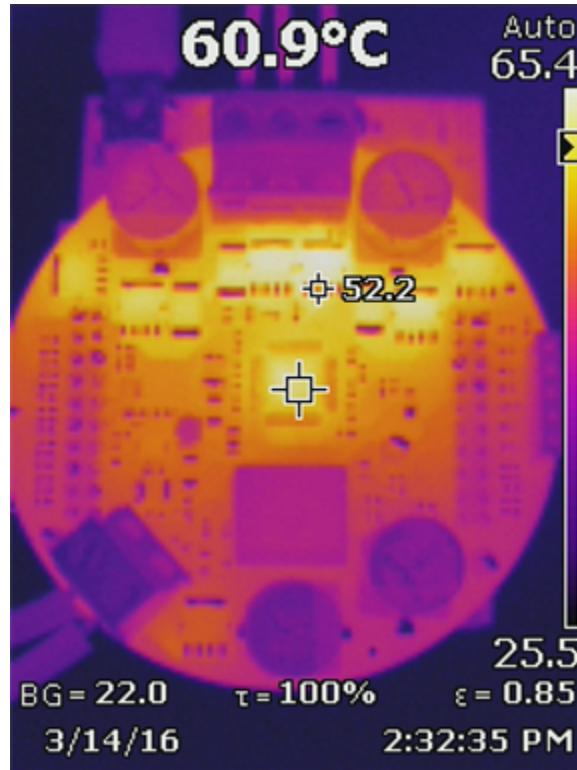
Figure 96. Thermal Image – 25% Brake

In Figure 97 the dynamometer brake is set to 30%, causing a power dissipation of 68 Watts in the dynamometer, and a total power from the 12-V supply of 91 Watts. The IR image shows that the top of the high-sde FET for phase B is at about 77 degrees, about 50 degrees above room temperature.
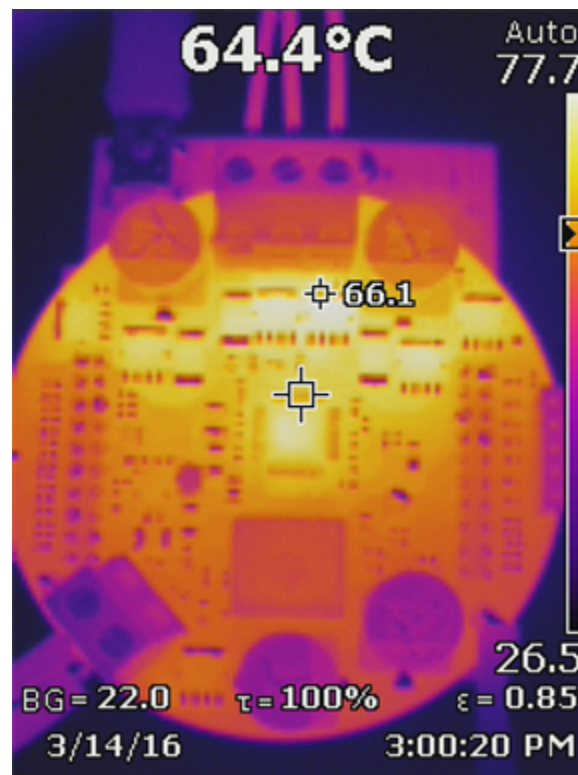
Figure 97. Thermal Image – 30% Brake

8 Design Files

To download the latest version of th electrical schematics for this board, see the design files at http://www.ti.com/tool/TIDA-00901.

8.1 Bill of Materials

To download the bill of materials (BOM), see the design files at TIDA-00901.

Table 18. BOM

ITEM	DESIGNATOR	QTY	PART NUMBER	DESCRIPTION
1	!PCB1	1	TIDA-00901	Printed Circuit Board
2	C1, C2, C3	3	UMK107AB7105KA-T	CAP, CERM, 1 µF, 50 V, ±10%, X7R, 0603
3	C4, C5	2	GRM21BR71H105KA12L	CAP, CERM, 1uF, 50 V, ±10%, X7R, 0805
4	C6, C7, C14, C32, C37	5	C1608X7R1H104K	CAP, CERM, 0.1uF, 50 V, ±10%, X7R, 0603
5	C8, C9, C12, C13	4	EEE-FT1H331AP	CAP, AL, 330 µF, 50 V, ±20%, 0.3 Ω, SMD
6	C10, C11	2	C1608X7R1H103K	CAP, CERM, 0.01 uF, 50 V, ±10%, X7R, 0603
7	C15 – C18	4	C0603C104J4RACTU	CAP, CERM, 0.1 µF, 16 V, ±5%, X7R, 0603

Table 18. BOM (continued)

ITEM	DESIGNATOR	QTY	PART NUMBER	DESCRIPTION
8	C19	1	C0402C104K4RACAUTO	CAP, CERM, 0.1 µF, 16 V, ±10%, X7R, AEC-Q200 Grade 1, 0402
9	C20, C22	2	C0603C473K1RACTU	CAP, CERM, 0.047uF, 100V, ±10%, X7R, 0603
10	C21, C23, C34, C41	4	C1608X7R1C105K	CAP, CERM, 1 µF, 16 V, ±10%, X7R, 0603
11	C24	1	GRM31CR71H475KA12L	CAP, CERM, 4.7 µF, 50 V, ±10%, X7R, 1206
12	C25 – C27, C36, C39, C40	6	GRM188R71C102KA01D	CAP, CERM, 1000pF, 16 V, ±10%, X7R, 0603
13	C28, C29, C31	3	GRM188R71C222KA01D	CAP, CERM, 2200pF, 16 V, ±10%, X7R, 0603
14	C30	1	C2012X7R1A106M125AC	CAP, CERM, 10 µF, 10 V, ±20%, X7R, 0805
15	C33	1	C3225X7R1H106M250AC	CAP, CERM, 10 µF, 50 V, ±20%, X7R, 1210
16	C35	1	GRM31CR71A226KE15L	CAP, CERM, 22 µF, 10 V, ±10%, X7R, 1206
17	C38	1	GRM033R71A103KA01D	CAP, CERM, 0.01 µF, 10 V, ±10%, X7R, 0201
18	C42	1	GRM32ER72A225KA35L	CAP, CERM, 2.2 µF, 100 V, ±10%, X7R, 1210
19	D1	1	CD0603-S0180	Diode, Switching, 90 V, 0.1 A, 0603 Diode
20	D2	1	LTST-C170KRKT	LED, Red, SMD
21	D3	1	LTST-C190KFKT	LED, Orange, SMD
22	D4	1	BAT54CDW-7-F	Diode, Schottky, 30 V, 0.2 A, SOT-363
23	J1	1	282856-2	Terminal Block, 5 mm, 2-pole, Tin, TH
24	J2	1	282856-3	Receptacle, 3 × 1, 5 mm, R/A, TH
25	J3, J4	2	CRD-081413-A-G	Receptacle, 2.54 mm, 10 × 2, Gold, TH
26	J5	1	PPTC051LFBN-RC	Receptacle, 2.54 mm, 5 × 1, Tin, TH
27	L1	1	XAL1010-222MEB	Inductor, Shielded, Composite, 2.2 µH, 32 A, 0.00255 Ω, SMD
28	L2	1	SPM3012T-4R7M	Inductor, Shielded, Ferrite, 4.7 µH, 1.5 A, 0.27 Ω, SMD
29	L3	1	BLM15AX601SN1D	Ferrite Bead, 600 Ω at 100 MHz, 0.5 A, 0402
30	Q1	1	BC846BLT1G	Transistor, NPN, 65 V, 0.1 A, SOT–23
31	Q2 – Q7	6	SQJ858AEP	MOSFET, N-CH, 40 V, 58 A, PowerPAK_SO-8L
32	Q8	1	SQJ422EP-T1-GE3	MOSFET, N-CH, 40 V, 75 A, PowerPAK_SO-8L
33	R1, R2, R14, R19, R21, R24, R29	7	CRCW040210K0JNED	RES, 10 k, 5%, 0.063 W, 0402
34	R3 – R5	3	CRE2512-FZ-R007E-3	RES SMD 0.007 Ω 1% 3 W 2512

Table 18. BOM (continued)

ITEM	DESIGNATOR	QTY	PART NUMBER	DESCRIPTION
35	R6 – R9	4	CRCW040225K5FKED	RES, 25.5 k, 1%, 0.063 W, 0402
36	R10 – R13	4	CRCW04024K99FKED	RES, 4.99 k, 1%, 0.063 W, 0402
37	R15	1	ERJ-2GE0R00X	RES, 0, 5%, 0.063 W, 0402
38	R16 – R18	3	CRCW04021K00JNED	RES, 1.0 k, 5%, 0.063 W, 0402
39	R20	1	CRCW0402100RFKED	RES, 100, 1%, 0.063 W, 0402
40	R22, R23, R25	3	CRCW040256R0JNED	RES, 56, 5%, 0.063 W, 0402
41	R26, R27, R28	3	CRCW040215K0JNED	RES, 15 k, 5%, 0.063 W, 0402
42	R30, R31	2	CRCW0402330RJNED	RES, 330, 5%, 0.063 W, 0402
43	TP1, TP3	2	5006	Test Point, Compact, Black, TH
44	TP2	1	5005	Test Point, Compact, Red, TH
45	U2	1	LMT86QDCKRQ1	SC70 Analog Temperature Sensor with Class-AB Output, DCK0005A
46	U3	1	DRV8305NPHPQ1	Three Phase Automotive Gate Driver with Three Integrated Current Shunt Amplifiers and Voltage Regulator, PHP0048G
47	U4	1	LM53600NQDSXRQ1	Synchronous Buck Regulator for 650 mA, DSX0010A
48	FID1, FID2, FID3	0	N/A	Fiducial mark. There is nothing to buy or mount.

8.2 PCB Layout Recommendations
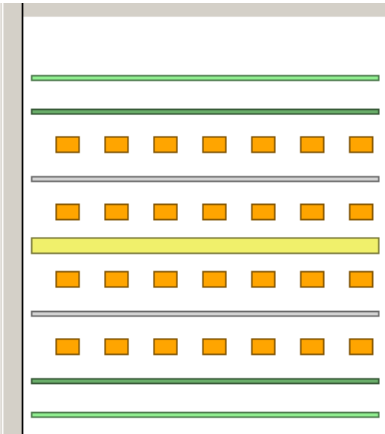
8.2.1 General Notes on Noise Sensitive Traces and Components

- Route voltage feedback traces away from other noisy traces or components, such as clock lines. Avoid routing things under the switch node of a power inductor altogether if possible
- Feedback nodes are generally high impedance lines which are quite sensitive to disturbances. The switch node can radiate a significant amount of energy and could couple noise into FB traces or other sensitive lines. Placing these traces on the other side of the board (with ground planes between them) helps mitigate ill effects as well.
- Analog and control loop components must be placed such that their trace lengths back to the IC are minimized.

The feedback and compensation nodes are especially high impedance and thus susceptible to picking up. As these are critical in the operation of the devices control loop, poor placement and routing of these components and traces may effect the performance of the device by introducing unwanted parasitic inductances and capacitances.

8.2.2 PCB Layering Recommendations

This design uses a 4-layer board, with an internal ground plane to shield the bottom signal layer from the switch nodes found on the top layer. Figure 98 shows the layer stack-up used in this board.

Layer Name	Type	Material	Thickness (mil)	Dielectric Material	Dielectric Constant	
Top Overlay	Overlay					
Top Solder	Solder Mask/Cov...	Surface Material	0.4	Solder Resist	3.5	
Top Layer	Signal	Copper	2.8			
Dielectric1	Dielectric	Prepreg	10	FR-4	4.2	
GND	Signal	Copper	2.8			
Dielectric 3	Dielectric	Core	28	FR-4	4.2	
PVDD	Signal	Copper	2.8			
Dielectric 2	Dielectric	Prepreg	10	FR-4	4.2	
Bottom Layer	Signal	Copper	2.8			
Bottom Solder	Solder Mask/Cov...	Surface Material	0.4	Solder Resist	3.5	
Bottom Overlay	Overlay					

Figure 98. Layer Stack Up, GND Plane and PVDD Layer Separating Top Layer Circuits From Bottom Layer Signals

- Wherever practical, keep power traces and pours on the same layer. This isn't always possible due to routing requirements.
- Keeping power traces and pours on the same layer minimizes the inductance of the path (by using as few vias as possible) by keeping individual power traces on the same layer, and reduce any noise coupling between planes by reducing overlap. Unfortunately, due to the number of different rails in this design, and the routing requirements needed to get them to the EVM connectors, this wasn't completely possible on this board.

8.2.3   General Power Supply Considerations

- Input capacitors should be placed as close to the IC as possible to reduce the parasitic series inductance from the capacitor to the device it is supplying. This is especially important for DCDC converters as the inductance from the capacitor to the high-side switching FET can cause high voltage spikes and ringing on the switch node, which can be damaging to components and cause problems for EMI.

- Place the input capacitors in order of descending size/value, with the smallest being closest to the device input pin. Contrastingly, place the output capacitors in order of descending size/value, with the largest being closest to the device's output pins/power inductor.

- Use wide copper areas/traces for routing outputs of the converters to the connectors or loads. This reduces the I*R drop along the power path and thus improves load regulation.

- The resistivity of a trace drops as the width of the trace increases ($R \propto 1/W$). If not using DCDC/linear converters capable of differential remote sensing, care must be taken that the voltage drop from the location of regulation (close to the converter) to the load is not significant. While there isn't really a maximum limit on this, there is a minimum. PCB traces, like wires, are rated for current ranges based on their cross-sectional area. This depends not only on the width but also on the thickness/height of the trace. Calculators are available online for calculating minimum trace width.

- Minimize the loop area and series path inductance of the switching return current in a DCDC converter. It is preferable that this be on the same layer and can be achieved by careful placement of the components.

- Since it is not always convenient to guarantee a good return path on the same layer, we can drop ground vias to an internal plane which is not broken up providing a more direct return path. The figure below shows the use of these ground vias where it was not possible to create a small loop on the top layer.

- The power inductors should be close to the switch node pins of the ICs, minimizing the distance from the pin to the inductor, but maintaining large area as much as possible. The goal is to minimize both the parasitic inductance, as well as reduce the radiated emissions from the node:

  – If a bootstrap capacitor is used, place this component as close to the power inductor as practical.

Figure 99 shows that the PVDD power connections are placed on large polygons on both the top layer and the middle layer of the board, and as suggested above, numerous layer-to-layer vias are used to connect these two planes. Figure 111 shows the Ground plane layer, which form almost a complete plane on the interior of the board. The inherent capacitance between these layers provides additional capacitance between the PVDD and GND nodes.
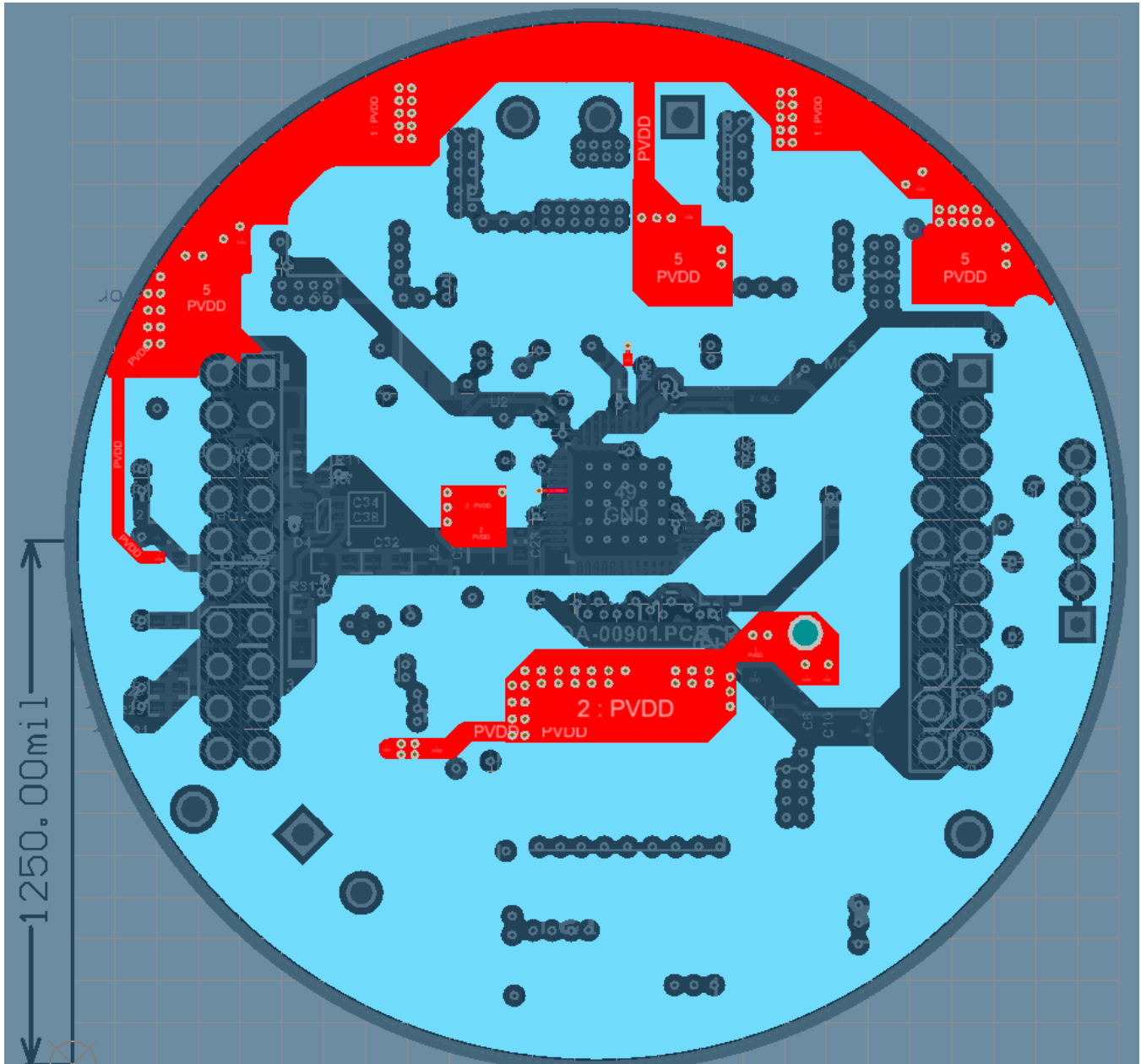
Figure 99. PVDD on Top and Middle Layers

8.2.4 12-V Protection Circuitry

Place input protection circuitry as close to the battery terminal inputs as possible, rather than close to the downstream circuit it is protecting, to reduce the inductance of the path. First of all, this means that the protection circuits will be as quick as possible to react to any transients. Second of all, in the event of a reverse polarity event, the FET controlled by the DRV8305-Q1 will shut off quickly and this could cause inductive kicks due to the interrupted current flow – the severity of this kick is a function of the inductance (and therefore the length/width) of the power path. Lastly, this provides a close, tight loop for the current/return path back to the battery terminals while the input filtering capacitors shunt a transient.

Figure 100 shows the placement of reverse-battery protection and input filtering components. Figure 101 shows the routing of reverse-battery protection and input filtering components.
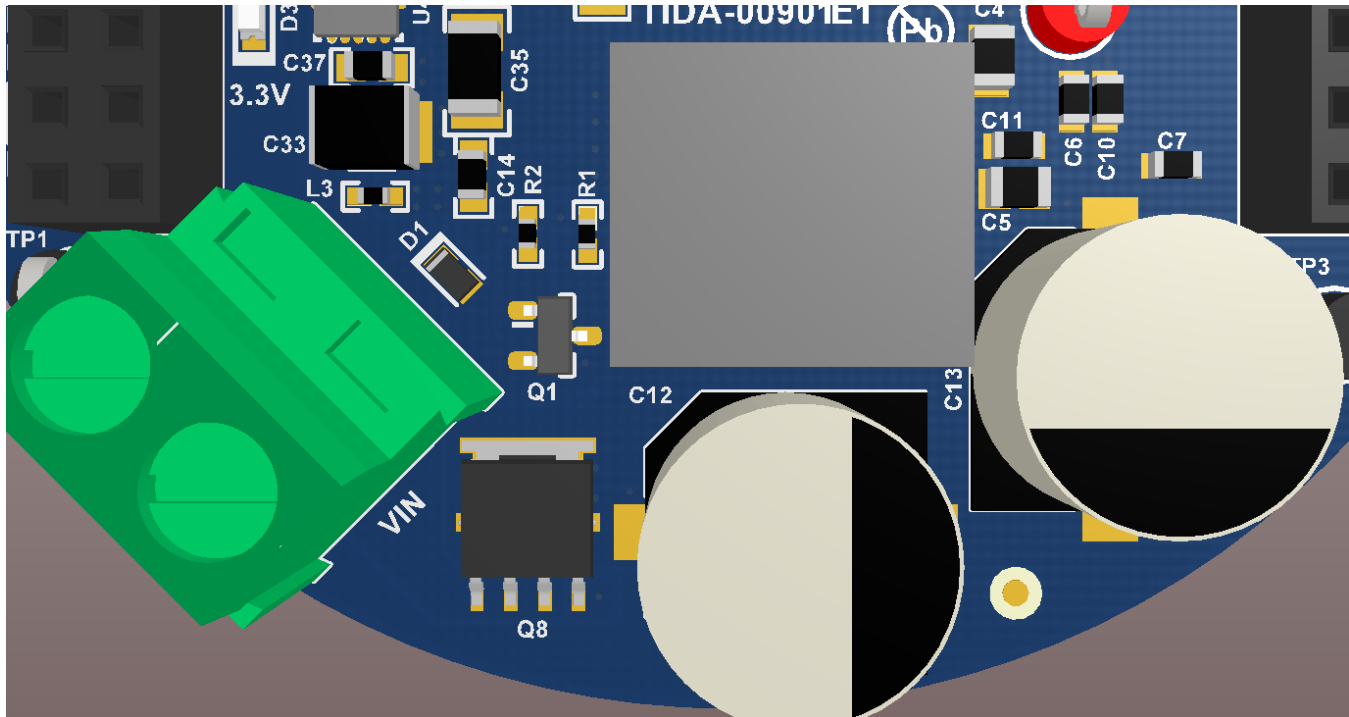
Figure 100. Placement of Reverse-Battery Protection and Input Filtering Components
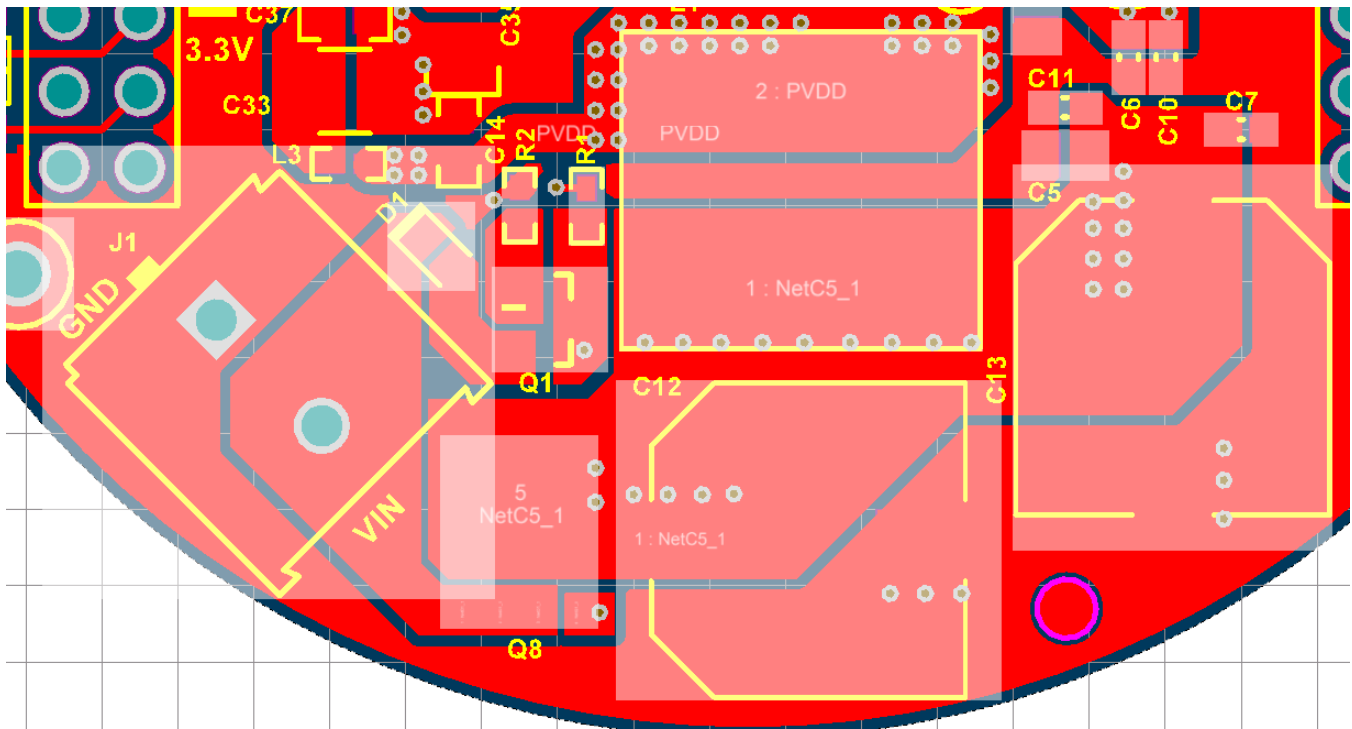
Figure 101. Routing of Reverse-Battery Protection and Input Filtering Components

8.2.5   3.3-V Buck Regulator

The following list of layout considerations is in order of importance:

1. Place high frequency input bypass capacitor, (C37), as close to the LM53600-Q1 as possible.
2. Connect AGND and GND to the DAP immediately adjacent to the LM53600-Q1.
3. Do not interrupt the ground plain under the loop containing the LM53600-Q1's VIN and GND pins and C37.
4. The boot capacitor, C32, should be close to the LM53600-Q1 and the loop from the SW pin, through the boot capacitor and into the BOOT pin should be kept as small as possible.
5. Keep the SW node as small as possible. It should be wide enough to carry the converter's full current without significant drop.
6. C33 with at least 4.7 µF of bypassing should be close to the LM53600-Q1's input.
7. Place C34, the VCC pin's bypass, and C38, the bypass for FB for fixed voltage devices and BIAS for adjustable devices as close to the LM53600-Q1 as possible.
8. The first output the trace from the output inductor to the output node should run by an output capacitor before joining the rest of the output node.
9. Keep C35 with at least 10µF close to the LM53600-Q1's output (output inductor and GND).
10. Clear the layer beneath the SW node.

Figure 102 and Figure 103 show the placement and routing for the 3.3-V buck regulator.
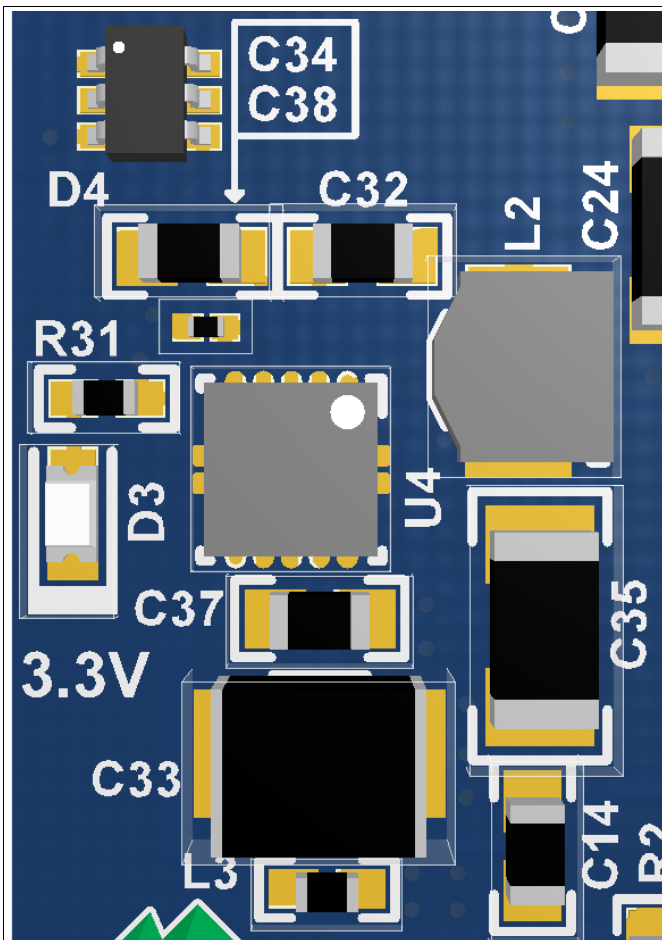
Figure 102. Placement for the 3.3-V Buck Regulator
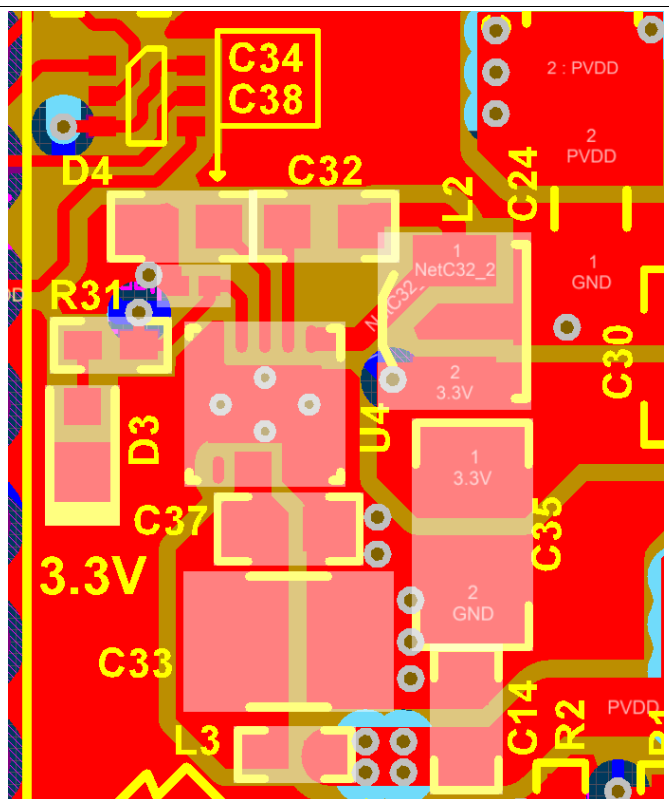
Figure 103. Routing for the 3.3-V Buck Regulator

8.2.6   Motor Gate Driver

The following layout recommendations were followed when designing the PCB for the DRV8305:

- The DVDD bypass capacitor (C23) and AVDD 1-µF bypass capacitor (C21) must connect directly to the adjacent GND pin to minimize loop impedance for the bypass capacitor.
- The CP1 and CP2 0.047-µF flying capacitors (C20 and C22) must be placed directly next to the DRV8305 charge pump pins.
- The VCPH 2.2-µF and VCP_LSD 1-µF bypass capacitors (C41 and C42) should be placed close to their corresponding pins with a direct path back to the DRV8305-Q1 GND net.
- The PVDD 4.7-µF bypass capacitor (C24) should be placed as close as possible to the DRV8305 PVDD supply pin.
- Use the proper footprint as shown in the Mechanical, Packaging, and Orderable Information section.
- Minimize the loop length for the high-side and low-side gate drivers. The high-side loop is from the DRV8305 GH_X to the power MOSFET and returns through SH_X. The low-side loop is from the DRV8305 GL_X to the power MOSFET and returns through SL_X.

Figure 104 and Figure 105 show the placement and routing for 3-Phase automotive gate driver.
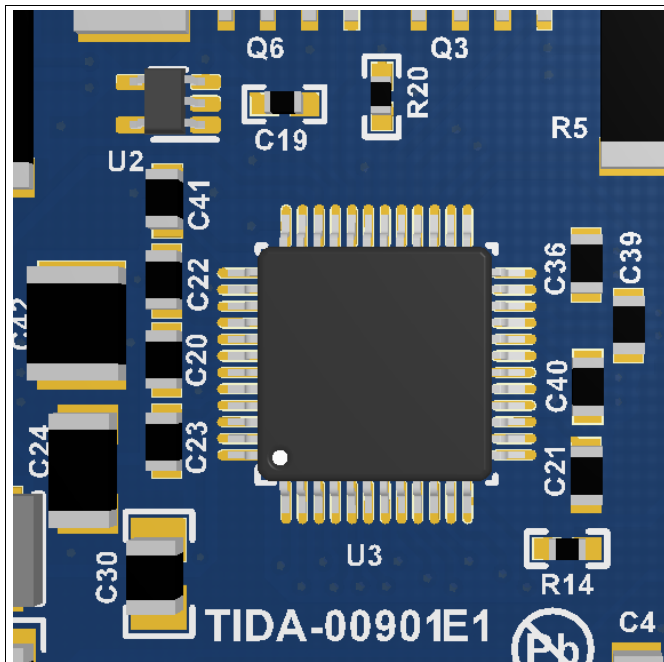
Figure 104. Placement for 3-Phase Automotive Gate Driver
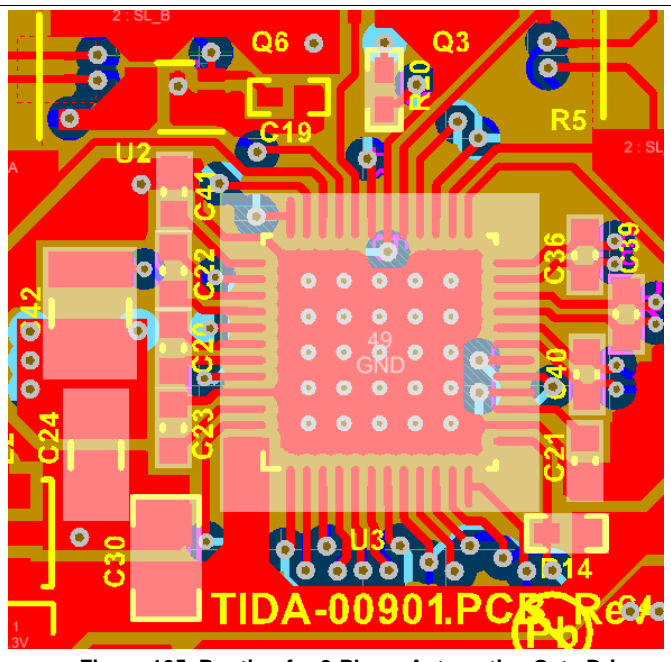
Figure 105. Routing for 3-Phase Automotive Gate Driver

8.2.7 Motor Drive Circuit

The components related to the drive stage for each phase of the motor are grouped together, and the layout of each of the phases is similar. The power FETs and associated components are located on the top side of the board, as is the DRV8305-Q1 gate driver (U3). The two power FETs for each motor phase are located in close proximity, and such that the shared output node MOT_A, MOT_B, or MOT_C connects them with solid current path. The current sense resistor (R3, R4, R5) for each phase is also located as close as possible to the motor phase traces.

C8 and C9 (330 uF) and C1, C2, and C3 (1 uF) provide a low-inductance reservoir of charge near the high-side FETs. They should be located in close proximity to the drive stages to reduce any resistance or inductance between the stored charge and the drive FETs.

Figure 106 shows the layout of the motor drive stages.
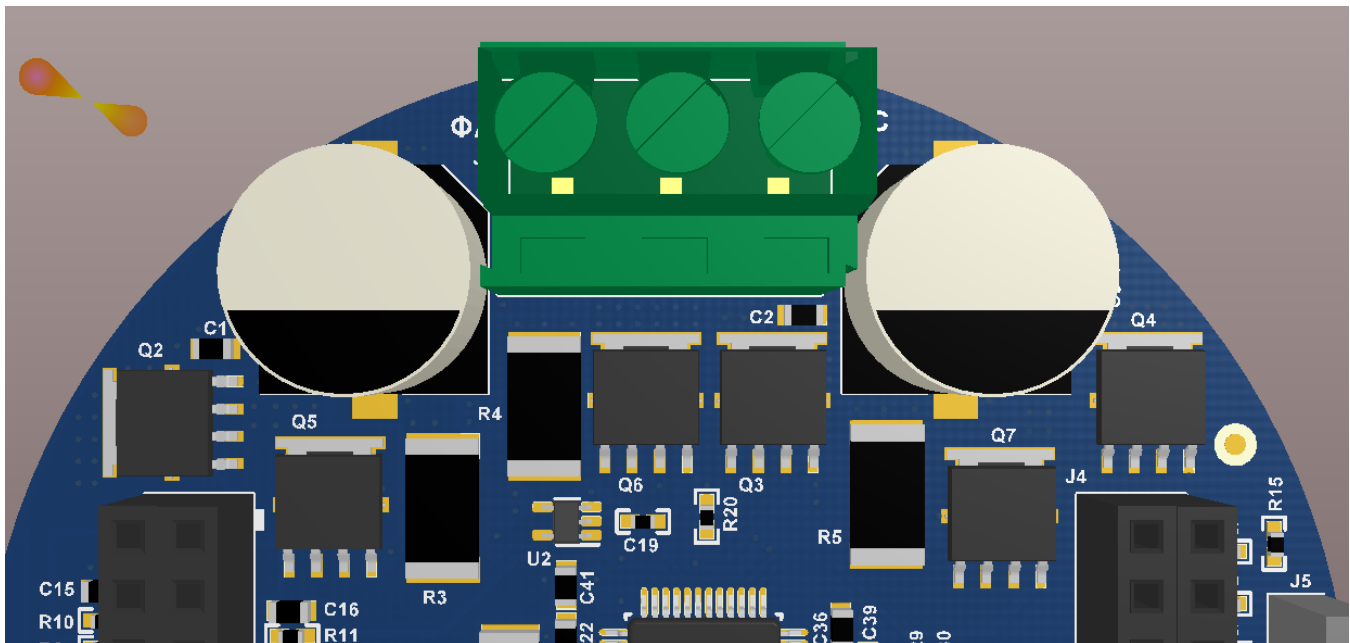
Figure 106. Layout of Motor Drive Stages

8.2.8 Differential Signals

In the case of differential signals, such as the motor current feedback across the current sense resistors, use symmetry to ensure that any noise picked up on one line is also picked up approximately equally on the other line.

Figure 107 shows the layout symmetry used to reduce differential-mode noise on analog signal.
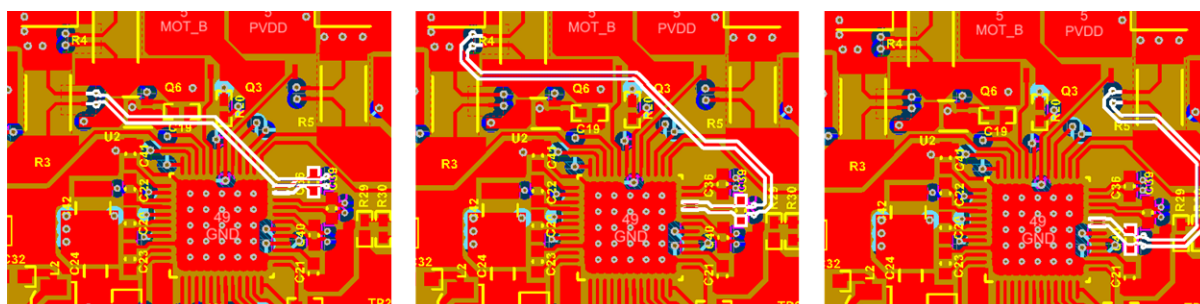
Figure 107. Layout Symmetry Used to Reduce Differential-Mode Noise on Analog Signal

8.3   Layout Prints

The following figures are for reference; to download the layout prints for each board, see the design files at http://www.ti.com/tool/TIDA-00901.
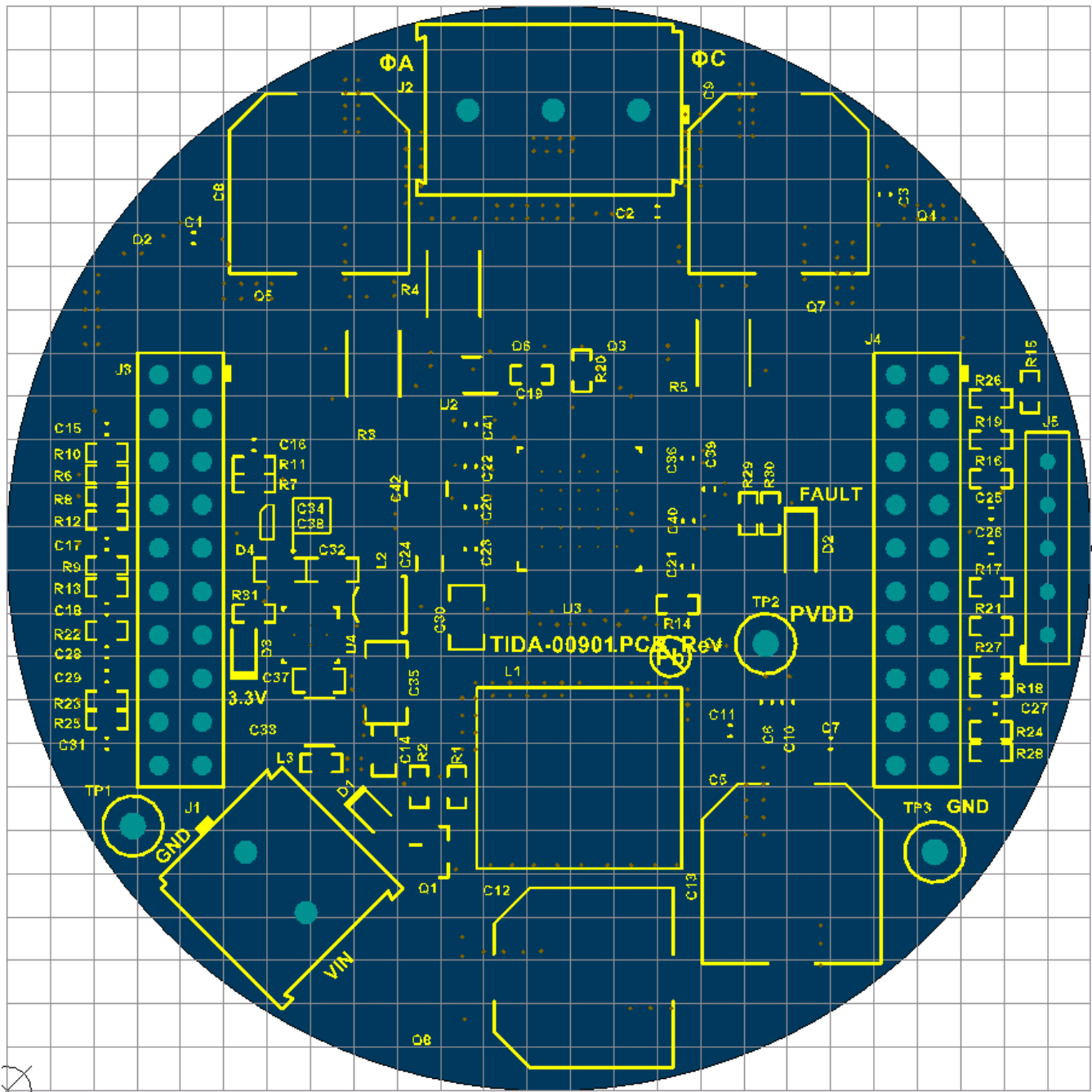
Figure 108. Top Silkscreen
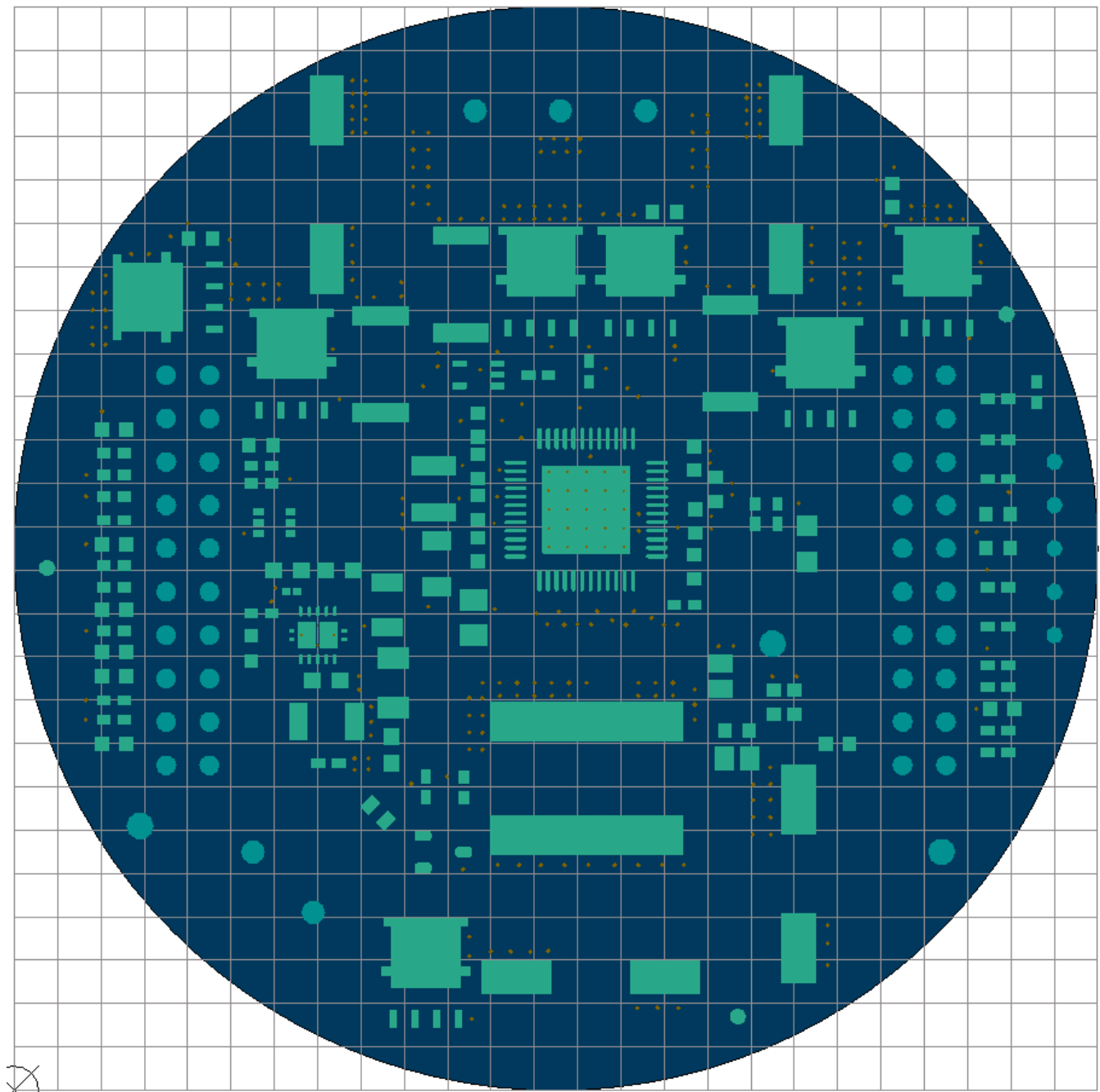
Figure 109. Top Solder Mask
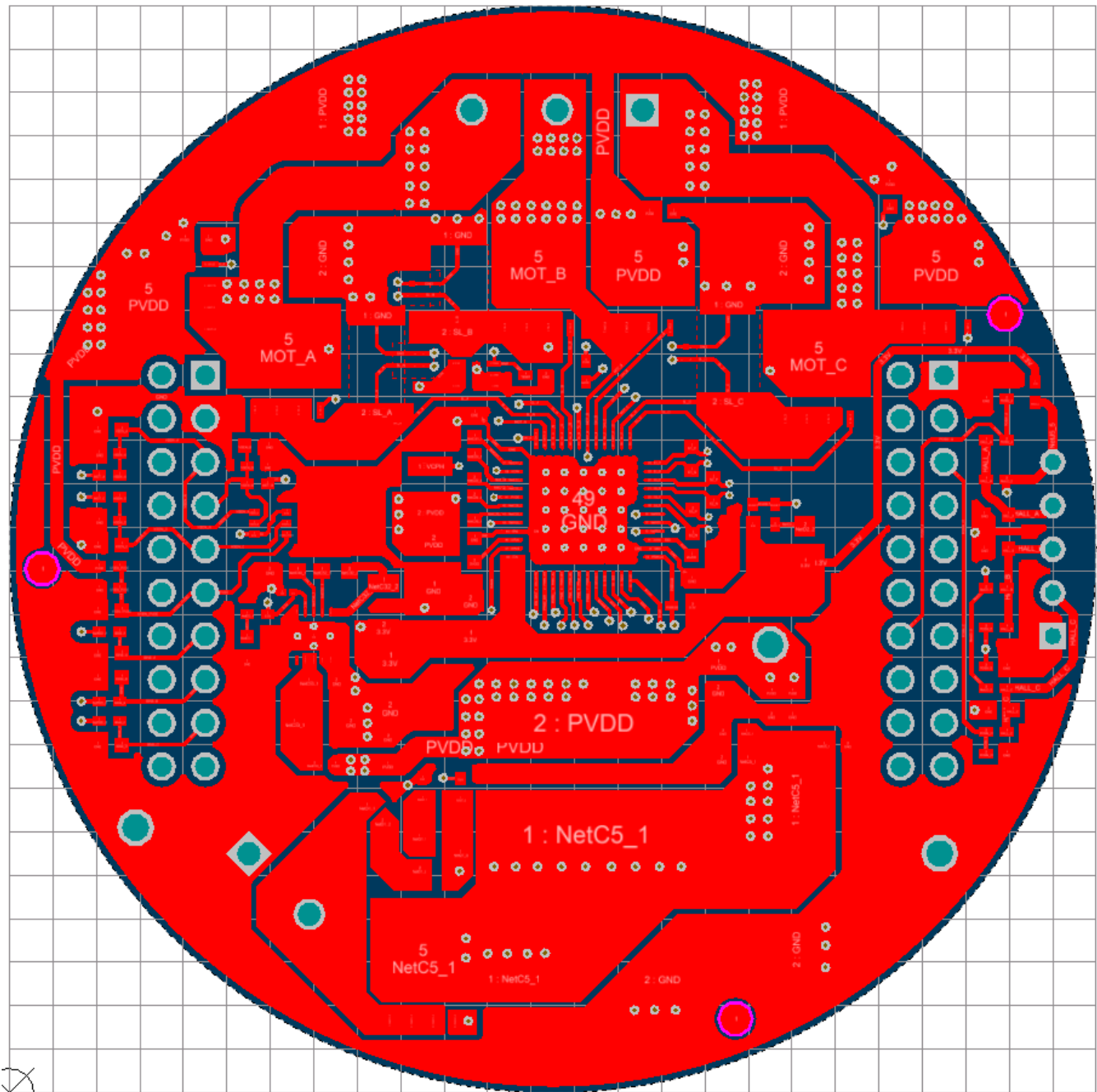
Figure 110. Top Layer
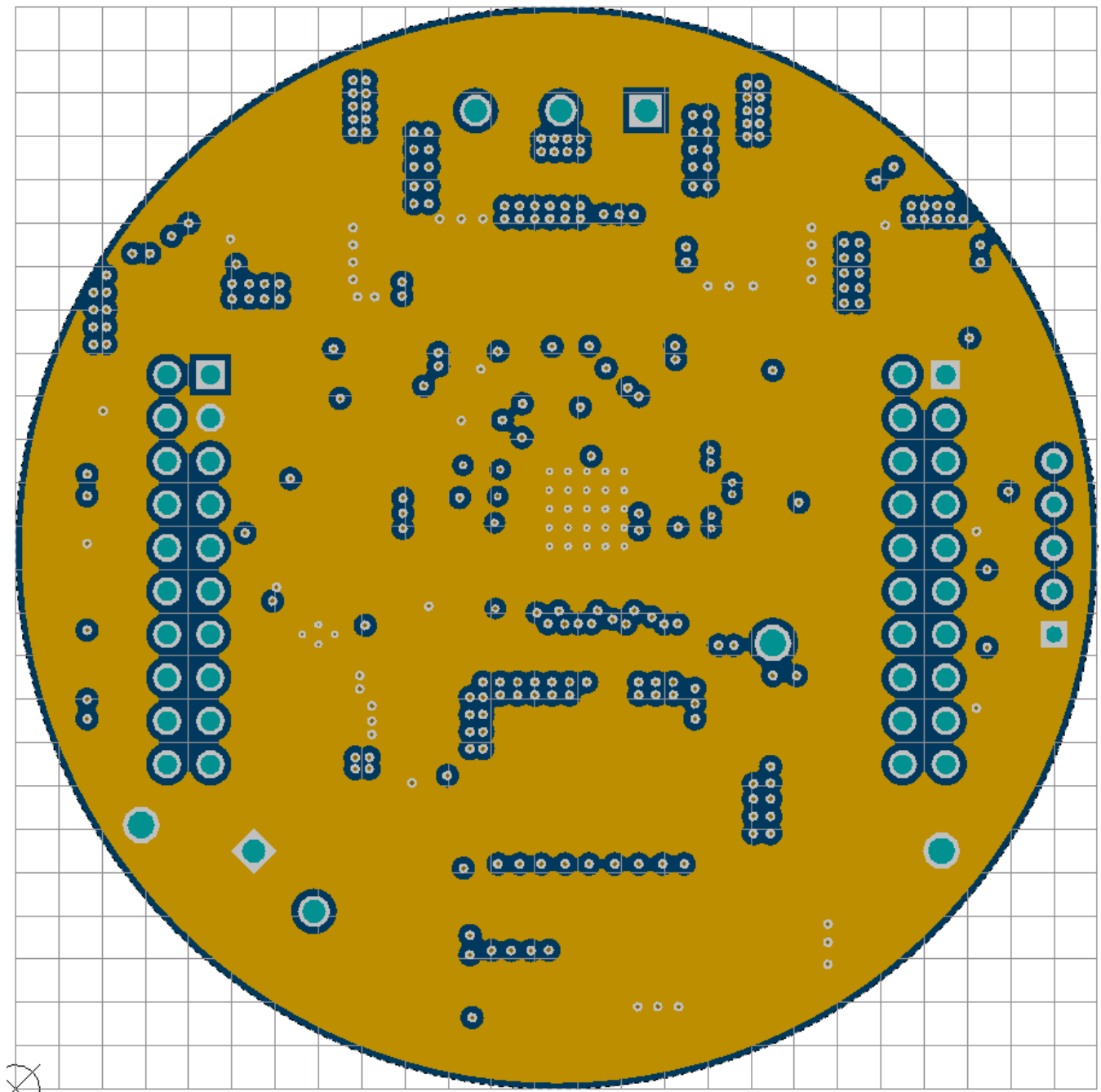
Figure 111. Layer 2 – Ground
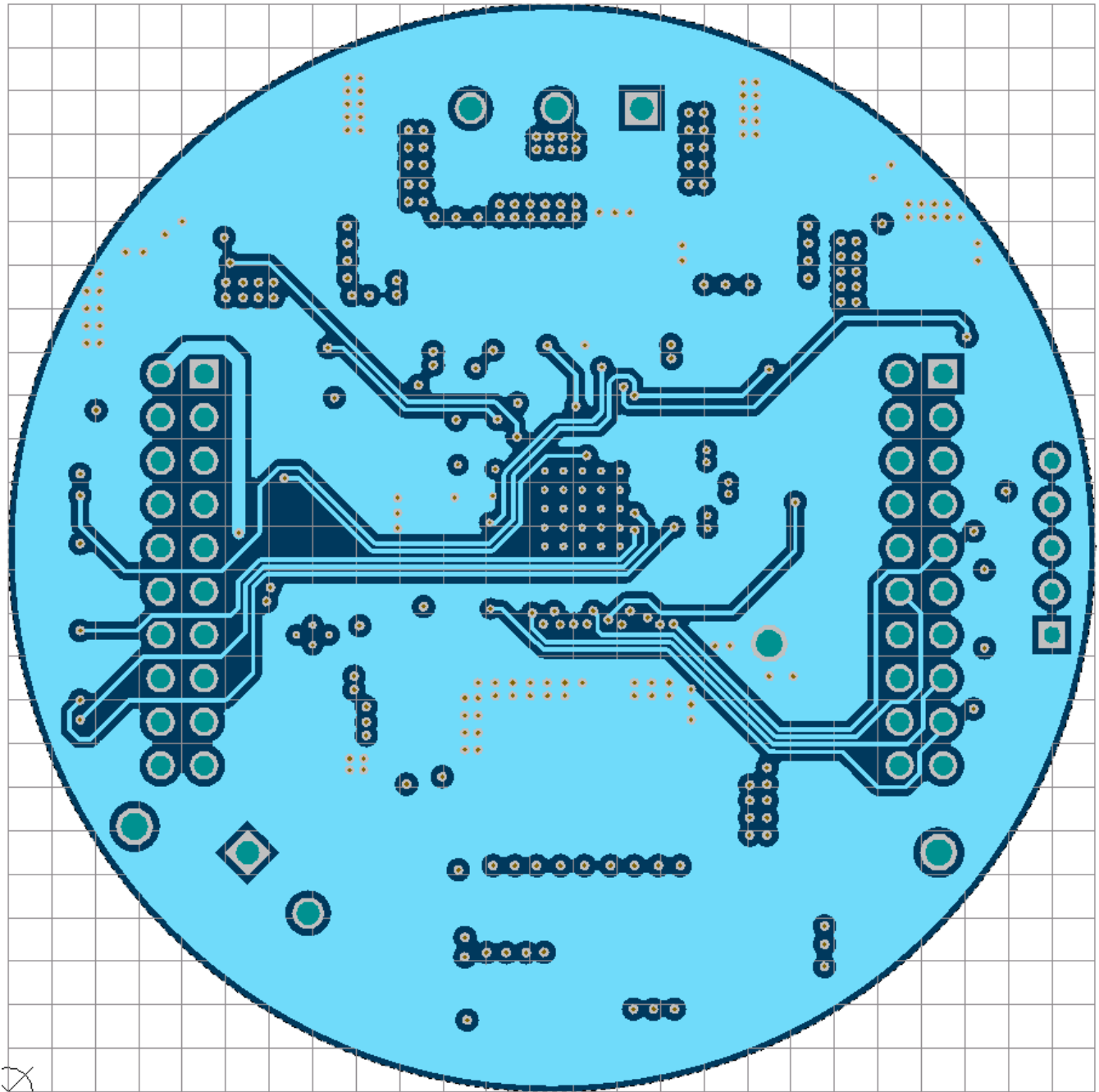
Figure 112. Layer 3 – Power
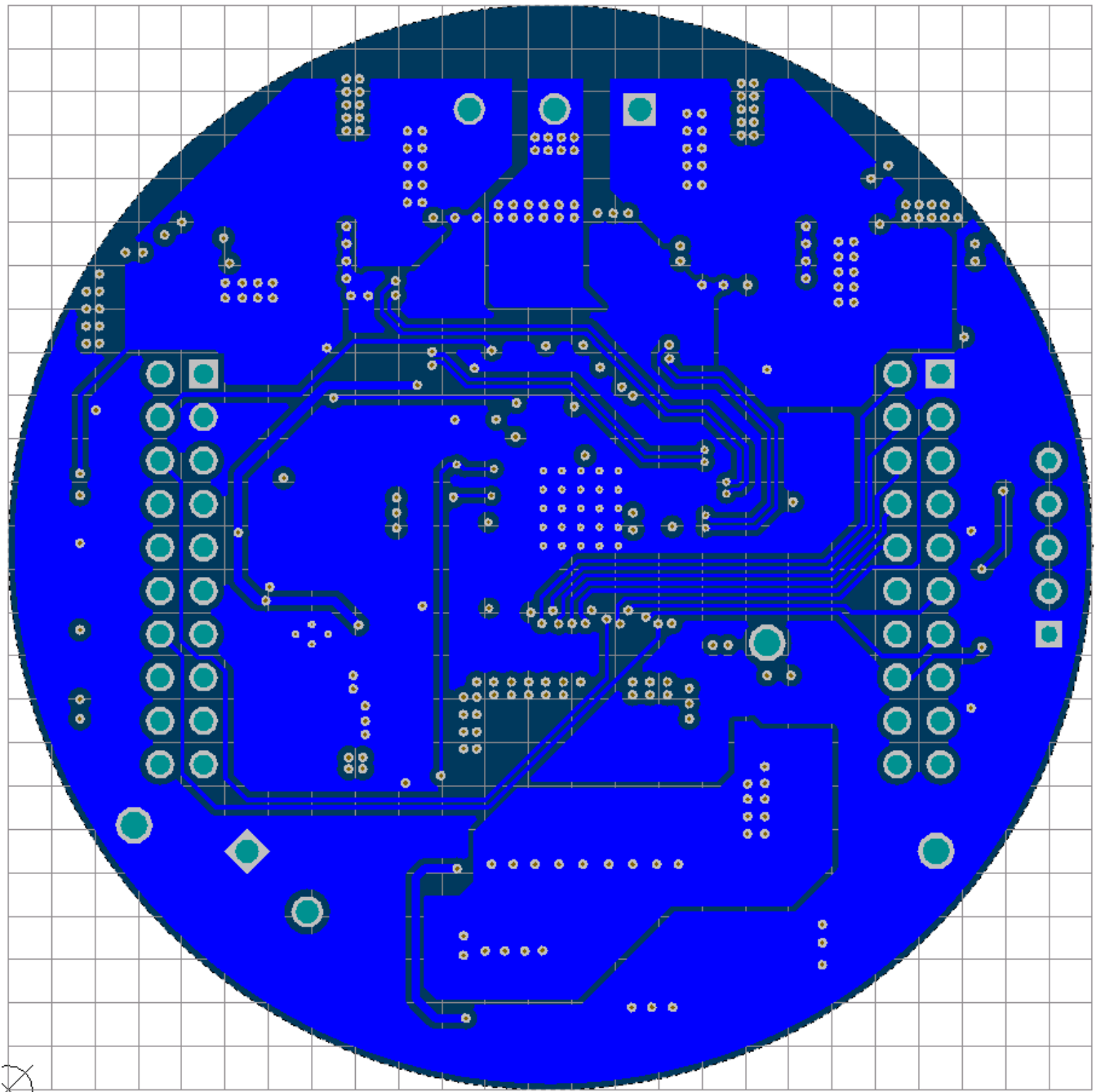
Figure 113. Bottom Layer
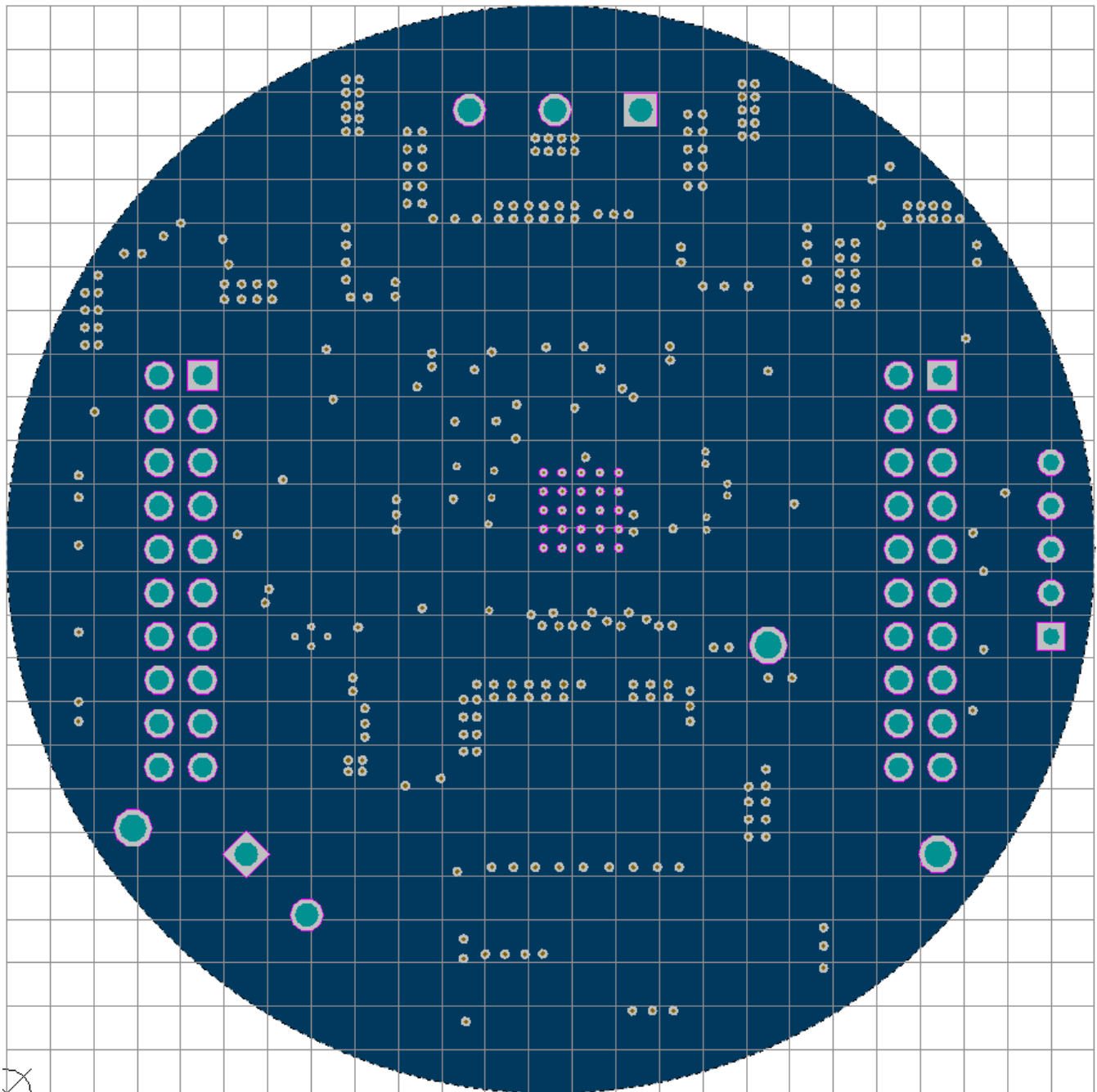
Figure 114. Bottom Solder
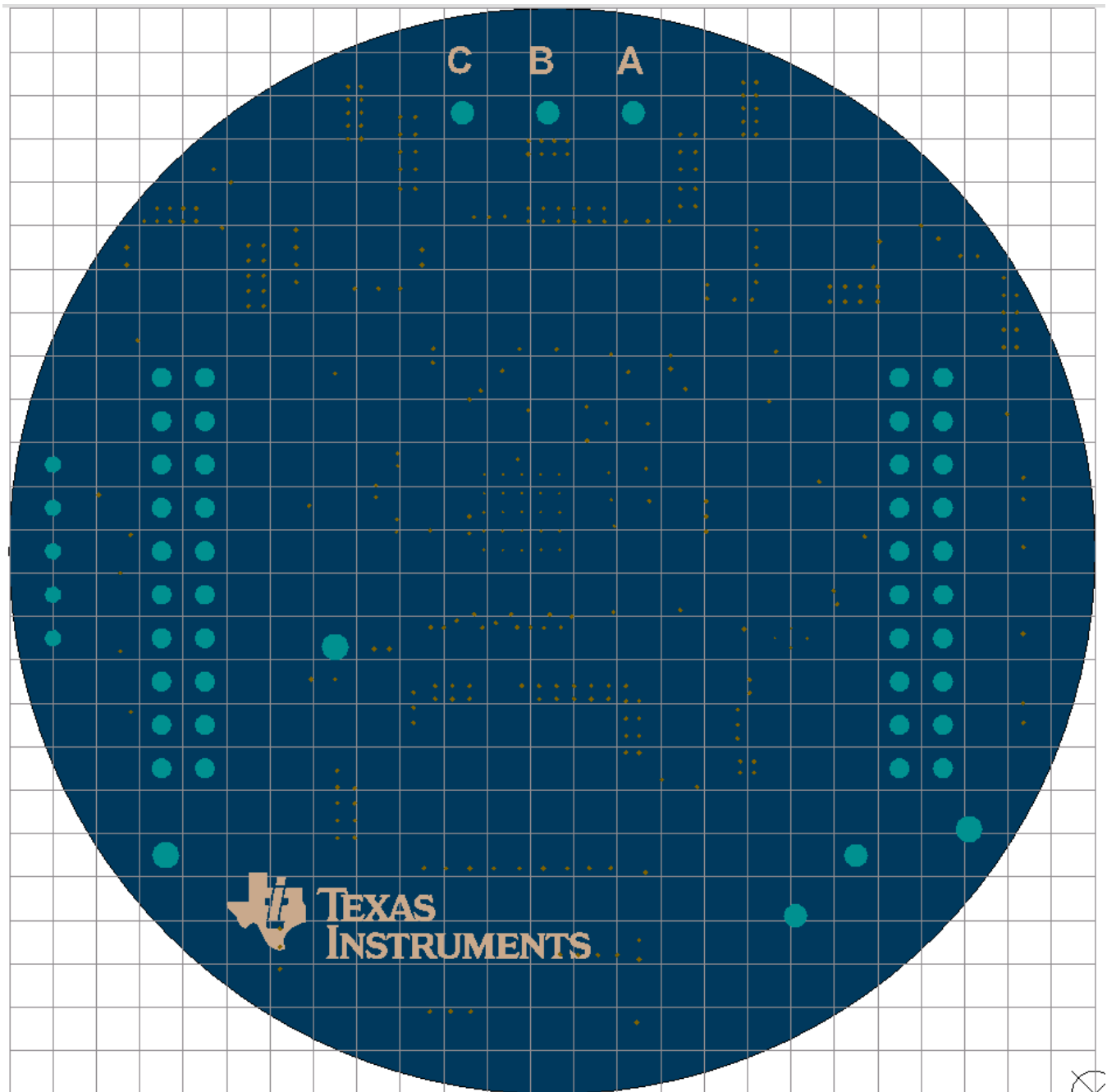
Figure 115. Bottom Silkscreen (Flipped)
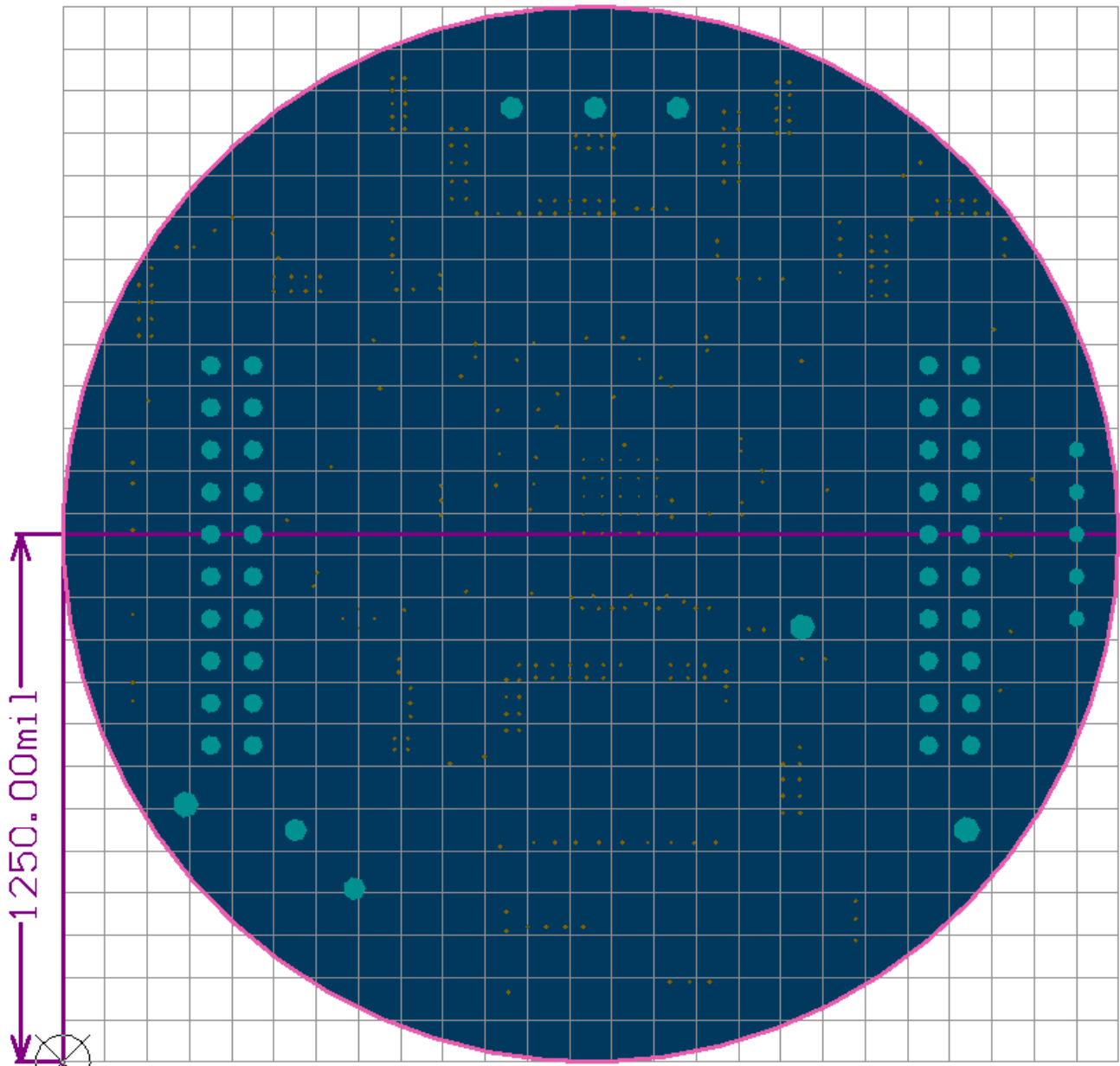
Figure 116. Mechanical Dimensions

8.4   Altium Project and Gerber Files

To download the Altium project and Gerber files for each board, see the design files at TIDA-00901.

9   Software Files

To download the Code Composer Studio Integrates Development Environment, see
http://www.ti.com/tool/CCSTUDIO.

To download the MotorWare Software packages, see http://www.ti.com/tool/MOTORWARE.

10   References

1. *DRV8305-Q1 Three-Phase Automotive Smart Gate Driver With Three Integrated Current Shunt Amplifiers and Voltage Regulator* (SLVSD12).
2. *LMT86/LMT86-Q1 SC70/TO-92, Analog Temperature Sensors with Class-AB Output* (SNIS169).
3. *LM53600/01-Q1, 0.65A/1A, 36V Synchronous, 2.1MHz, Automotive Step Down DC-DC Converter* (SNAS660).
4. *DRV5013 -Q1 Automotive Digital-Latch Hall Effect Sensor* (SLIS162C).
5. *TMS320F28026F, TMS320F28027F InstaSPIN-FOC Software Technical Reference Manual* (SPRUHP4).
6. *Understanding IDRIVE and TDRIVE in TI Motor Gate Drivers* (SLVA414).
7. *Simple Success with Conducted EMI from DC-DC Converters* (SNVA489).
8. MotorWare Software, http://www.ti.com/MotorWare
9. InstaSPIN / MotorWare GUI, http://www.ti.com/tool/instaspinuniversalgui
10. Webench Design Center, http://www.ti.com/webench.

11   Terminology

ADC: Analog-to-Digital Converter

BOM: Bill of Materials

Buck: Step-down switching-mode voltage converter

CAN:Controller Area Network

CCS: Code Composer Studio

EMC: Electromagnetic Compatibility

EMF: Electromotive Force

FET: Field Effect Transistor

FOC: Field Oriented Control

GND: Ground

IR: Infrared

MOSFET: Metal Oxide Semiconductor Field Effect Transistor

OEM: Original Equipment Manufacturer

PCB: Printed Circuit Board

RC: Resistor Capacitor

RCD: Resistor Capacitor Diode

SPICE: Simulation Program

TIDA: TI Design

12 About the Author

CLARK KINNAIRD is a Systems Applications Engineer at Texas Instruments. As a member of the Automotive Systems Engineering team, Clark works on various types of motor drive end-equipment, creating reference designs for automotive manufacturers. Clark earned his Bachelor of Science and Master of Science in Engineering from the University of Florida, and his Ph.D. in Electrical Engineering from Southern Methodist University.

Appendix A Appendix

A.1   WEBENCH Simulation Models

Figure 117 shows the WEBENCH electrical schematic for the LM53600-Q1 3.3-V buck regulator.
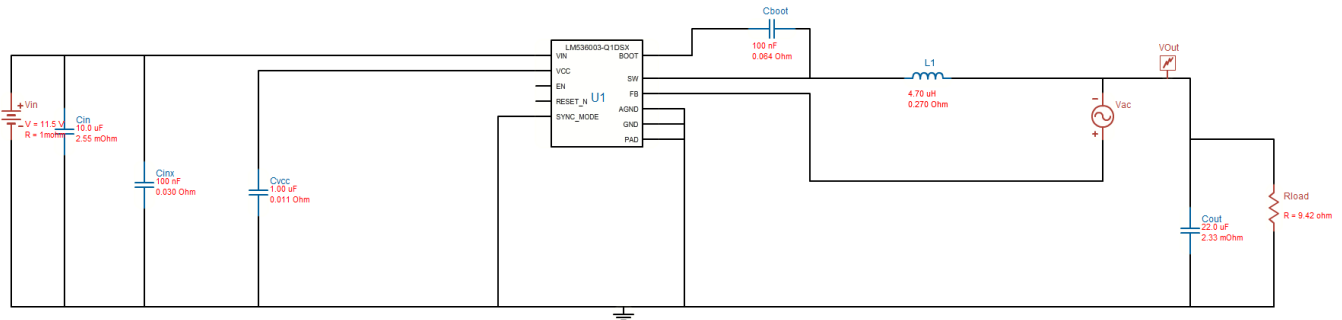
Figure 117. WEBENCH Electrical Schematic for the LM53600-Q1 3.3-V Buck Regulator.

A.2   TINA Simulation Models

shows the TINA simulation schematic for motor current feedback circuit.
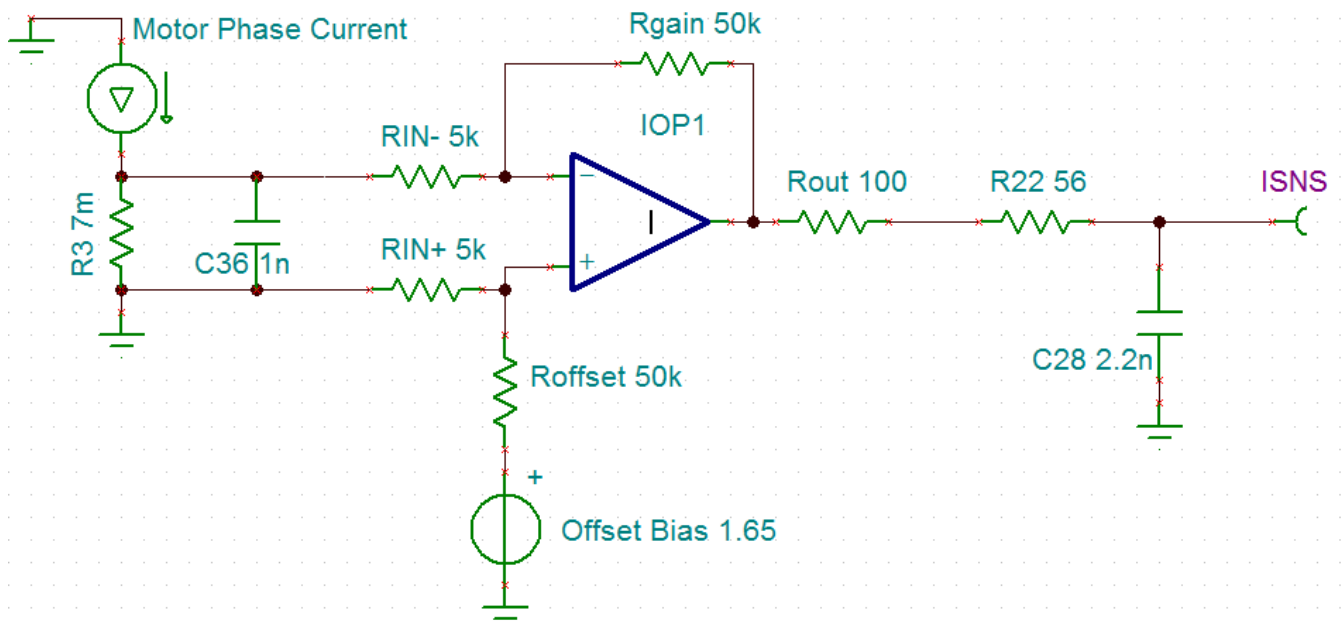
Figure 118. TINA Simulation for Motor Current Feedback Circuit

Figure 119 shows the TINA simulation schematic for VBAT input filtering.
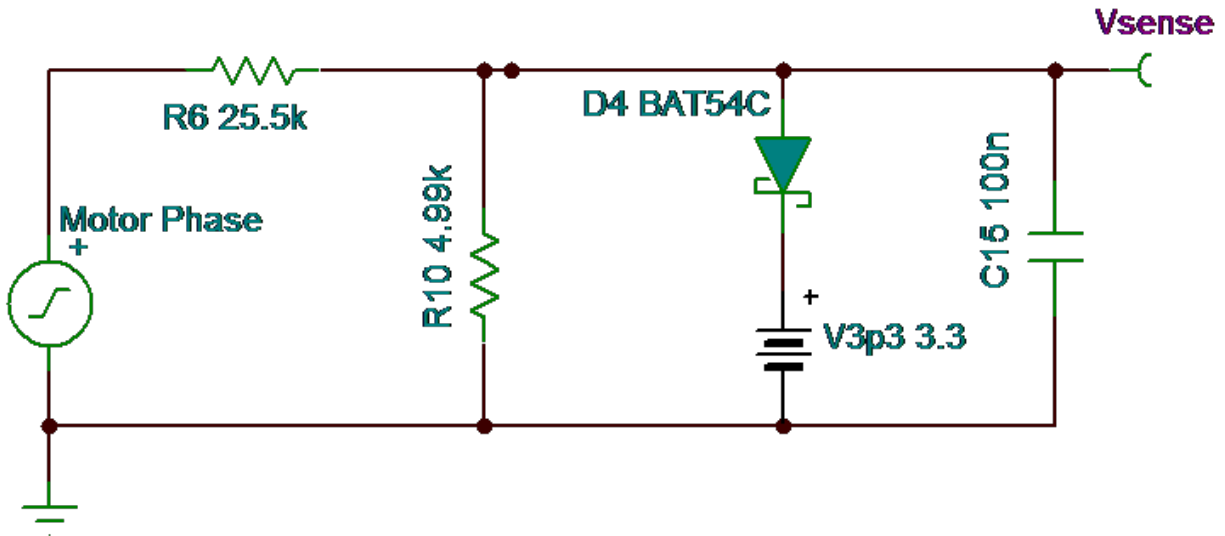
Figure 119. TINA Simulation Schematic for Motor Voltage Feedback Circuit

Figure 120 shows the TINA simulation schematic for VBAT input filtering.
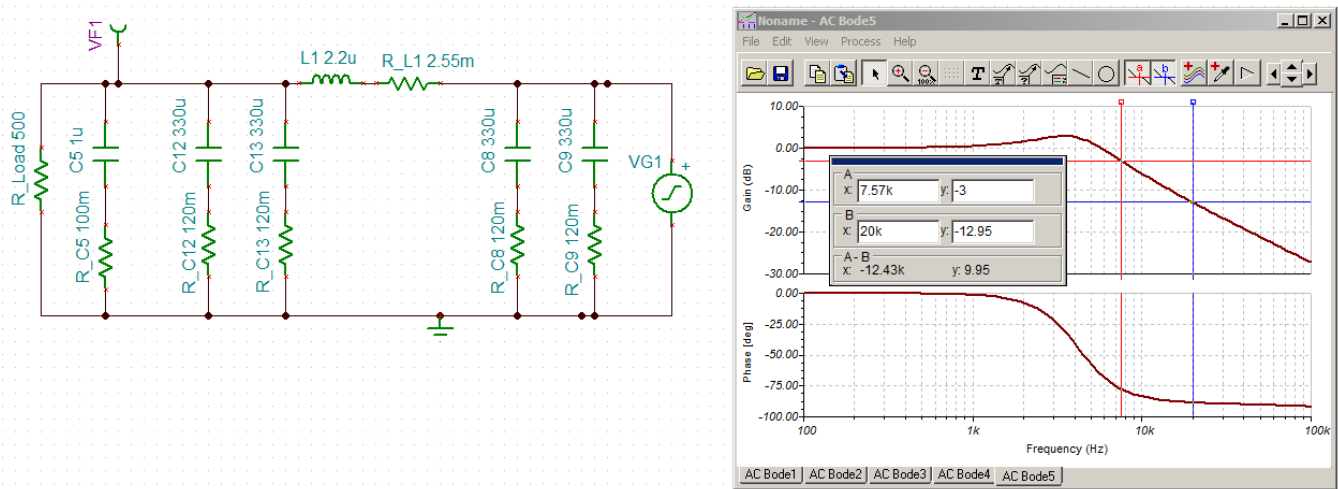
Figure 120. TINA Simulation Schematic for VBAT Input Filtering

A.3 Motor Specifications

shows the motor specifications.

Table 19. Motor Specifications

PARAMETER	UNITS	DT4260-24-055-04 (BLY172S-24-400)	RP34-313V24-100	IHN06576
Vendor		Telco (Anaheim Automottion)	ElectroCraft	Custom
Rated Voltage	V	24	24	24
Rated Speed	RPM	4,000	2,400	
Rated Power	W	77	545	
BACK EMF Constant	V / kRPM	3.35	10.2	
Electrical Poles		4	4	
Phase Resistance	Ω	0.8	0.2	0.6
Phase Inductance	mH	1.2	1	0.628
Stall Torque	N - m		221	
Peak Torque	N - m		773	
Electrical Time Constant	msec	1.5	6	
Rotor Inertia	in-oz-sec^2	0.00068	0.0385	
Weight	kg	0.45	4.1	1.4
Shaft Diameter	mm			7.9
Frame Size	mm	42		70